

**BIOENERGETICS AND MAJOR DEPRESSIVE DISORDER-
INVESTIGATIONS OF MITOCHONDRIA FUNCTION IN A
HUMAN CELLULAR MODEL**



DISSERTATION

ZUR ERLANGUNG DES DOKTORGRADES
DER NATURWISSENSCHAFTEN (DR. RER. NAT.)
DER FAKULTÄT FÜR BIOLOGIE UND VORKLINISCHE MEDIZIN
DER UNIVERSITÄT REGENSBURG

vorgelegt von
Kerstin Kuffner
aus
Viechtach
im Jahr
2020

Das Promotionsgesuch wurde eingereicht am:

20.02.2020

Die Arbeit wurde angeleitet von:

Prof. Dr. Christian Wetzel

Unterschrift:

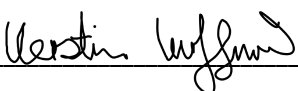


Table of contents

Acknowledgements	9
Abbreviations.....	10
Abstract	12
Zusammenfassung	14
1 Introduction.....	16
1.1 Mitochondria – the vital force in our cells	16
1.1.1 Mitochondria structure and the site of action	16
1.1.2 Mitochondria in the cellular metabolism.....	19
1.1.3 Fission and fusion: a dynamic network.....	21
1.2 Major Depressive Disorder – a multifactorial disease	24
1.2.1 Classification and diagnostics	24
1.2.2 Early and new theories for manifestation.....	26
1.3 The risk factor stress - impact on mitochondria and mood.....	28
1.3.1 The stress response in the human body	28
1.3.2 Benefits of acute stress	29
1.3.3 Sustained stress and its deleterious consequences.....	30
1.4 Mitochondria and disease – what we know so far	33
1.4.1 Mitochondriopathies	33
1.4.2 Mitochondrial disruption in neurodegenerative diseases.....	34
1.4.3 Dysfunction of mitochondria and psychiatric disorders.....	35
1.5 From fibroblasts via induced pluripotent stem cells through to induced neurons - a cellular model for MDD	36
1.6 Bioenergetic imbalance in MDD – hypothesis and aim of the thesis.....	38
2 Materials.....	41
2.1 Lab supplies.....	41
2.2 Reagencies, chemicals and kits	41

2.4 Antibodies	43
2.5 Culture media and buffer compositions	43
3 Methods	45
3.1 Study participants	45
3.2 Adult human dermal fibroblasts.....	46
3.2.1 Culturing conditions	46
3.2.2 Passaging, freezing and thawing procedure.....	46
3.2.3 Automated cell counting with CASY Cell Counter	47
3.3 Reprogramming of adult human dermal fibroblasts into induced pluripotent stem cells using Epi5 plasmids.....	47
3.1 Coating with Vitronectin.....	47
3.2 Preparation of Epi5 plasmids	47
3.3 Preparation and electroporation of human fibroblasts.....	48
3.4 Coating for iPSCs and NPCs	48
3.5 Induced pluripotent stem cells	49
3.5.1 Culturing conditions	49
3.5.2 Passaging, freezing and thawing procedure.....	49
3.6 Neural induction and expansion of neural progenitor cells	50
3.7 Immunocytochemical staining.....	51
3.8 Assessment of respiratory properties: Seahorse XFp Flux Analyzer	51
3.10 Normalization of respiratory experiments.....	53
3.10.1 Normalization by Hoechst staining.....	53
3.10.2 Normalization by Bichinoic Acid Assay	53
3.11 Luminescent assay for ATP content	54
3.12 Live cell imaging.....	55
3.12.1 Mitochondrial membrane potential measurements with JC-1	55
3.12.2 Analysis of intracellular Ca ²⁺ with Fura-2 dye	56
3.13 Determination of the mitochondrial content.....	57

3.13.1 gDNA extraction.....	57
3.13.2 Quantitative Real-Time Poly Chain Reaction.....	58
3.14 Data analysis and statistics	60
4 Results.....	61
4.1 Patient and control cohort.....	61
4.2 Differences in mitochondrial metabolism in peripheral cells: Fibroblasts show alterations in mitochondria-related functions.....	62
4.2.1 Mito Stress Test: ETC function and glycolysis	63
4.2.2 ATP content.....	69
4.2.3 Bioenergetic properties and mitochondria-related homeostasis in fibroblasts	70
4.3 Mitochondrial content: mtDNA copy number in fibroblasts.....	74
4.4 Successful reprogramming of fibroblasts into iPSCs and induction of NPCs	75
4.4.1 Cultivation and reprogramming of human dermal fibroblasts.....	75
4.4.2 Quality control for pluripotency	76
4.4.3 Differentiation of neural progenitor cells.....	77
4.5 Alterations of the mitochondrial metabolism in cells of the CNS: Neural progenitor cells depict changes in energy supply.....	78
4.5.1 Mito Stress Test: ETC and glycolysis	79
4.5.2 ATP content.....	84
4.5.3 Bioenergetics and mitochondria-related homeostasis in NPCs.....	85
5 Discussion.....	88
5.1 Fibroblasts from MDD patients show lower respiratory rates and altered bioenergetic functions	88
5.2 Enhanced metabolism in fibroblasts due to hormonal and metabolic stressors	90
5.3 Similar mitochondrial densities in MDD and control fibroblasts.....	93
5.4 Decreased mitochondria-related metabolism in MDD NPCs	94
5.5 Effects of the synthetic hormonal stressor dexamethasone in NPCs.....	96

6 Conclusion and future perspectives	98
List of references	101
List of figures.....	114
List of tables.....	116
Appendix.....	118

Acknowledgements

Danksagung

Allen voran möchte ich mich bei meinem Doktorvater Prof. Dr. Christian Wetzl bedanken. Vielen Dank, Christian, für deine Unterstützung, die Ratschläge und Ermutigungen. Danke aber auch für das entgegengebrachte Vertrauen und die Freiheiten, die du mir geschenkt hast. Ohne dich wäre diese Arbeit nicht die zu der sie geworden ist.

Ein weiterer Dank geht an meine Mentoren und Prüfer Prof. Dr. Stephan Schneuwly, Prof. Dr. Iris-Tatjana Kolassa und Prof. Dr. Oliver Bosch. Zudem möchte ich dem ganzen GRK2174 unter der Leitung von Prof. Dr. Inga Neumann und meiner 2. PI innerhalb des GKR PD Dr. Caroline Nothdurfter, sowie Prof. Dr. Rainer Rupprecht als Leiter des Lehrstuhls für Psychiatrie und Psychotherapie danken.

Des Weiteren möchte ich mich bei Dr. Leopold Größer, Dr. Konstantin Drexler und Prof. Dr. Mark Berneburg der Dermatologie des UKR für die Durchführung der Hautstanzen bedanken. Ein weiterer Dank für die Kollaborationen geht auch an Prof. Dr. Markus Riemenschneider der Neuropathologie des UKR und Prof. Dr. Richard Warth für die Leihgabe des Seahorse XFp Flux Analyzers.

Ein herzliches Dankeschön geht auch an Dr. Vladimir Milenkovic. Vielen Dank, Vladi, für die Weitergabe deiner technischen und wissenschaftlichen Expertise, aber auch die Aufmunterungen durch deine Witze und deinen Charme. Du trägst maßgeblich zu der guten Stimmung im Labor bei!! Bei den technischen Assistentinnen – allen voran Tati – möchte ich mich bedanken. Heike, Doris und Anett – auch eure Hilfe schätze ich sehr.

Zudem gilt mein Dank Christoph und Julian, die mich während meines ersten Jahres unterstützt – und bestens unterhalten – haben. Danke auch an Kati für die Zusammenarbeit im Labor und die immer nette Gesellschaft im Büro während meines zweiten Jahres. Treuste und definitiv unterhaltsamste (lauteste?) Begleiterin war Steffi, die keine Gelegenheit ausgelassen hat mit mir Späße zu machen und herzlich zu lachen. Du „Gaudibletzal“! Das werde ich vermissen!

DANKE euch allen Laborkollegen - ihr habt mir diese Zeit zu einer wunderschönen gemacht!

Bei meinen Kollegen des GRK 2174 möchte ich mich auch bedanken, insbesondere aber bei Lisa und Felix, welche nicht nur Kollegen waren, sondern zu echten Freunden geworden sind.

Zu guter Letzt geht natürlich auch ein riesen Dankeschön an meine Eltern und Thassilo, die mich vor allem im letzten Jahr immer wieder aufgebaut und ermutigt haben, nicht aufzugeben. Danke für euer offenes Ohr, euren Zuspruch und eure Geduld. Danke, dass ihr immer für mich da wart und an mich geglaubt habt.

Abbreviations

ACL	ATP-citrat-lyase
ACTH	adrenocorticotropic hormone
AD	Alzheimer's Disease
ADP	adenosine diphosphate
ADs	antidepressants
ALS	Amyotrophic Lateral Sclerosis
APP	amyloid precursor protein
ATP	adenosine triphosphate
A β	amyloid- β -peptide
B2M	beta-2-microglobulin
BCA	bichinoic acid
BDNF	brain-derived neurotrophic factor
BMI	body-mass-index
BPD	Bipolar Disorder
BSA	bovine serum albumin
CON	control
CPEO	Chronic Progressive External Ophthalmoplegia
CRP	C-reactive protein
Cyt c	Cytochrome c
DEX	dexamethasone
DNA	desoxiribonucleic acid
drp1	dynammin-like protein 1
ECAR	extracellular consumption rate
EHS	Engelbreth-Holm-Swarm
ER	endoplasmic reticulum
ETC	electron transport chain
FCCP	carbonyl cyanide-4-(trifluoromethoxy)phenylhydrazone
FCS	fetal calf serum
GABA	gamma-aminobutric-acid
GAL	galactose
GC(R)	gluccocortocoids (receptor)
GLS	glutaminase
GSH	glutathione
GTP	guanosintripophosphate
HAM-D	Hamilton Depression Scale
HD	Huntington's Disease
HPA axis	Hypothalamus-Pituitary-Adrenal axis
HTRA2	high-temperature requirement protein A2
IL	interleukin
IMM	inner mitochondrial membrane
iN	induced neuron
iPSC	induced pluripotent stem cell
IMS	Intermembrane space
KSS	Kearns Sayre Syndrome
LRRK2	leucine-rich-repeat kinase 2
MAM	mitochondria-associated membrane
MAOIs	monoamine oxidase inhibitors

MAPK	mitogen-activated protein kinase
MDD	Major Depressive Disorder
MELAS	Mitochondrial Encephalomyopathy-Lactic Acidosis and Stroke-like Episodes
MERF	myoclonic epilepsy and ragged red fibres
Mfn 1/2	Mitofusin 1/2
MILS	maternally inherited Leigh Syndrome
MMP	mitochondrial membrane potential
MnSOD	mitochondrial superoxide dismutase
MSRA	methionine sulfoxide reductase A
mt	mitochondrial
Mt-TL1	mitochondrially encoded tRNA leucine 1
N	non-treated
NMDA	<i>N</i> -Methyl-D-aspartic acid
NPC	neural progenitor cell
OCR	oxygen consumption rate
OMM	outer mitochondrial membrane
OPA1	optic atrophy 1
OXPHOS	oxidative phosphorylation
P	phosphate
PBMC	peripheral blood mononuclear cell
PBS	phosphate buffered saline
PD	Parkinson's Disease
PFA	paraformaldehyde
PGC-1 α	proliferator-activated receptor-coactivator 1- α
PINK	PTEN-induced kinase 1
PrimFibM	Primary Fibroblast Medium
PTEN	phosphatase and tensin homologue
RNA	ribonucleic acid
ROS	reactive oxygen species
RT-PCR	real-time poly chain reaction
SEM	standard error of the mean
SIRT	sirtuins
SMAC	second mitochondrial activator of caspases
SN	substantia nigra
SOD 1/2	Superoxide dismutase 1/2
SSRIs	selective serotonin reuptake inhibitors
SZ	Schizophrenia
TCA cycle	tricarboxylic acid cycle
TCAs	tricyclic antidepressants
TIM	translocase of the inner membrane
TNF	tumour necrosis factor
TNFR1	tumour necrosis factor receptor 1
TOM	translocase of the outer membrane
TRX-2	thioredoxin-2
TSPO	Translocator Protein 18 kDa
UCP	uncoupling protein
VDAC	voltage-gated anion channel

Abstract

Major Depressive Disorder (MDD) is a severe disease with almost 300 million people suffering worldwide (WHO 2019). By 2030, MDD is suggested to be identified as the global leading cause of disease burden. Only about 60% of patients react to a classical antidepressant (ADs) treatment and even if the subject is successfully treated and remission is achieved, the depressive disorder still imposes a considerable burden. Rarely, all of the symptoms disappear during remission and still depict an impairment to the patients' daily life (Lépine and Briley 2011). The treatment of symptoms cannot be the sole 'cure' for MDD, rather a treatment of the cause is needed. Yet, the cause of MDD cannot be broken down to one single mechanism or factor, it is rather a variety of malfunctions leading to the manifestation of MDD.

This study hypothesized the involvement of mitochondria and a bioenergetic imbalance for MDD patients. The mitochondrial respiration, the adenosine triphosphate (ATP) content, as well as the mitochondrial membrane potential (MMP) and the Ca^{2+} homeostasis were investigated in human cellular model. The mitochondria-related functions were assessed in somatic cells (human dermal fibroblasts) and neural progenitor cells (NPCs) derived from iPSCs of 16 MDD patients and 16 gender- and age-matched healthy control subjects.

Individuals with MDD showed significantly impaired mitochondrial functioning in fibroblasts under standard culturing conditions: basal and maximal respiration, spare respiratory capacity, non-mitochondrial respiration and ATP-related turnover is lower in Seahorse XFp Flux Analyzer respiratory measurements. Moreover, MDD fibroblasts harbor lower ATP levels determined by a bioluminescence assay. Measurements with the cationic dye JC-1 reveal a significantly more negative MMP in MDD fibroblasts, whereas the assessment of cytosolic Ca^{2+} with the ratiometric dye Fura-2 does not result in any significant differences.

Additionally, fibroblasts were exposed to metabolic stress (galactose, 7 days) and hormonal stress (dexamethasone, 7 days). After the exposure to stress, the differences in bioenergetics in MDD fibroblasts were widely abolished and fibroblasts of both groups showed an overall significantly increased metabolism.

In order to investigate the bioenergetics on a neuronal cellular level, the fibroblasts were episomally reprogrammed into iPSCs and differentiated into NPCs. Despite this process,

the mitochondria-related alterations discovered in MDD fibroblasts were also detectable in NPCs: A significantly lower basal and non-mitochondrial respiration and proton leak-related oxygen consumption were discovered in respiratory measurements. Whereas ATP levels did not exhibit any significant differences, MDD NPCs showed a significantly more positive MMP and a trend towards altered Ca^{2+} homeostasis could be shown. Similar to the observations in fibroblasts, the differences between MDD patients and controls are not present after the exposure to hormonal stress (dexamethasone, 7 days).

The results of the present study underpin the theory of a bioenergetic imbalance in MDD. It is likely that a mitochondrial dysfunction contributes to the pathophysiology of MDD and suggests that these alterations contribute to the biomolecular manifestation of depressive symptoms.

Those differences in electron transport chain (ETC) function and the altered mitochondria-related properties depict a basis for further investigations of disease-causing mechanisms. Furthermore, it might open new ways to gain insight into ADs-acting pathways, which could demonstrate a promising tool for new therapeutical approaches.

Zusammenfassung

Die Unipolare Depression, mit weltweit mehr als 300 Millionen Betroffenen, ist eine schwerwiegende Krankheit (WHO 2019). Es wird prognostiziert, dass die Unipolare Depression bis zum Jahr 2030 die weltweit führende Krankheitsbelastung darstellt. Auf eine Behandlung mit klassischen Antidepressiva sprechen nur in etwa 60% der Patienten an und selbst wenn eine Remission erreicht wird, erlegt die Depression den Betroffenen noch immer eine Last auf. Selten sind die Patienten während der Remission symptomfrei und leiden unter den damit einhergehenden täglichen Einschränkungen (Lépine und Briley 2001). Die alleinige Behandlung der Symptome kann nicht die „Heilung“ der Depression sein - vielmehr wird eine Behandlung der Ursache benötigt. Der Grund für die Entstehung einer Depression kann jedoch nicht an einem einzigen Mechanismus oder Faktor festgemacht werden. Es ist eher eine Vielzahl an Fehlfunktionen, welche schlussendlich zur Manifestation einer Depression führen.

Im Zuge dieser Studie wird eine Beteiligung der Mitochondrien als einer dieser Faktoren vermutet und es wird angenommen, dass ein bioenergetisches Ungleichgewicht in depressiven Patienten vorliegt. In einem humanen Zellmodell werden die mitochondriale Respiration, der Gehalt an Adenosin-Triphosphat (ATP), wie auch das mitochondriale Membranpotential (MMP) und der Ca^{2+} -Haushalt untersucht. Diese mit Mitochondrien assoziierten Funktionen werden in somatischen Zellen (humanen dermalen Fibroblasten) und neuronalen Vorläuferzellen von 16 depressiven Patienten und 16 alters- und geschlechtsangepassten gesunden Kontrollen betrachtet.

Die Fibroblasten von Personen mit einer Unipolaren Depression zeigen signifikant eingeschränkte mitochondriale Funktionen unter Standard-Kulturbedingungen: Basale und maximale Respiration, respiratorische Reservekapazität, nicht-mitochondriale Respiration und die ATP-produktionsabhängige Atmung sind verringert in Seahorse XFp Flux Analyzer Messungen. Außerdem besitzen Fibroblasten von Patienten einen niedrigeren ATP Gehalt, welcher mit Hilfe eines Biolumineszenz Assays bestimmt wurde. Messungen mit dem kationischen Farbstoff JC-1 resultieren in einem signifikant negativeren MMP in Patientenfibroblasten, wohingegen keine signifikanten Unterschiede in den Messungen des zytosolischen Ca^{2+} mittels des ratiometrischen Farbstoffes Fura-2 festgestellt werden können.

Zudem wurden die Fibroblasten eine Woche lang metabolischem Stress in Form von Galaktose und hormonellem Stress durch die Zugabe des synthetischen Glukokortikoids Dexamethason ausgesetzt. Durch die Anwendung dieser Stressprotokolle wurden die bioenergetischen Unterschiede in den Patientenfibroblasten weitestgehend aufgehoben und Patienten- als auch Kontrollfibroblasten zeigen generell eine gesteigerte metabolische Aktivität.

Um die Bioenergetik auf einem neuronalen Zellelevel zu untersuchen, wurden die Fibroblasten zu induzierten pluripotenten Stammzellen reprogrammiert und zu neuronalen Vorläuferzellen differenziert. Trotz dieses Prozesses können die Veränderungen in der Mitochondrienfunktion, welche vor der Reprogrammierung in den Patientenfibroblasten gemessen wurden, auch in den neuronalen Vorläuferzellen nachgewiesen werden: Eine signifikant verringerte basale und nicht-mitochondriale Atmung wurden in Respirationsexperimenten ermittelt. Obgleich der ATP-Gehalt der neuronalen Vorläuferzellen sich zwischen Patienten und Kontrollen nicht unterscheidet, konnte ein signifikant verringertes MMP und ein Trend zu einer veränderten Ca^{2+} -Homöostase gezeigt werden. Ähnlich den Beobachtungen in Fibroblasten, sind die Unterschiede in Patienten und Kontrollen auch bei neuronalen Vorläuferzellen nach hormonellem Stress (Dexamethason, 7 Tage) nicht mehr vorhanden.

Die Ergebnisse dieser Studie untermauern die Theorie eines bioenergetischen Ungleichgewichts bei einer Unipolaren Depression. Es ist sehr wahrscheinlich, dass eine mitochondriale Dysfunktion zur Pathophysiologie der Unipolaren Depression beiträgt und es gibt Hinweise, dass diese Veränderungen einen Einfluss auf die biomolekulare Manifestation der depressiven Symptome haben.

Die veränderte Funktion der Elektronentransportkette und die abweichenden Eigenschaften bezüglich der Mitochondrien legen einen Grundstein für weitere Untersuchungen von Mechanismen, welche Depressionen verursachen. Des Weiteren könnten diese Entdeckungen neue Wege und Möglichkeiten bieten, einen Einblick in Wirkmechanismen von Antidepressiva zu gewinnen, welche wiederum eine vielversprechende neue Methode darstellen neue therapeutische Ansätze zu eröffnen.

1 Introduction

1.1 Mitochondria – the vital force in our cells

1.1.1 Mitochondria structure and the site of action

The human body harbors trillions of mitochondria. For a eukaryotic cell's function mitochondria are vital. Hundreds to thousands of small bacteria-sized (0.5-1 μM) mitochondria ensure the cell's energy supply. The number of mitochondria varies among cell type, tissue and organ, depending on the energetic needs. Muscle and cardiac cells, neurons and liver cells, for instance, contain up to 2,000 mitochondria, whereas red blood cells do not have them at all. However, mitochondria do not only vary in number, but also in size and shape. Mitochondria have – among many others – one key function: the provision of the cell with energy in form of ATP, which is pivotal for the maintenance of the cell's proper function and survival. To fulfill this crucial task, mitochondria have a special structure: They are double-membraned, with an outer (OMM) and an inner membrane (IMM), an intermembrane space (IMS), cristae and the matrix (Alberts et al. 2002).

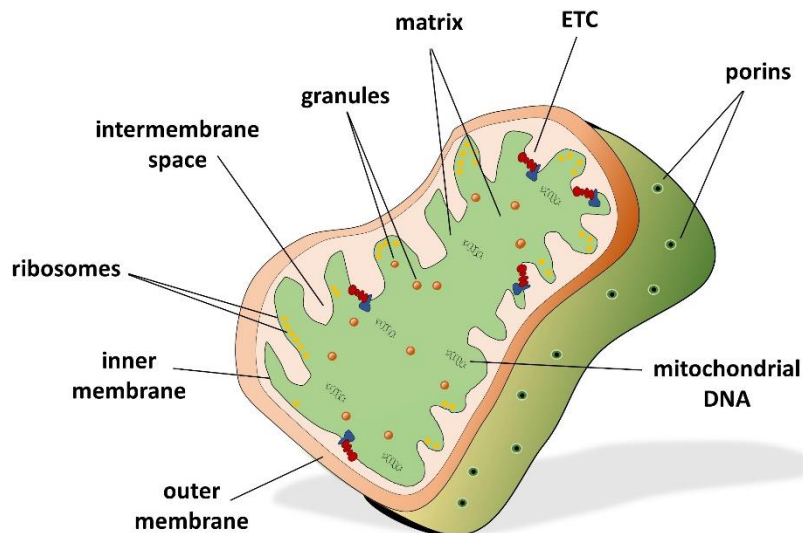


Figure 1 The organization of the mitochondrion. The outer membrane encloses the inner membrane possessing cristae, where the ETC machinery is located. The matrix of the mitochondrion contains granules, ribosomes and the mtDNA.

The mitochondrion is enclosed by OMM that is equipped with porins for the exchange of metabolites. Between the OMM and the IMM is the IMS. The smooth OMM, consisting of a lipid-double layer, has numerous embedded proteins. Large integral proteins called porins form the connection between the cell's cytosol and the IMS. Those porins are the major junction to the cells' surrounding and they are responsible for the transport of nucleotides, ions and metabolites (Alberts et al. 2002). One of these important gateways from outside to the IMS of mitochondria is the voltage-gated anion channel (VDAC) that extends over the OMM. VDAC is described as a large aqueous pathway from a single 30 kDa protein; a channel, that does not only have the purpose of the exchange of small hydrophilic molecules across the OMM. VDAC displays multi-faceted features and is able to form complexes with proteins and enzymes and responds to the protein concentration of the cytoplasm (Colombini 2004). Hence, VDAC, in association with the Translocator Protein 18 kDa (TSPO), for example, depicts a noteworthy equipment of the OMM setup and therefore the entire mitochondrial structure (Shoshan-Barmatz, Pittala, and Mizrachi 2019).

Enzymes and proteins also run through the IMM. The TOM complex in the OMM and the TIM complex situated in the IMM are multimeric protein assemblies which enable protein transport across the double membrane. Most importantly, the proteins of the ETC are embedded into the IMM. To extend the membrane and enlarge its surface, the IMM has cristae. The cristae are foldings of the IMM and just like the number, size and shape of the mitochondria itself, they differ widely along cell types. Muscle cells and neurons, for instance – cells types that require a high energetic demand - show large cristae in order to gain some extra space for the machinery of oxidative phosphorylation (OXPHOS): the process which creates chemical energy (Alberts et al. 2002).

The matrix contains the mitochondrial DNA (mtDNA). The mtDNA is a small, circular and multi-copy genome. It includes 37 mitochondrial genes whereof 13 mt genes are coding for essential components of the mitochondrial ETC and the ATP synthase. Each mitochondrion can contain 2–10 copies of mtDNA (Robin and Wong 1988).

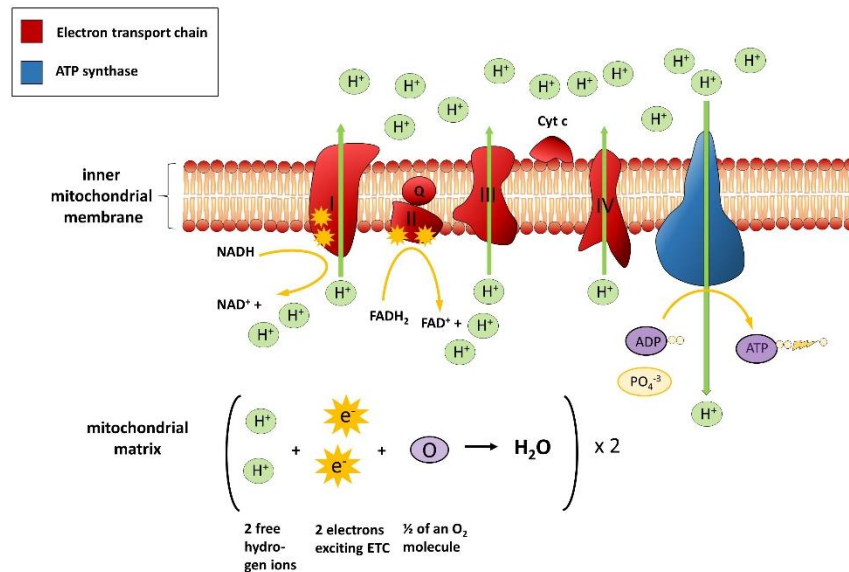


Figure 2 The ETC and the mechanism of OXPHOS in mitochondria. Through the transfer of electrons at the Complexes I-IV of the respiratory chain the reduction equivalents and the pumping of protons from the mitochondrial matrix the mitochondrial membrane potential is built up. This electrochemical gradient drives the ATP synthase that converts ADP and inorganic phosphate the cell's most valuable energy carrier ATP.

The respiratory chain is the “site of action” and through OXPHOS the final products of the tricarboxylic acid (TCA) cycle and glycolysis are metabolized. Via OXPHOS basically the metabolism of sugars is completed and the mitochondrion fulfills its major function in the cell: the energy supply in form of ATP. In the respiratory chain, the reduction equivalents NADH and FADH₂ derived from the TCA cycle are oxidized through serial redox reactions. Besides H₂O and CO₂, 36 molecules of ATP are synthesized. The respiratory chain is built up of four protein complexes and the ATP synthase located at the IMM. At Complex I (NADH Ubiquinone-Oxidoreductase) two electrons are transferred from NADH/H⁺ to ubiquinone. Two further electrons are transferred from FADH₂ to ubiquinone at Complex II, called the Succinate-Ubiquinone-Oxidoreductase. At the third Complex (Ubiquinone-Cytochrome-c-Oxidoreductase) two molecules of Cytochrome c (Cyt c) are reduced by the transfer of two electrons from ubiquinol. Finally, at Complex IV (Cyt c-Oxidase), Cyt c is reoxidized under the reduction of O₂ to H₂O. Besides the transport of electrons along the reduction equivalents, protons are pumped from the matrix of the mitochondrion into the IMS. Therefore, an electrochemical gradient is built up over the IMM. This proton motive force drives the ATP synthase and enables the generation of ATP from ADP+P_i (Alberts et al. 2002).

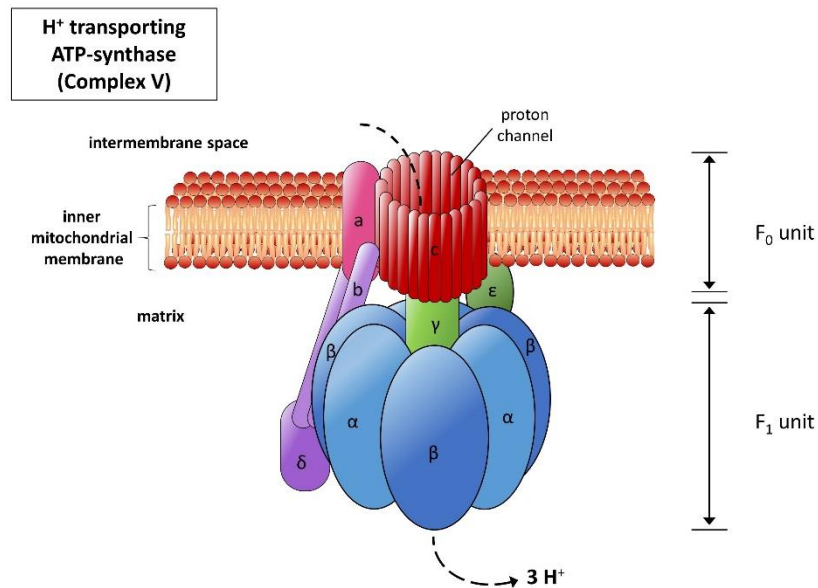


Figure 3 The ATP synthase. The ATP synthase is located at the IMM and consists of two subunits, which are in turn built up of several subunits. The hydrophobic F₀ (consisting of a, b, c) is situated in the membrane and forms a proton channel: it converts the flux of the protons through the membrane into a rotation, with whose help the ATP synthase is driven. The hydrophilic F₁-subunit (put together by the alpha, beta, gamma, delta and epsilon unit), sticks out of the IMM into the matrix, where from ADP and P_i ATP are synthesized. The OSCP-subunit also belongs to the F₁-complex and plays an important role when it comes to stabilization of the F₁-subunit against the rotation of the F₀-subunit.

1.1.2 Mitochondria in the cellular metabolism

The mitochondrion's key function, the OXPHOS, cannot be seen as a separate mechanism, independently passing off in the mitochondrion. Mitochondria are involved in a network of metabolic pathways and the products of these important metabolic pathways are transformed into energy and eventually, mitochondria are the organelles keeping the cell alive. Metabolites from lipid degradation, glycolysis and the TCA cycle convert in the mitochondrion.

Oxidative metabolism of both glucose and free fatty acids result in the generation of the key metabolite Acetyl-CoA. During the oxidation of one molecule glucose into two molecules pyruvate, net 2 ATP and 2 NADH are generated. Pyruvate is converted by enzyme complex pyruvate dehydrogenase into two molecules of Acetyl-CoA, which is trafficked from the cytosol into the mitochondrion. During β -oxidation fatty acids are broken down in a four-step reaction: The β -carbon is oxidized to ketone followed by the cleavage of the α - and the β -carbon which yields after all one molecule Acetyl-CoA and the reduction equivalents NADH and FADH₂. In the TCA cycle, Acetyl-CoA is oxidized in an eight steps process in the mitochondrial matrix outside the cristae. Each molecule of Acetyl-CoA yields 3 molecules of NADH and one molecule of FADH₂. These reduced

nucleotide coenzymes subsequently transfer electrons to molecular oxygen via the ETC and ATP is generated from ADP and inorganic phosphate (Alberts et al. 2002). Mitochondria are the main source of endogenously produced reactive oxygen species (ROS). ROS are a byproduct of OXPHOS which is produced by the ETC through the reduction of O_2 to superoxide. In order to prevent oxidative stress by overwhelming amounts of ROS, cells harbor an antioxidative defense (Roma et al. 2017). The mitochondrial enzymes superoxide dismutase (SOD) and thioredoxin-2 (TRX2) scavenge free radicals and strive for an equilibrium in the cell. Another endogenous antioxidant system with mitochondrial involvement is the glutathione (GSH) peroxidase system (Tanaka et al. 2002).

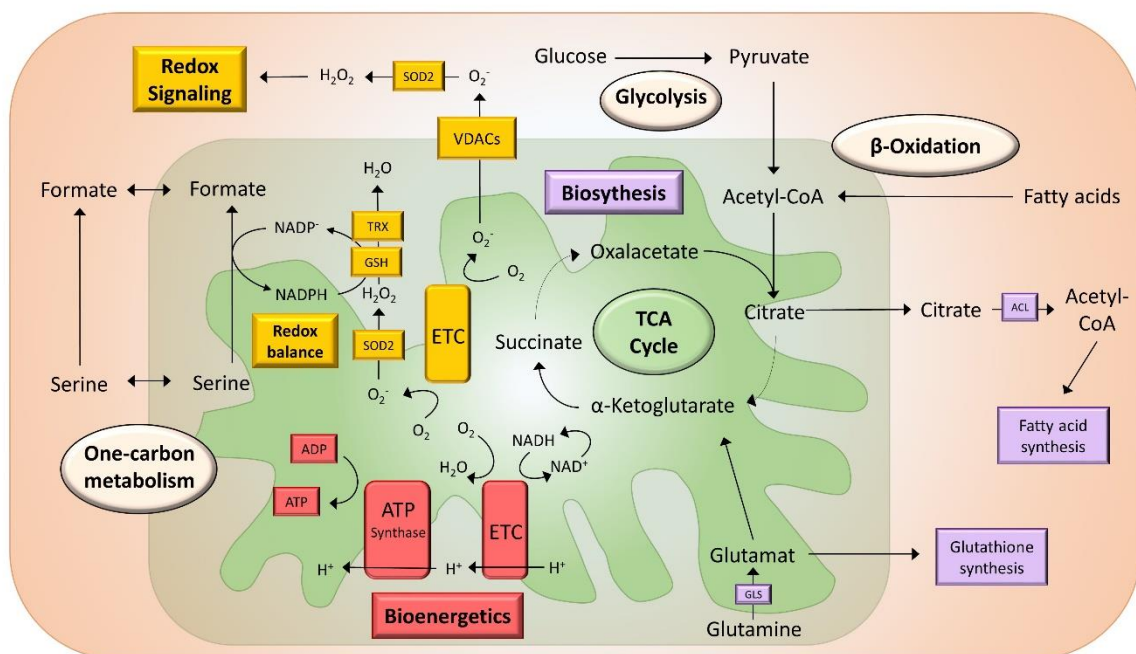


Figure 4 Mitochondria in the cellular metabolism. Mitochondria are involved in crucial cellular functions including biosynthesis as well as degradation of metabolites, bioenergetics and energy supply and balance and signaling of ROS. The key processes – glycolysis, β-oxidation of fatty acids, the TCA cycle and one-carbon metabolism – in the cell and in the mitochondrion and their interplay are depicted.

However, ROS is necessary for the cell and its production is imperative for redox homeostasis. Balanced ROS levels are vital for the cell's homeostasis. ROS signalling is not only part of the immune system, but it also mediates cell proliferation and apoptotic pathways to ensure proper regulation of the cell cycle and programmed cell death (Roma et al. 2017). Ca^{2+} homeostasis is the second key player in cell survival and apoptosis. Ca^{2+} as second messenger molecule mediates intracellular signalling cascades as well as cell-

cell-signalling (Clapham 2007). Mitochondria regulate cytosolic Ca^{2+} levels and consequently Ca^{2+} -mediated signalling. Mitochondrial Ca^{2+} levels are crucial for the rate of OXPHOS. Uncoupling proteins 1, 2 and 3 (UCP1, UCP2, UCP3) are embedded in the IMM and belong to the superfamily of mitochondrial ion transporters (Ricquier and Bouillaud 2000). UCP1 accounts for heat production by inducing a H^+ leak that uncouples OXPHOS, whereas UCP2 and UCP3 contribute to many cellular processes including mitochondrial free-radical production, apoptosis, hormone secretion and they are implicated in glucose and fatty acid metabolism (Dejean et al. 2004; Harper et al. 2002; Krauss et al. 2003; Mookerjee et al. 2010). Most importantly, UCP2 and UCP3 were shown to be fundamental for mitochondrial Ca^{2+} transport (Graier, Trenker, and Malli 2014).

Besides those transport systems, Ca^{2+} signalling and buffering is accomplished by interfaces of the mitochondria and the endoplasmic reticulum (ER) and are entitled mitochondria-associated ER membranes (MAMs). Proteins in MAM either are involved in physical connection between ER and mitochondria or modify the tethering complexes in MAMs. Mitofusin 1/2 (Mfn1/2), a mitochondrial fusion GTPase, which situated to the OMM, is part of the MAM complex. MFN1/2 plays a role in mitochondrial fusion and together with OPA1, another mitochondrial fusion GTPase, which located at the IMM, regulates the merging of mitochondria (De Brito and Scorrano 2008; Cipolat et al. 2004; Detmer and Chan 2007).

1.1.3 Fission and fusion: a dynamic network

Mitochondria are highly dynamic organelles and change their shapes and distribution constantly. Mitochondria's shapes range from small vesicles, short rods and reticular networks spanning the entire cell. Their rapid changes in shape and location, allow mitochondria a fast adaptation to energetic needs and they are essential to mitochondrial health, wherefore damaged organelles or precipitates are restored and removed. Mitochondrial fission and fusion events are balanced and have been identified as a critical process in mitochondrial morphology and function. As mentioned beforehand, and most importantly, fission and fusion control the shape length and number of mitochondria. Additionally, the shape of mitochondria affects the ability of cells to distribute their mitochondria to specific subcellular locations. By continuous merger and division, the exchange of lipid membranes and intra-mitochondrial content is ensured (Charmandari, Tsigos, and Chrousos 2005; Gold et al. 2002; Kyrou, Chrousos, and Tsigos 2006; Detmer

and Chan 2007). Defects in fission and fusion come with severe diseases. Dysregulation of those two processes are associated with an energetic defect, giving the hint that mitochondrial structure and function are tightly related (Bertholet et al. 2016; Lee and Yoon 2016). Mfn1 and Mfn2 are responsible for OMM fusion, whereas OPA1 regulates the fusion of the IMM. Fission events in mammals are mediated by the dynamin-like protein 1 (drp1), which is predominantly a cytosolic protein (Meeusen et al. 2006; Yonashiro et al. 2009). Fibroblasts that lack both, Mfn1 and Mfn2, show reduced respiratory capacity and individual mitochondria show great heterogeneity in shape and membrane potential. Cells that lack OPA1 show similar defects, with an even greater reduction in respiratory capacity (Chen, Chomyn, and Chan 2005).

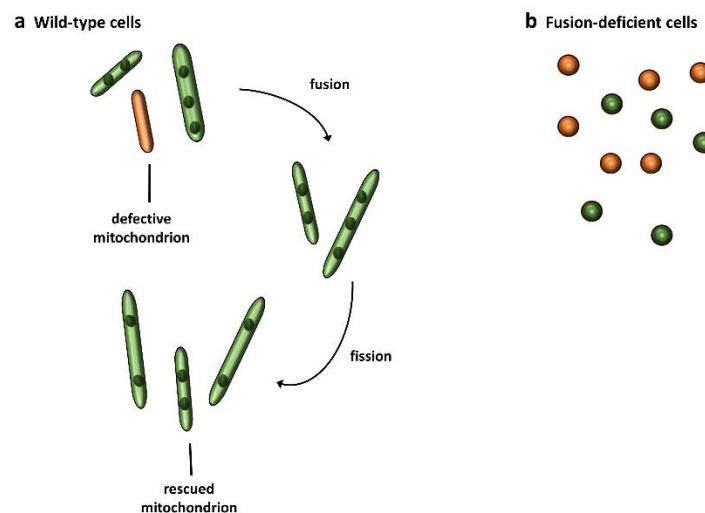


Figure 5 Fission and Fusion events. (a) Wild-type cells with intact mitochondrial dynamics. Functioning mitochondria are shown in green, whereas mitochondria with defects and lack of mtDNA are shown in orange. By fusion events the deficiencies in non-functional mitochondria can regain its function and mtDNA by fusing with a neighbouring mitochondrion. The fused mitochondrion then undergoes fission, with both daughter mitochondria receiving mtDNA nucleoids. (b) Cells with fusion-deficient properties. The mitochondria are fragmented since fission events are still happening. Cells lack mtDNA nucleoids accumulate because there is no pathway for defective mitochondria to regain mtDNA. Fusion-deficient cells can maintain mtDNA nucleoids, but such nucleoids serve a much smaller mitochondrial mass.

Hence, mitochondrial dynamics are extremely important for mitochondrial function. Mitochondria should not be seen as separate organelles but as a population of organelles with heterogeneous functions. Information and contents are being exchanged and deficient mitochondria can be rescued by others. A few mitochondria might be non-functional owing to the loss of essential components. However, this dysfunction is transient, since mitochondrial fusion provides a pathway for these defective

mitochondria to regain essential components (figure 5). An essential prerequisite for proper mitochondrial function is mitochondrial DNA (mtDNA) which is organized in nucleoids. The mtDNA genome encodes important subunits of the respiratory Complexes I, III and IV, and is therefore indispensable for OXPHOS. When mitochondrial fusion is abolished, a large fraction of the mitochondrial population loses mtDNA nucleoids (Chen, McCaffery, and Chan 2007). When mitochondria divide, most daughter cells inherit at least one mtDNA nucleoid. If this inheritance fails, fusion events compensate for that and the mtDNA is restored in the daughter cell. Since in cells with disturbed mitochondrial dynamics, the exchange of contents does not take place, the restoration of mtDNA nucleoids probably accounts for the heterogeneity in mitochondrial MMP and the reduced respiratory capacity. Cells with a lack of fusion capability, however, still harbour a significant number of mtDNA nucleoids. Due to fission events, the functional mitochondrial mass gets reduced. Furthermore, not only the mtDNA gets restored by mitochondrial fusion, but also other components like substrates, metabolites and specific lipids can be recovered in disturbed mitochondria (Detmer and Chan 2007). Concluding, the mitochondrial mass is strongly influenced by mitochondrial dynamics and might reflect the cell's health or disease state. The cellular mtDNA content is regulated by the nuclear DNA that encodes for in mtDNA replication, transcription, translation and repair. Molecular defects in the genes responsible for mtDNA biogenesis and therefore a reduction of mtDNA content. It is known that mtDNA depletion and a lack of the maintenance of mtDNA integrity can lead to a series of disorders. Those diseases include, for instance, Leigh-like encephalopathy with dystonia, deafness and lactic acidosis combined with encephalomyopathy, but also mitochondrial hepatoencephalopathy with hepatic and neurologic symptoms during infancy (Dimmock et al. 2008; Ostergaard et al. 2007; Sarzi et al. 2007; Wong et al. 2008).

Studies also reported alterations of the mitochondrial mass in mood disorders. MtDNA copy number is reduced in leucocytes of Schizophrenia (SZ) and Bipolar Disorder (BPD) patients and could be correlated to the severity of disease and the anti-psychotic treatment. They suggested a link between mitochondrial dysfunction and psychosis-like symptoms (Kumar et al. 2018). Decreased number of mtDNA in leucocytes was revealed for MDD (Kim et al. 2013). Decreased mtDNA copy numbers were also discovered with increasing duration of the Posttraumatic Stress Disorder (PTSD) symptoms, whereas the copy number is highest in the initial phase of PTSD (Bersani et al. 2016). Moreover, for patients with MDD, anxiety disorder or adjustment-disorder an increased mtDNA copy

numbers in peripheral blood is reported and it is positively correlated to the severity of disease (Karabatsiakos et al. 2014). It might be assumed that higher mtDNA copy numbers compensate for dysfunctional mitochondrial metabolism and the resulting energetic deficiencies (Wang et al. 2017).

1.2 Major Depressive Disorder – a multifactorial disease

1.2.1 Classification and diagnostics

Sadness, emptiness, hopelessness, a loss of interest and pleasure – MDD has many faces. The severe disease is of high heterogeneity and multifaceted in the clinical picture. Symptoms include changes in mood, cognition, interest, but also troubles in decision-making, anxiety, anhedonia, problems in volition and motivation and changes with respect to psycho-motility and energy. Furthermore, appetite and therefore weight and the circadian rhythm can be affected. According to *Diagnostic and Statistical Manual of Mental Disorders V (DSM V)* classification two out of three main symptoms - a depressed mood, anhedonia and the lack of drive and some of the side symptoms, respectively somatic symptoms include troubles in cognition, reduced self-esteem, feelings of guilt and/or hopelessness, changes in appetite, sleep disturbances and the expression of meaninglessness of life – so suicidal ideation – must be present for at least 2 weeks nearly every day. MDD is diagnosed based on physician-administered or patient self-administered interview and is still subjective since it depends on the individual clinical judgment (Bilello 2016; Young et al. 2016). MDD state is evaluated through a questionnaire that determines the severity of depression. The Hamilton Depression Scale (HAM-D) ranges from 0 (no depression) to 10-20 scores (mild depression) to 21-30 scores (medium severe depression). More than 30 points are considered as a severe MDD. Classification according to *ICD-10 Classification of Mental and Behavioral Disorders. Clinical Descriptions and Diagnostic guidelines (ICD-10)* provides the following categories:

- F32.0: Mild depressive episode: Two or three of the symptoms are present. The subject is generally impaired and is seeking for help, however he/she is still able to fulfill occupational and private routine.
- F32.1: Medium severe depressed episode: Usually four or more of the symptoms are present. The subject has severe troubles continuing daily routine.

- F32.2: Severe depressed episode without psychotic symptoms: Several of the symptoms are present to a torturous extent. Subjects typically exhibit a loss of self-esteem and worthlessness and affected persons utter suicidal thoughts and actions. Persons additionally suffer from somatic symptoms, e.g. agitation, sleep disturbances or loss of appetite or libido.
- F32.3: Severe depressed episode with psychotic symptoms: State of disease is described as F32.2, but additionally subjects suffer from hallucinations and delusional ideas, psychomotor inhibitions or stupor, so that daily social activities are impossible and persons are in danger of life due to suicide and a lack of imbibition and ingestion.
- 32.8: Other depressive episode.
- 32.9: Depressed episode, not specified.

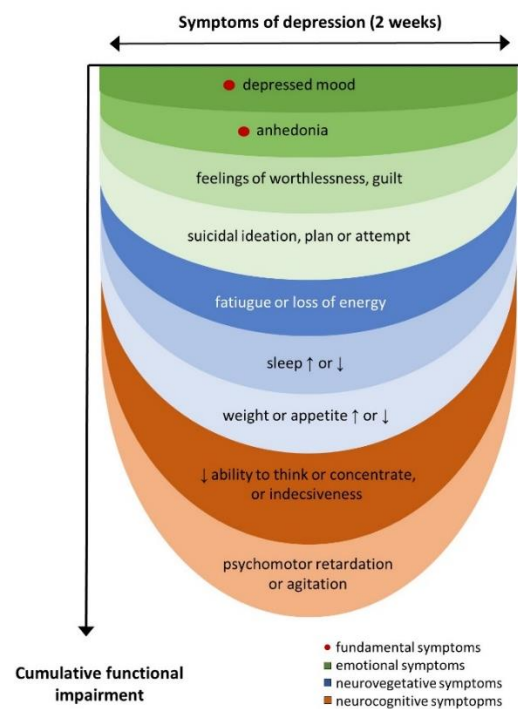


Figure 6 Symptoms of MDD and its increasing impact on daily performance. A combination of symptoms concerning emotional status, vegetative and cognitive function must be present over a period of 2 weeks. Increasing number of a combination of manifestations causes cumulative functional impairment. Main symptoms for depression are marked with a red dot. The color green indicates emotional symptoms, blue color stands for neurovegetative symptoms and orange depicts neurocognitive symptoms.

MDD has a severe impact on the affected persons. It is a disease with tremendous societal, economic and emotional burden and results in an impairment in social or occupational functioning and therefore impairs daily living (Kessler and Bromet 2013). MDD is

considered as a global burden with 1 to 17% of affected people in adults, 3 to 6% in adolescents, and 12 to 38% in elderly (Gururajan et al. 2016; Kessler and Bromet 2013; Rantamaki and Yalcin 2016). MDD is one of the leading causes of mental disability worldwide, with an estimated lifetime prevalence of up to 20–30% (Weissman et al. 1996). Moreover, women are affected more frequently than men (Kessler and Bromet 2013). MDD is highly comorbid with somatic diseases like diabetes, asthma and arthritis, but also with neurodegenerative disorders like Alzheimer's disease (AD), Parkinson's diseases (PD) and Huntington's disease (HD) (Kupfer, Frank, and Phillips 2012; Réus et al. 2016).

MDD is a multifactorial disease including, genetic and epigenetic factors, the exposure to stress or traumatic events and the interaction with other psychological or environmental factors and even personality itself plays a role in the manifestation of MDD (Rantamaki and Yalcin 2016; Schneider and Prvulovic 2013). It is assumed, that for MDD patients neuronal circuits are affected and neuronal connectivity is altered, leading to functional neuroanatomical modifications (Rantamaki and Yalcin 2016). From a molecular point of view, neurobiological, but also neuroendocrine, neurotrophins as well as oxidative stress and inflammatory processes contribute to the manifestation of MDD and several theories for the development of the disease merged the last decades.

1.2.2 Early and new theories for manifestation

The oldest hypothesis that is postulated with regard to the manifestation of MDD is the monoaminergic theory of depression. It claims that the underlying pathophysiologic basis for the manifestation of MDD is a lack of monoamines like serotonin, norepinephrine and/or dopamine in the synaptic cleft. Tricyclic antidepressants (TCAs) and selective serotonin reuptake inhibitors (SSRIs) are the most common treatments for the MDD (Bartl et al. 2014; Eisenhofer, Kopin, and Goldstein 2004). These medications elevate the level of neurotransmitters in the brain by either prolonging their presence in the synaptic cleft or blocking their presynaptic auto-receptors. Depressive symptoms are effectively reversed by monoamine oxidase inhibitors (MAOIs) and TCAs, however with a delayed onset. Drugs acting on the monoaminergic system usually need at least 2 to 8 weeks before a therapeutic effect can be observed and each drug is only efficient in around two third of MDD patients (Sonnenberg et al. 2008). Besides that, the observed discrepancy

between pharmacological and biochemical function of ADs and their clinical mood altering responses remains unclear (Leonard 2007).

Therefore, additional neurotransmitter systems came into play and newer theories postulate that monoamine deficiency cannot be the sole underlying reason for the development of depression. The neuroplasticity theory of depression includes other transmitters like Glutamate and γ -butyric acid (GABA), but also the Brain-Derived-Neurotrophic factor (BDNF). The glutamatergic system may be also implicated in MDD (Hashimoto 2009). Fast-acting drugs like Ketamine, which is an antagonist of the NMDA-receptor, revealed antidepressant effects (Dutta, McKie, and Deakin 2015). Moreover, it is likely that the glutamatergic system is involved in the manifestation of MDD, since increased glucocorticoid levels, which are released under conditions of chronic stress that associated with depression, lead to enhanced glutamatergic transmission, elevated NMDA receptor expression and increased extracellular glutamate levels (Lu et al. 2003). Glutamate and GABA are both involved in synaptic plasticity and various studies implicated GABA in the pathophysiology of depression (Krystal, Sanacora, and Duman 2013; Luscher, Shen, and Sahir 2011).

Synaptic plasticity is an important process in the brain including synaptogenesis, alterations in dendritic function, neurite extension, synaptic remodelling and modification of synaptic neurotransmissions. ADs treatment can – at least partly - reverse this disturbed plasticity which contributes to a pathological state (Pittenger and Duman 2008; Wood et al. 2004). The modulation of receptors for serotonin and noradrenaline through ADs treatment, different downstream pathways get activated that have a common function which is the regulation of gene expression, e.g. BDNF, which is crucial for the formation of neuronal networks (Yu and Chen 2011).

Numerous studies also suggest that inflammation may contribute to symptoms relevant to a number of psychiatric disorders and particularly depression. Inflammation and depression are linked and there is strong evidence that one goads the other, in the sense that inflammatory responses can lead to depression and depression can lead to inflammation. It is known that patients with inflammatory diseases are more likely to show greater rates of MDD. Moreover, patients with high inflammation have been shown to react poorly to conventional ADs therapies (Felger 2018). A large number of people with MDD show elevated peripheral inflammatory biomarkers, even in the absence of a medical illness. Several studies have reported increased circulating inflammatory cytokines, such as interleukin (IL)-1, IL-6, and tumor necrosis factor (TNF), their soluble

receptors, and acute phase reactants, like C-reactive protein (CRP), in patients with MDD (Maes 1999; Maes et al. 1992; Sluzewska 1999). And coming back to neurogenesis and alterations in brain signaling pattern, inflammatory mediators have been found to alter glutamate and monoamine neurotransmission as well as glucocorticoid receptor (GR) resistance (Amodeo, Allegra Trusso, and Fagiolini 2018).

A dysfunction of GRs, elevated levels of glucocorticoid hormones and the accompanied disturbed feedback mechanism of the hypothalamus-pituitary-adrenal (HPA) axis is strongly associated with MDD (Vreeburg et al. 2009). ADs act on the upregulation of the HPA axis and moderate the hyperactivity by ameliorating many of the neurobiological disturbances in depression and relief depressive symptoms (Anacker et al. 2001).

1.3 The risk factor stress - impact on mitochondria and mood

1.3.1 The stress response in the human body

The human stress response is a homeostatic mechanism that provides a better chance of survival when the body is under threat. It mobilizes neural and hormonal networks to optimize cognitive, cardiovascular, immunological and metabolic function.

The HPA axis is the key pathway in the human stress response and reacts immediately to a real or perceived stressor. It is the central mediator of the “fight or flight” reaction.

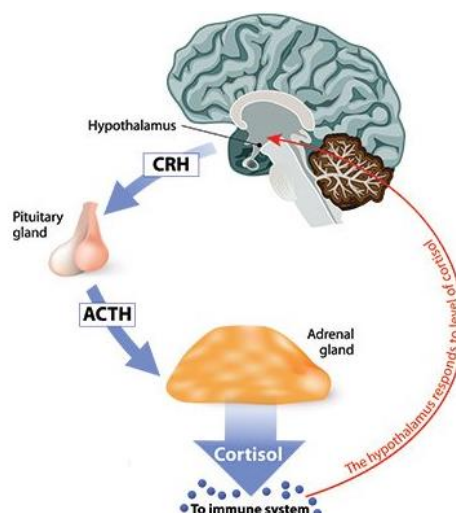


Figure 7 The Hypothalamic-Pituitary-Adrenal Axis. An internal or external stressor induced the releases of CRH from the hypothalamus which causes a release of ACTH from the pituitary gland. ACTH acts on the adrenal glands and elevated levels of Cortisol follows. Cortisol action is regulated by a negative feedback mechanism on the hypothalamus. Source: <https://images.agoramedia.com/everydayhealth/gcms/What-Is-Cortisol-722x406.jpg>

The HPA axis is a complex combination of organs and transmitters with a feedback mechanism. Internal, e.g. the circadian rhythm, and external signals, like stress, trigger the hypothalamic release of corticotropin releasing hormone (CRH), which acts on the anterior pituitary, which in turn stimulates the synthesis and secretion of adrenocorticotrophic hormone (ACTH) in the pituitary gland. ACTH then acts on the adrenal cortex to stimulate the production and secretion of Cortisol, a glucocorticoid (GC). The GCs that are released, mediate through GRs which are expressed throughout the entire body and trigger negative feedback mechanism by also targeting the hypothalamus and anterior pituitary. The production and release of CRH and ACTH are inhibited and thereby limit both, the intensity and duration, of the GC increase (Oakley and Cidlowski 2013). Hence, the stress response is crucial for our homeostasis and survival and comes along with beneficial adaptations on a cellular and molecular level.

1.3.2 Benefits of acute stress

Not just the release of CRH, ACTH and GCs are typical for the stress response, but also the release of catecholamines, adrenaline and noradrenaline, as well as pro-inflammatory factors TNF- α , IL-1 and IL-6. Altogether, the secreted substances ensure the fast response that includes effective blood supply in the brain, the cardiac muscle and the skeletal muscle. Furthermore, the energy production is enhanced by recruiting substrates like glucose, fatty acids and amino acids from storages. Besides that, the optimal ATP availability to vital tissues is orchestrated (Charmandari, Tsigos, and Chrousos 2005). Mitochondria are the pivotal organelle when it comes to biosynthetic activities and the supply of energy. Together with their involvement in Ca²⁺ metabolism, signaling, the regulation of thermogenesis and the generation of ROS, as well as the decision makers over cell survival or apoptosis, they are the first organelles to react to stressors (Klinedinst and Regenold 2014). Oxygen consumption and total energy expenditure are increased during the initial phase of the acute stress. Several signalling pathways are activated to meet energy demands during stress situations. Firstly, a higher number of mitochondria are recruited and they increase their volume. The expression and the activity of OXPHOS units are enhanced and the uncoupling of the respiratory chain and consequently energy in the form of heat is released. Besides that, the ROS level is regulated which is in turn important for signalling and defence and finally, an apoptotic

cascade is triggered, depending on the nature of the stressor (Goldenthal and Marin-Garcia 2004).

Mitochondrial function is affected and enhanced through GR action. GRs are expressed in mitochondria in several cell types (Demonacos et al. 1995). There is evidence that short-term exposure to stress and the concentration of GCs is associated with induction of mitochondrial biogenesis and enzymatic activity of the ETC units. For instance, by acute exposure of skeletal muscles to the synthetic GC dexamethasone, the transcription primarily of nuclear genes, but also mtDNA-encoded genes, affecting mitochondrial function and biogenesis, are initiated (Mikes et al. 2002). Mitochondrial biogenesis and OXPHOS and consequently adaptive thermogenesis in adipose tissue as well as in the skeletal muscle are stimulated by the catecholamines that are released. In brown adipose tissue energy saved from OXPHOS of substrates is dissipated as heat instead of the storage in form of ATP: this process is denominated as 'uncoupling'. The process of uncoupling is beneficial for the cell, as it attenuates mitochondrial ROS production and protects against cellular damage (Brand and Esteves 2005). Another signalling pathway that is activated during acute stress is the peroxisome proliferator-activated receptor-coactivator 1- α (PGC-1 α) signalling pathway. Cytokines, such as TNF- α , IL-1, which are immediately released, trigger the transcriptional activity of PGC 1- α via direct phosphorylation and activation the mitogen-activated protein kinase (MAPK) pathway. This results in stabilization and activation of PGC-1 α protein, which is the master regulator of mitochondrial biogenesis. PGC 1- α switches on gene expression that drives mitochondrial biogenesis and OXPHOS, again directing the metabolism towards mitochondrial uncoupling and energy expenditure (Michael et al. 2001; Wu et al. 2006).

Taken together, the acute effects of stress on the human body and the downstream effects are beneficial and necessary for the reaction to a stressor in general. But what happens when the perceived or actual stressor is persistent and the human body is steadily exposed to stress?

1.3.3 Sustained stress and its deleterious consequences

Chronic exposure to stress results in reversal of the beneficial effects. The long-term cortisol exposure becomes maladaptive, which can lead to a broad range of problems including the metabolic syndrome, obesity, cancer, mental health disorders, cardiovascular disease and increased susceptibility to infections (Björntorp and Rosmond 2000; Pufall 2015a; Steckler, Holsboer, and Reul 1999; Strüber, Strüber, and Roth 2014a).

However, starting with the initial process leading to these serious diseases: the activation of the HPA axis and the release of GCs, adrenaline and cytokines. Prolonged exposure to GCs causes respiratory chain dysfunction, increased ROS generation, mitochondrial structural abnormalities, apoptosis and cell death. Even if the release of GC is crucial and necessary in a stressed state, an overload of cortisol – regardless if naturally secreted or synthetic GCs administered through pharmacological treatments – is associated with various serious diseases (Charmandari, Tsigos, and Chrousos 2005; Chrousos 2000; Gold et al. 2002; Kyrou, Chrousos, and Tsigos 2006). The beneficial PGC1- α signalling, which is necessary for mitochondrial biogenesis, can become maladaptive and is detrimental to the cell in response to persistent stressors. PGC-1 α overexpression for instance, caused hepatic insulin resistance, manifested by higher glucose production and diminished insulin suppression of gluconeogenesis (Liang et al. 2009). Another study was able to show, also in a murine model, that the overexpression of PGC1- α leads to cardiomyopathy (Russell et al. 2004). Abnormally increased mitochondrial biogenesis leads to an elevated level of ROS. Increased oxidative damage in form of elevated levels of stress markers and genetic modification, namely telomere shortening, was revealed in children of mother with chronic psychological stress (Epel et al. 2004). In this context, especially the NF- κ B pathway is highly sensitive to changes in the intracellular redox environment and thus can be activated by oxidative stress. Mitochondrial gene expression can be negatively regulated in response to cellular TNF- α stimulation (Cogswell et al. 2003). Moreover, exceeded TNF- α release induces apoptosis in several cell types. TNF- α mediated apoptosis requires binding of the cytokine to its receptor TNFR1. This triggers a downstream activation of caspase 8 increasing Cyt c release which is followed by a loss of the MMP and the induction of apoptosis (Micheau and Tschopp 2003). Moreover, mtDNA is sensitive to oxidative damage. Mutations in the mtDNA can lead to altered transcription and expression of the ETC enzymes, which causes pathologic changes of mitochondrial function (Shokolenko et al. 2009).

It is known that chronic stress alters ingestion behavior. Nutrient overload and a carbohydrate- and lipid-rich diet leads to an excess of GC and is associated with abdominal obesity. It is very likely that overweight is accompanied by the development of diseases affecting metabolism, e.g. metabolic syndrome, type-2 diabetes and cardiovascular disease (Krempler et al. 2002; Patti et al. 2003). Disruptions of the OXPHOS and mtDNA abnormalities cause changes in PGC 1- α expression and UCP2. PGC 1- α and UCP2 play a

crucial role in proton leak and thermogenesis and they are linked diabetes and the metabolic syndrome (Brand and Esteves 2005).

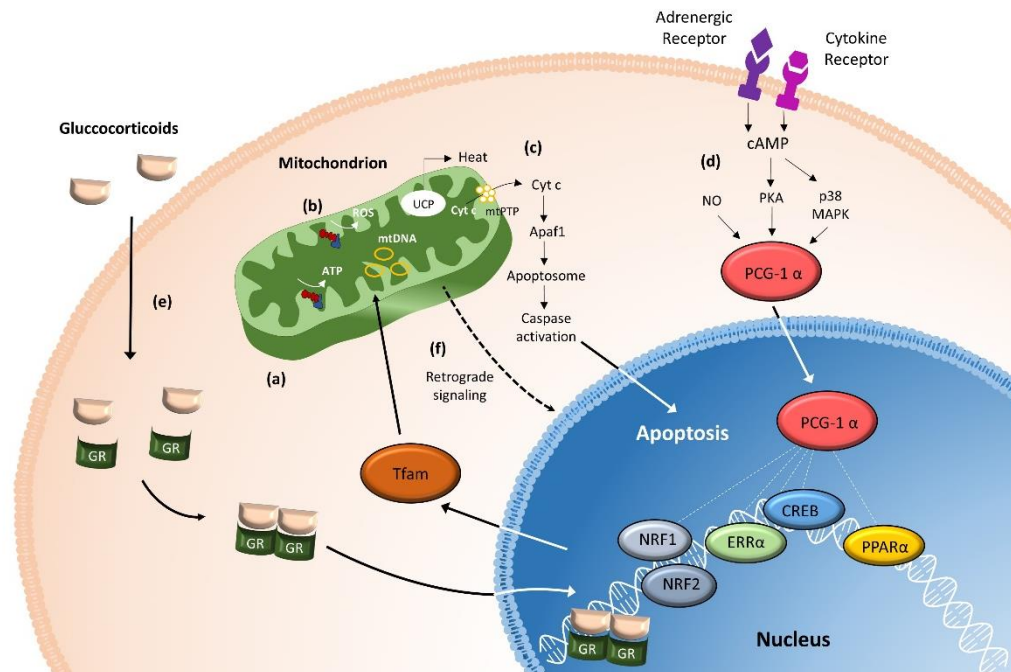


Figure 8 Mitochondrial functions in the stress response. This figure summarizes important mitochondrial functions including (a) the energy production through OXPHOS, (b) the generation of ROS and (c) the induction of apoptosis by opening of the mitochondrial permeability transition pore (mtPTP). By the release of Cyt c and the activation of Apaf1, the Apoptosome is triggered downstream and caspase activation follows. Alongside, the mitochondrion's most important signaling pathways are shown. (d) By adrenergic receptor activation, cAMP and PKA are activated. By cytokine receptor activation, the p38 MAPK pathway is triggered, which in results an activation of the major upstream regulator of mitochondrial function-related gene expression, the PGC-1 α . Exposure to stressors, such as cold temperature, fasting, exercise, cachexia or chronic infection activates PGC-1 α . (e) The release of GC during the stress response nuclear and mitochondrial genes regulating mitochondrial biogenesis and function are activated and the GRs can enter the mitochondrion and regulate mtDNA transcription. (f) A 'mitochondria-specific stress response' takes place by a retrograde signalling from the mitochondrion to the nucleus.

Elevated diurnal GC levels are a characteristic for depressed subjects and they remain high even after remission from a depressed episode (Beluche et al. 2009; Belvederi Murri et al. 2014). A constant state of stress in form of high cortisol levels constitutes one important neurobiological characteristic of depression (Stetler and Miller 2011). Chronic stress, which is defined as stress ongoing for more than 12 months, is a stronger predictor of depressive symptoms than acute stressors (Hammen 2005). There is clear evidence, that the severity and number of negative, stressful events increases the probability for an onset of a depressed phase (Kendler, Karkowski, and Prescott 1998). Resuming the facts of persisting stress, the long-term elevation of cortisol and its molecular downstream

effects as one of the biggest risk factors for the manifestation of MDD, a fundamental role of dysfunctional mitochondria and their pathogenic impact is reasonable.

1.4 Mitochondria and disease – what we know so far

1.4.1 Mitochondriopathies

Primary and secondary mitochondriopathies are described as clinical, biochemical and genetic diseases. The disorders are caused either by mutations of the maternally inherited mitochondrial genome or nuclear DNA mutations. The clinical manifestation of a mitochondriopathy is in the first place not dependent on the localisation of the mutation or the cell type, organ or the affected person, but rather on the distribution across cell types and the extent of the mtDNA mutations. Besides the genetic variation of the mtDNA itself, epigenetic factors contribute to the clinical picture (Finsterer 2004). Mitochondriopathies can be distinguished according to different aspects. Firstly, primary and secondary mitochondriopathies are differentiated. Primary mitochondriopathies include mutations in the mtDNA or the nDNA, or in both. A secondary mitochondriopathy is defined by a normal mitochondrial DNA, however the mitochondria are structurally modified. Secondary mitochondriopathies prevail along muscle dystrophies, glycogenosis or myositis. The biochemical defect is another aspect. Myopathies can be considered and categorized according to the molecular changes: defects in the respiratory enzymes, respectively substrate transporters or protein shuttles, alterations in the β -oxidation or pyruvate oxidation or the citrate cycle (Morgan-Hughes 1996). Alternatively, it can be distinguished among the clinical symptoms. Those symptoms are of high variety and range from muscle dystrophies, ophthalmoplegia and vision loss, to metabolic diseases like diabetes. Epilepsy and physical or mental retardation are typical for mitochondriopathies, too (Walker and Collins 1996). Clinically classified mitochondrial symptoms are for example Chronic Progressive External Ophthalmoplegia (CPEO), Kearns Sayre Syndrom (KSS), Mitochondrial Encephalomyopathy- Lactic Acidosis and Stroke-like Episodes (MELAS), myoclonic epilepsy and ragged red fibres (MERRF) or maternally inherited Leigh Syndrome (MILS). It is known, that people primarily diagnosed with a mitochondriopathy, show comorbidities with psychiatric disorders. A high comorbidity of mitochondrial MELAS in SZ and bipolar affective disorder has also been documented (Oexle and Zwirner 1997; Prayson and Wang 1998; Siciliano et al. 2003). Moreover, an acute confused state and SZ-like hallucination syndrome are sometimes observed in

patients with MELAS. Cases of mitochondrial encephalopathies presenting MDD or BPD have also been reported (Kato and Kato 2000).

1.4.2 Mitochondrial disruption in neurodegenerative diseases

Mitochondrial dysfunction and abnormalities have been reported in several neurological disorders. Typical neurodegenerative disorder with mitochondrial involvement are Alzheimer's disease (AD), Parkinson's disease (PD), Amyotrophic Lateral Sclerosis (ALS) or Huntington's disease (HD). The most common cause for these illnesses is mitochondrial ageing and as a consequence thereof, an accumulation of mtDNA mutations and the net production of ROS. Throughout lifespan, increasing number of large scale deletions and point mutations are acquired (Corral-Debrinski et al. 1992). Several IS proteins including Cyt c, second mitochondrial activator of caspases (SMAC) and high-temperature requirement protein A2 (HTRA2) have pro-apoptotic functions when released to the cytoplasm. An accumulation of deletions and point mutations in genes that are responsible for apoptosis, are considered to contribute to a diminished mitochondrial function and survival. Defects in ROS scavenging enzymes like mitochondrial superoxide dismutase (MnSOD) or methionine sulfoxide reductase A (MSRA) are related to a shortened mitochondrial life span. Oxidative damage notably contributes to AD-related pathology. For instance, deficiencies in the MnSOD enzyme activity was shown to increase amyloid- β -peptide ($A\beta$) levels, which is the primary component of senile plaques (Velliquette, O'Connor, and Vassar 2005). Moreover, amyloid precursor protein (APP), which gives rise to $A\beta$, was detected to interact with the ER and mitochondria directly. An exceed of APP blocks the mitochondrial protein import machinery and causes mitochondrial dysfunction and impaired energy metabolism (Anandatheerthavarada et al. 2003).

A characteristic for PD is neuronal loss in the substantia nigra pars compacta (SN). Surviving nigral neurons may contain intracytoplasmic inclusions called Lewy bodies. The presence of Lewy bodies in the SN constitutes the histologic diagnosis. Lewy bodies consist largely of fibrillar α -synuclein and its aggregation is promoted by Complex I inhibition in cell culture and PD animal models. The functional disruption and the elevation of oxidative stress on PD are induced by mutations in further nuclear encoded genes like phosphatase and tensin homologue (PTEN)-induced kinase 1 (PINK1), leucine-

rich-repeat kinase 2 (LRRK2) which directly or indirectly involve biogenetic metabolism and mitophagy (Swerdlow 2009).

For ALS, progressive weakness, muscle atrophy, spasticity, and eventual paralysis are typical. The neurological disruptions origin from a degeneration of upper and lower motor neurons. Frequent mutations detected in ALS include changes in genes encoding for SOD1, which protects for oxidative damage and which is implicated in apoptosis. SOD1 is considered to be a cytoplasmic enzyme, but it is also identified to be membrane-associated in mitochondria. Mutations in SOD1 in mice exhibit altered mitochondrial morphology and SOD1 accumulation, which underpins that mutant SOD1 drives neurodegeneration by damaging mitochondria (Gurney et al. 1994; Wong et al. 1995). Moreover, Complex I, II and III activities have been reported to be increased in vulnerable and non-vulnerable regions of patients with SOD1 mutations, whereas Complex IV activity was decreased in the spinal cord and skeletal muscle.

Abnormalities in mitochondrial morphology in skeletal muscles, liver and spinal cord motor neurons were detected in ALS patients (Borthwick et al. 2001; Comi et al. 1998). Moreover, Ca^{2+} homeostasis is altered in mitochondria of skeletal muscles of ALS patents. Despite of an increased number of local mitochondrial in synaptic terminals of motor neurons, Ca^{2+} -mediated processes in mitochondria appear to be disrupted (Siklós et al. 1996). In familial ALS patients Cyt c activity was reduced, indicating changes in proper mitochondrial metabolism and cellular survival (Comi et al. 1998).

HD is defined by a mutation of the Huntingtin gene on chromosome 4 and characterized as a hyperkinetic movement disorder. Various metabolism-related enzymes including the ETC complexes are altered in HD. The contribution of Huntingtin in particular remains unclear. However, Huntingtin was shown to be associated with the mitochondrial membrane and therefore it is likely to be involved in Ca^{2+} handling. Furthermore, Huntingtin is reported to disrupt PGC-1 α and thereby affecting mitochondrial metabolism (Swerdlow 2009).

1.4.3 Dysfunction of mitochondria and psychiatric disorders

Several brain disorders including MELAS, Leigh Syndrome, Friedrich's Ataxia as well the aforementioned neurodegenerative diseases AD, PD, ALS and HD result from mtDNA mutations. It is suggested that a malfunction of ROS production and disturbed mitochondrial metabolism contribute to the manifestation. Other studies also implicate the effect of oxidative stress on the development of mood disorders (Barton et al. 2003;

Forlenza and Miller 2006; Ozcan et al. 2004). Psychiatric symptoms also occur in subjects with mitochondriopathies. Several cases were documented that report of mitochondrial disorders with a comorbidity of psychiatric diseases including BPD, MDD, psychosis, anxiety disorders, and personality changes. Depressive episodes are reported with CPEO, whereas MELAS is highly correlated with SZ and BPD (DiMauro and Moraes 1993; Oexle and Zwierner 1997; Prayson and Wang 1998; Siciliano et al. 2003). Hence, brain metabolism seems to be disrupted which is caused by mtDNA mutation. These mutations causing mitochondrial abnormalities induce a patho-psychological state. Vice versa, in subjects primarily diagnosed with mental illnesses, especially MDD, bioenergetic deficits can be detected.

1.5 From fibroblasts via induced pluripotent stem cells through to induced neurons - a cellular model for MDD

In order to study mitochondrial metabolism in psychiatric disorders, a suitable model is needed. Whereas postmortem studies of brains can provide information about genetic variations, protein expression, changes in brain structures and volume alterations of different regions as well as the network of brain cells, several factors may interfere with tissue and molecular preservation of these samples and induce changes in the post-mortem state of the brain compared to pre-mortem (Ferrer et al. 2008). Therefore, functional and enzymatic studies are preferably conducted in intact, living cells from MDD subjects. Moreover, mitochondria constantly undergo fusion and fission, form networks and crosstalk with other subcellular compartments (Picard et al. 2011). This emphasizes also the need to analyze mitochondrial function without, or at least with minimal, cell disruption and with an as close as possible physiological environment, declining observations with isolated mitochondria or even frozen or fixed tissue. Nevertheless, brain studies in patients with MDD revealed that cellular bioenergetics are imbalanced and are related to mitochondrial dysfunction (Iosifescu et al. 2008; Stork and Renshaw 2005; Videbech 2000). Recent investigations in intact peripheral cells present bioenergetic changes in peripheral blood mononuclear cells (PBMCs), muscle cells, platelets and fibroblasts in correlation with a MDD state. Gardner et al. discovered a decreased ATP production and enzyme ratios comprising Complex I+III/Complex IV and the Complex II+III/Complex IV ratios in mitochondria of muscle cells in MDD patients (Gardner et al. 2003). Another study revealed that MDD patients lacking any ADs

treatment or pharmacological interventions exhibited significantly increased nitric oxide levels and a heightened MMP in platelets compared with those observed in control subjects (Moreno et al. 2013). Hroudová et al. also investigated platelets and were able to unveil reductions in mitochondrial physiological respiration, maximal capacity of the ETC and a lower respiratory rate after Complex I inhibition (Hroudová et al. 2013). Human fibroblasts of MDD patients show on a mRNA and miRNA level changes induced by metabolic stress. Those alterations indicate MDD-associated impairments in molecular pathways which are involved in guiding metabolism and energy production, cell survival, proliferation and migration (Garbett et al. 2015).

Moreover, patients with MDD had significantly lower basal and maximal respiratory rates in PBMCs than controls (Karabatsiakakis et al. 2014).

Lorenz et al. investigated the mitochondrial metabolism and defects in the mtDNA not in somatic cells as the aforementioned studies, but in iPSCs derived from human fibroblasts, NPCs and induced neurons (iN). They were able to show that despite the process of reprogramming, the parental mtDNA profile is retained. Moreover, they revealed that cells from iPSCs via NPCs through to iN exhibit a metabolic switch towards OXPHOS. The differentiated NPCs from patients carrying a deleterious homo-plasmic mutation mtDNA mutation showed defective ATP production and abnormal MMP besides an altered Ca^{2+} homeostasis, which might display a potential cause of neural impairment. The results of the study of Lorenz et al. highlighted that iPSC-derived NPCs provide an effective model for the investigation of bioenergetic changes, not only due to genetic changes that take place during development, but also that the cell types itself throughout neural development are a suitable model (Lorenz et al. 2017). Another study also emphasizes the importance of NPC investigation and their metabolic switch from aerobic glycolysis to OXPHOS, on which neurons rely on for their energy provision. They demonstrated the importance of this developmental changes since this process is critical for neural development. Defects during neuronal development cause neurological as well as neurodegenerative diseases (Zheng et al. 2016).

Klein Gunnewiek et al. elucidated mitochondrial dysfunction by the means of iPSC stem cell technology. They generated and observed excitatory cortical neurons with normal and impaired mitochondrial function due to the common pathogenic m.3243A>G mutation causing MELAS. iN with high levels of mtDNA mutations showed mitochondrial dysfunction, delayed neural maturation, receded dendritic complexity and less functional

synapses with a reduced network activity. These structural changes and failed proper integrity of iN are suggested to be a result of impaired metabolism in neurons bearing pathogenic mutation. These observations are proposed to enhance the susceptibility to neuropsychiatric manifestation because of a mitochondrial disease (Klein Gunnewiek et al. 2019).

A study highlighted iPSC-derived neurons as a model to investigate mental disorders – BPD in the particular case – and its potential for developing new therapies and drugs aiming for clinical treatment. iN of BPD patients exhibited mitochondrial abnormalities and a hyperexcitability which could be reversed by lithium treatment in neurons derived from patients who also responded to lithium (Mertens et al. 2015).

Various studies proved iPSCs, NPCs and iN as models for the investigation of metabolic changes, as well as an appropriate *in vitro* system to examine potential mitochondrial defects and bioenergetic alterations throughout development in disease. The iPSC technology from somatic cells to neural cell types is a suitable way to approach the implication of mitochondria in MDD in the present study.

1.6 Bioenergetic imbalance in MDD – hypothesis and aim of the thesis

In the present study, we focus on the association of mitochondria function and MDD. Potential pathomechanisms related to mitochondrial dysfunction and the bioenergetics imbalance in cells from MDD patients compared to healthy subjects should be elucidated. Based on the recent findings by Garbett et al., Hroudová et al., Karabatsiakos et al. and others, we hypothesize that mitochondria function is altered in somatic cells of MDD patients, as well as in neural cells.

In a first approach, the bioenergetic core function, the function of the ETC and OXPHOS, is examined in human dermal fibroblasts by the Seahorse XFp Flux Analyzer. It enables the assessment of the respiratory flux by the direct measurement of the oxygen consumption rate (OCR), which can be seen as a measure of the efficiency of the ETC. In the presence of the naturally available substrates, the OCR can be correlated to the function of the different respiratory complexes. The application of chemical compounds interfering with the ETC reveals the activity and capacity. Besides that, the aim is to investigate the overall energetic state in both, MDD fibroblasts and fibroblasts from controls. Measurements

with the Seahorse XFp Flux Analyzer allow the assessment of the proton secretion, the extracellular acidification rate (ECAR), which is a measure for glycolysis.

In addition, the energetic capacity in form of ATP is investigated by the direct measurement of the ATP content using a bioluminescence-based assay in order to unravel differences in MDD fibroblasts and control fibroblasts.

The ETC builds up an electro-chemical gradient between the IMS and the mitochondrial matrix, which is degraded by the ATP synthase and uncoupling proteins. This MMP over the IMM serves as an indicator for the bioenergetic state of mitochondria and might give a hint at a bioenergetic imbalance resulting from mitochondrial malfunction. Therefore, an objective is the assessment of the MMP in live cell imaging experiments with the help of the cationic dye JC-1.

Another objective of this thesis is to observe the homeostatic function of mitochondria and to elucidate potential differences in MDD cells and cells from healthy subjects. Mitochondria in association with the ER possess a Ca^{2+} -buffer function, which is closely related to the negative MMP. Alterations in the MMP might result in higher or lower cytosolic Ca^{2+} levels and consequently changes in cellular Ca^{2+} -mediated signaling.

Peripheral, non-neuronal cells are suitable for the investigation of mitochondrial functions and their implication in psychiatric disorders – like this case for MDD disease modeling. Nevertheless, in the focus of interest of this thesis is also to investigate whether potential alterations in the mitochondrial function in fibroblasts are also detectable in precursor-like state of neurons, the neural progenitor cells (NPCs). Reprogrammed somatic cells and cells that undergo the differentiation process experience changes in their energetic demands. Therefore, the cell's metabolism adapts and metabolism switches from efficient OXPHOS to fast but less efficient glycolysis and back to OXPHOS. NPCs are an intermediate state between iPSCs and iNeurons, and as this developing cell stage is pivotal to neuronal growth and differentiation, the research focus of this thesis is the mitochondrial (dys)function and bioenergetic (im)balance in MDD NPCs. This study hypothesizes, that also neural cells from MDD patients harbor alterations in their mitochondrial function. Therefore, the goal is to reprogram fibroblasts into iPSCs (Takahashi and Yamanaka 2006) and differentiate those into NPCs by the application of different growth factors and to control for proper neural induction by immunocytochemical staining (Yan et al. 2013). Similar to the focus of research in somatic cells, an important objective is to conduct the respiratory experiments with the Seahorse XFp Flux Analyzer in NPCs derived from MDD patients and compare their properties to

those from NPCs from healthy controls. Moreover, another objective is to determine the ATP levels in NPCs by a bioluminescence assay.

Likewise in fibroblasts, it is hypothesized that possible changes in the respiration also cause differences in the MMP in NPCs and go along with alterations in their Ca^{2+} homeostasis. In order to investigate this issue, live cell imaging experiments are conducted with NPCs. The cationic dye JC-1 is used to assess the MMP and cytosolic Ca^{2+} levels are determined with the ratiometric dye Fura-2.

Furthermore, the impact of hormonal stress in form of Dexamethasone (1 μM , 7d) and metabolic stress induced by the replacement of glucose by galactose (10 mM, 7d) on mitochondria function and metabolism is a main objective.

Whether the differences in the bioenergetics, which might be unveiled in the previously described approaches, are actually due to an ETC malfunction or simply by a reduced mitochondrial mass, the mitochondrial DNA copy number is determined in patient and control cells.

This study aims for a better insight into mechanisms related to the manifestation of MDD and seeks for shedding light on the indispensable proper function of a small but crucial organelle – the mitochondrion – assuring not only a healthy body, but also a healthy mind.

2 Materials

2.1 Lab supplies

Table 1 Lab supplies used in the present study

Material	Manufacturer
6-well-/12-well-/24-well-plate	Corning Incorporated; Tewksbury, Massachusetts
Agilent Seahorse XFp Flux Cartridge	Agilent Technologies; Santa Clara, California
Agilent Seahorse XFp Flux Miniplate	Agilent Technologies; Santa Clara, California
cell strainer 100 μm	Greiner Bio One; Kremsmünster, Austria
chamber for coverslip (\varnothing 25 mm)	Warner Instruments; Hamden, Connecticut
coverslips, glass (\varnothing 25 mm, \varnothing 12 mm)	Menzel Gläser; Braunschweig, Germany
cryo Vials 2mL	Lab Solute by Th. Geyer; Renningen, Germany
Eppendorf cups (0.5mL- 5 mL)	Eppendorf; Hamburg, Germany
Erlenmeyer flask 250 mL	Corning Incorporated; Tewksbury, Massachusetts
Falcon tubes (15 mL, 50 mL)	Corning Incorporated; Tewksbury, Massachusetts
mircoplates 96-well (black bottom)	Greiner Bio One; Kremsmünster, Austria
mircoplates 96-well (transparent)	Greiner Bio One; Kremsmünster, Austria
parafilm	PECHINEY Plastic Packaging; Chicago, Illinois
Pasteur pipette	Carl Roth; Karlsruhe, Germany
petridish (\varnothing 10 cm)	Sarstedt; Nümbrecht, Germany
pipette 0.1-10 μL	Eppendorf; Hamburg, Germany
pipette 10 μL - 200 μL	Eppendorf; Hamburg, Germany
pipette 100 μL - 1000 μL	Eppendorf; Hamburg, Germany
pipette filter tips	Sarstedt; Nümbrecht, Germany
pipette tips (10 μL , 200 μL , 1200 μL)	Sarstedt; Nümbrecht, Germany
pipettor	Brand GmbH&Co. KG; Wertheim, Germany
stripette, glass (5 mL)	Corning Incorporated; Tewksbury, Massachusetts
stripettes, plastic (1 mL, 5 mL, 10 mL, 25 mL)	Corning Incorporated; Tewksbury, Massachusetts
T75 flask	Sarstedt; Nümbrecht, Germany

2.2 Reagencies, chemicals and kits

Table 2 Chemicals required for the experiments of the study

Reagency	Manufacturer
0.5 M EDTA pH 8.0	Invitrogen by Life Technologies; Carlsbad, California
Accutase	Gibco by Life Technologies; Carlsbad, California
Advanced DMEM	Gibco by Life Technologies; Carlsbad, California
Agilent Seahorse XF Base Medium	Agilent Technologies; Santa Clara, California
Antibiotic/Antimycotic solution	Sigma-Aldrich; St. Louis, Missouri
Antimycin A	Cayman Chemical Company; Ann Arbor, Michigan
CASYton buffer	OMNI Life Science; Bremen, Germany
dexamethasone	Cayman Chemical Company; Ann Arbor, Michigan
dextrose	Carl Roth; Karlsruhe, Germany
ethanol 100%	Merck; Darmstadt, Germany
Dispase	STEMCELL Technologies; Vancouver, Canada
DMEM	Gibco by Life Technologies; Carlsbad, California
DMEM/F12	Gibco by Life Technologies; Carlsbad, California
DMSO	Sigma-Aldrich; St. Louis, Missouri
DPBS	Gibco by Life Technologies; Carlsbad, California
E7 Medium	STEMCELL Technologies; Vancouver, Canada

FCCP	Cayman Chemical Company; Ann Arbor, Michigan
FCS	Sigma-Aldrich; St. Louis, Missouri
FCS dialyzed	PAN Biotech; Aidenbach, Germany
Fluorescent Mounting Medium	Dako; Carpinteria, California
Fura-2/AM ("Fura-2")	Gibco by Life Technologies; Carlsbad, California
galactose	Carl Roth; Karlsruhe, Germany
gentamycin	Gibco by Life Technologies; Carlsbad, California
JC-1	Invitrogen by Life Technologies; Carlsbad, California
L-Glutamine	Sigma-Aldrich; St. Louis, Missouri
matrigel	Corning Incorporated; Tewksbury, Massachusetts
mTeSR	STEMCELL Technologies; Vancouver, Canada
mTeSR Supplement 50X	STEMCELL Technologies; Vancouver, Canada
NaOH	Carl Roth; Karlsruhe, Germany
Neural Induction Supplement	Gibco by Life Technologies; Carlsbad, California
Neurobasal Medium	Gibco by Life Technologies; Carlsbad, California
non-essential amino acids	Gibco by Life Technologies; Carlsbad, California
normal goat serum	Thermo Fisher Scientific; Carlsbad, California
Oligomycin	Cayman Chemical Company; Ann Arbor, Michigan
OptiMEM	Gibco by Life Technologies; Carlsbad, California
paraformaldehyde	Carl Roth; Karlsruhe, Germany
DPBS	Gibco by Life Technologies; Carlsbad, California
Penicillin-Streptomycin	Sigma-Aldrich; St. Louis, Missouri
Pluronic 10% F127	Thermo Fisher Scientific; Carlsbad, California
Rotenone	Cayman Chemical Company; Ann Arbor, Michigan
sodium butyrate	Sigma-Aldrich; St. Louis, Missouri
sodium pyruvate	Gibco by Life Technologies; Carlsbad, California
RNase free water	MACHERY-NAGEL; Düren, Germany
CryoStore CS10	BioLifeSolutions; Bothell, Washington
STEMdiff Neural Progenitor Freezing Medium	STEMCELL Technologies; Vancouver, Canada
Triton X-100	Sigma-Aldrich; St. Louis, Missouri
Trypan Blue	Sigma-Aldrich; St. Louis, Missouri
Trypsin	Sigma-Aldrich; St. Louis, Missouri
Vitronectin XF	STEMCELL Technologies; Vancouver, Canada

Table 3 Kits

Kit	Manufacturer
Pierce™ BCA Protein Assay Kit	Thermo Fisher Scientific; Carlsbad, California
CellTiter Glo Cell Viability Assay	Promega; Madison, Wisconsin
Seahorse XFp Mito Stress Kit	Agilent Technologies; Santa Clara, California
Human Dermal Fibroblast Nucleofector Kit VPD-1001	Lonza; Basel, Switzerland
QIAmp DNA Mini Kit	Qiagen; Hilden, Germany
Takyon Amplification Technologies	Eurogene; Seraing, Belgium

2.4 Antibodies

Table 4 Antibodies for Immunocytochemistry

Antibody (AB)	Dilution	Type of AB	Manufacturer
Hoechst	1:1000	primary	Gibco by Life Technologies; Carlsbad, California
Anti-PAX6 (mouse)	1:10	primary	PAX6 was deposited to the DSHB by Kawakami, A. (DSHB Hybridoma Product PAX6)
Anti-SOX2 ab97959 (rabbit)	1:1000	primary	Abcam; Cambridge, UK
Anti-mouse Cy3	1:1000	secondary	Thermo Fisher Scientific; Carlsbad, California
Anti-rat 488	1:1000	secondary	Gibco by Life Technologies; Carlsbad, California

2.5 Culture media and buffer compositions

Table 5 Primary Fibroblast Medium

Component	Volume
DMEM	500 mL
FCS	50 mL
Antibiotic/Antimycotic Solution	5 mL

Table 6 Primary fibroblast freezing medium

Component	Volume
Primary Fibroblast Medium	35 mL
FCS	10 mL
DMSO	5 mL

Table 7 E7 Medium

Component	Volume
TeSR-E7	480 mL
TeSR-E7 25X Supplement	20 mL

Table 8 mTeSR Medium

Component	Volume
mTeSR Basal Medium	400 mL
mTeSR Supplement 50X	100 mL
Gentamycin (2000X)	250 μ L

Table 9 Neural Induction Medium

Component	Volume
Neurobasal Medium	49 mL

Neural Induction Supplement	1 mL
------------------------------------	------

Table 10 Neural Expansion Medium

Component	Volume
Neurobasal Medium	24.5 mL
Advanced DMEM/F12 Medium	24.5 mL
Neural Induction Supplement	1 mL
Penicillin/Streptomycin	250 μ L

Table 11 Blocking buffer

Component	Volume
0.5% Triton-X100	1 mL
10% normal goat serum	1 mL
1X PBS	1 mL
ddH₂O	7 mL

Table 12 Antibody buffer

Component	Volume
0.5% Triton-X100	200 μ L
10% normal goat serum	200 μ L
1X PBS	1 mL
dd H₂O	8.6 mL

Table 13 Seahorse Assay Medium pH=7.4

Component	Volume
XFp Base Assay Medium	24 mL
1 M glucose	500 μ L
sodium pyruvate 100 mM	250 μ L
L-Glutamine 200 mM	250 μ L

Table 14 Ringer's solution, pH=7.4

Component	Volume
NaCl 140 mM	46.7 mL
KCl 5 mM	1 mL
MgCl₂ 2 mM	2 mL
HEPES 10 mM	50 mL
ddH₂O	900.3 mL

Table 15 Phosphate Buffered Saline pH=7.3

Component	Concentration
NaCl	137 mM
KCl	2.7 mM
Na₂HPO₄	8 mM
KH₂PO₄	1.4 mM

3 Methods

3.1 Study participants

Primary fibroblast lines were obtained by skin biopsy conducted by Dr. Leopold Größer, Dr. Konstantin Drexler and Prof. Dr. Mark Berneburg, Department of Dermatology, University Hospital of Regensburg, Regensburg, Germany. All 16 patients are diagnosed with MDD (Unipolar Depression, Hamilton Score > 18, diagnosed according to ICD-10) and responded to ADs medication. For the 16 gender- and age-matched healthy control subjects no current psychiatric disorder was recorded (Hamilton score 0-3).

Table 16 Study participants and controls

Patient	Gender	Age	Hamilton Score	Control	Gender	Age	Hamilton Score
MDD1	M	48	24	CON1	M	49	3
MDD2	F	49	21	CON2	F	50	0
MDD3	M	19	24	CON3	M	25	0
MDD4	M	48	20	CON4	M	45	1
MDD5	M	19	23	CON5	M	24	0
MDD6	F	24	23	CON6	F	25	1
MDD7	F	44	22	CON7	F	49	0
MDD8	F	44	22	CON8	F	53	0
MDD9	M	21	22	CON9	M	21	0
MDD10	M	21	21	CON10	M	20	1
MDD11	M	23	31	CON11	M	24	1
MDD12	F	23	34	CON12	F	23	0
MDD13	M	23	32	CON13	M	23	0
MDD14	M	30	28	CON14	M	27	0
MDD15	M	31	28	CON15	M	30	0
MDD16	M	34	25	CON16	M	35	0

Biopsy material of healthy skin (\varnothing 4 mm) is cut into 6 to 10 smaller pieces, put into 6 wells of a 6-well-plate, attached for 5-7 minutes and covered with Primary Fibroblast Medium (PrimFibM), consisting of DMEM/F12 supplemented with 10% fetal calf serum and 1% Antibiotic/Antimycotic solution (Anti/Anti). The primary fibroblasts determined passage 0 are cultured for 2-3 weeks until wells reach a confluence of 80-90%, then they are split (see 3.2) and transferred into T75 flasks for further growth.

3.2 Adult human dermal fibroblasts

3.2.1 Culturing conditions

Fibroblast cell lines are cultured at 37 °C and 5% CO₂ in PrimFibM in either 6-well-plates for experimental purposes or T75 flasks/ø10 cm petri dishes for further culturing. Cell cultures are checked daily under Olympus IX70 inverted cell culture transmitted-light microscope (Olympus Corporation; Tokyo, Japan). The medium is changed every other day.

3.2.2 Passaging, freezing and thawing procedure

When the cells reach around 80- 90% of confluence, they are prepared for splitting. The medium is aspirated and the cells are incubated with pre-warmed 1 mM PBS/EDTA for 15 min at 37°C in order to facilitate detachment. Subsequently, they are enzymatically detached by adding pre-warmed Trypsin for 5 min at 37 °C. By adding culture media, the reaction is stopped and the cell suspension is transferred into a 15 mL Falcon tube. After centrifugation for 5 min at 800 rpm, the cell pellet is resuspended properly in culture media and 200 µL are transferred into an Eppendorf cup for counting.

Cell counting was done with the CASY Cell Counter (OMNI Life Science; Bremen, Germany; see 3.2.3).

The volume with the desired amount of cells is seeded onto 6-well-plates or in a T75 flask/ø10 cm petri dish.

Table 17 Volumes for fibroblast splitting procedure

	1 well/6-well-plate	T75 flask/ ø10 cm petri dish
1 mM PBS/EDTA	1 mL	5 mL
Trypsin	0.5 mL	2 mL
PrimFibM (stopping reaction)	1.5 mL	8 mL
PrimFibM (resuspending)	2 mL	6-10 mL

For freezing, the cells are split as described above, apart from resuspending the cell pellet. After aspiration of the medium, the cell pellet is taken up in 1 mL of fibroblast freezing medium and transferred into a 1.5 mL cryo store vial. An evenly freezing of the sample is guaranteed by putting the vials into an isopropanol container. The cells are stored for short-term purposes at -80 °C and long-term at -196 °C.

For thawing, the fibroblasts in cryo vials are put shortly into the waterbath (37 °C) and afterwards, they are transferred into a 15 mL Falcon tube with 5-10 mL of PrimFibM. The suspension is centrifuged for 5 min at 800 rpm in order to eliminate the cell-toxic DMSO. The cell pellet is resuspended in 10 mL of PrimFibM and seeded into a T75 flask/ø10 cm petri dish.

All the experiments with primary fibroblasts were conducted under three different conditions: non-treated (N), galactose (GAL) and dexamethasone (DEX). The metabolic (GAL, 10 mM) or hormonal (DEX, 1 µM) stress inducing media are applied for 1 week under the culturing conditions as described above.

3.2.3 Automated cell counting with CASY Cell Counter

For accurate cell counting, 60 µL of the cell suspension are diluted in 6 mL CASYton buffer and measured automatically. The program determines average cell size, cell viability, total cell number and number of viable cells. The amount of viable cells is used for calculations of desired numbers of cells used in the experiments.

3.3 Reprogramming of adult human dermal fibroblasts into induced pluripotent stem cells using Epi5 plasmids

3.1 Coating with Vitronectin

15 µL hrVitronectin XF (250 µg/µL) are diluted in 6 mL PBS and 1 mL per 6-well-plate is prepared and polymerized for 1 h at room temperature. The wells are washed with 2 mL of PrimFibM before seeding the cells and 2 mL fresh PrimFibM are added to each well of a 6-well-plate. Per cell line one 6-well-plate is required.

3.2 Preparation of Epi5 plasmids

For the reprogramming, the VPD-1001 kit (Lonza; Basel, Switzerland) is used. The required plasmids are pCBX-EBNS, pCE-hsk, pCE-hUL, pCE-hOCT3/4 and pCE-mp53DD, as described in the publication of Takahashi and Yamanaka 2006. 600 ng of each plasmid are required. The plasmids are mixed with 82 µL of nucleofactor solution and 18 µL of the supplement.

3.3 Preparation and electroporation of human fibroblasts

The fibroblasts are split and counted as described in the previous chapter. The cell pellet of 600,000 cells is washed once with 3 mL of PBS in order to remove remaining PrimFibM. The cells are centrifuged again at 800 rpm for 5 min. The medium is aspirated and the cells are mixed with the solution containing the plasmids and the nucleofactor solution. The cell suspension is applied into the pre-cooled electroporation chambers. The cells are electroporated with program U-23 of the Amaxa Nucleofactor Electroporator (Lonza; Basel, Switzerland) and immediately put back on ice. 200 – 300 μ L of PrimFibM are added to the cell suspension and it is distributed equally drop by drop into the 6 wells of the 6-well-plate. Day 0 and day 1 after electroporation PrimFibM with 100 μ g of sodium butyrate is used. From day 2 on until day 7, E7 Medium with 100 μ M sodium butyrate is applied and the medium is changed every day. From day 8 on, E7 Medium without sodium butyrate is used and the medium is changed every day. From day 15, on clones should appear. The clones are marked with self-inking object marker (“cell dotter”) (Nikon; Tokyo, Japan) and picked with the help of a digital microscope (Primo Vert, Zeiss; Oberkochen, Germany) under sterile conditions and transferred into a new well of a 12-well-plate each by taking up the clone with a 200 μ L tip. The 12-well-plates are coated with Matrigel beforehand as described in the following chapter.

3.4 Coating for iPSCs and NPCs

iPSCs and NPCs require coated plates for attachment and optimal growth. Matrigel is a soluble basement membrane extract of the Engelbrecht-Holm-Swarm (EHS) tumor that polymerizes to form a reconstituted basement membrane (Kleinman et al., 1986). An aliquot Matrigel (volume dependent on manufacturer’s advice, usually 270 μ L – 300 μ L) is dissolved in cold 12 mL DMEM/F12 and for each well this solution and cold DMEM/F12 are added 1:1 into the pre-cooled plate. Afterwards, the plates can be stored for one to three weeks at 4 °C or polymerized at 37 °C for 30 min. Before the cell suspension is added to the wells, they need to be washed with DMEM/F12 in order to remove unpolymerized Matrigel. The table below lists the volumes required for the different plates. In case cover slips are added to the wells, they are placed into the wells before the solutions are added.

Table 18 Coating conditions

Plate type	DMEM/F12 with Matrigel	DMEM/F12
6-well-plate	1 mL	1 mL
12-well-plate	0.5 mL	0.5 mL
24-well-plate	250 μ L	250 μ L
XFp Seahorse Miniplate	100 μ L	100 μ L

3.5 Induced pluripotent stem cells

3.5.1 Culturing conditions

The iPSCs are kept under standard conditions (37 °C, 5% CO₂). The mTeSR Medium is changed every day and differentiated parts are marked and aspirated.

3.5.2 Passaging, freezing and thawing procedure

One well of a 6-well-plate of iPSCs is split in a 1:3 ratio. 6-well-plates are coated as described above and 1.5 mL of mTeSR Medium are put into each well. The medium is aspirated and per each 6 well 1 mL of pre-warmed Dispase is added. After 5 to 8 min the Dispase is aspirated and each well is washed three times with 1 mL of DMEM/F12. After the last washing step, 2 mL of DMEM/F12 is added and the previously marked differentiated spots and finally the DMEM/F12 are aspirated. 1.5 mL of mTeSR Medium are added. With the help of a disposable glass pipette the stem cell colonies are separated by gently scratching the bottom in grid pattern. With the help of a cell scraper the stem cell colonies are completely detached from the bottom. Per each new well, 0.5 mL of the cell suspension are added drop by drop and distributed by gently shaking horizontally.

For freezing purposes, after detaching the cells with the help of Dispase and the differentiated cells are removed as described before. The cells are detached with a cell scraper in DMEM/F12 and transferred into a 15 mL Falcon tube and centrifuged at 800 rpm for 5 min. The cell pellet is taken up in 1 mL CryoStore CS10 freezing medium, put into a cryo vial and stored at -80 °C.

For thawing, the cryo vial with the stem cells is put into a waterbath (37 °C) for maximum 5 min and the cell suspension is quickly transferred into a 15 mL Falcon tube containing 3 mL of DMEM/F12 in order to remove the cytotoxic component of the freezing medium. The suspension is centrifuged for 5 min at 800 rpm, the supernatant is aspirated and the

cell pellet is taken up into 2 mL of mTeSR Medium and seeded onto one well of a 6-well-plate.

3.6 Neural induction and expansion of neural progenitor cells

One day after splitting, the iPSC colonies for differentiation should have densities of $2\text{--}2.5 \times 10^4$. mTeSR Medium is changed to Neural Induction Medium (NIM). The medium is changed every other day from day 0 until day 4 of neural induction and from day 5 on every day, since cell densities increase during differentiation. After one week, the cells are split. The cells are detached with 1 mL pre-warmed Accutase for 5 min per one 6-well. The reaction is stopped by adding 2 mL of DPBS or DMEM/F12. The suspension is transferred into a 15 mL Falcon tube and centrifuged for 5 min at 800 rpm. The supernatant is aspirated and the cell pellet is resuspended in 2-3 mL of DPBS or DMEM/F12 and the suspension is passed through a 100 μm cell strainer placed on a 50 mL Falcon tube. Subsequently, the suspension is centrifuged at 800 rpm for 5 min and the cell pellet is resuspended in Neural Expansion Medium (NEM) with 5 μM ROCK-Kinase-Inhibitor. The cells are counted with the help of Trypan Blue in a Neubauer Chamber and approximately $6.0\text{--}7.0 \times 10^5$ cells are seeded onto one well of a 12-well-plate coated with Matrigel. The medium is changed every other day and the NPCs of passage 0 are grown until they reach confluence.

NPCs are split by aspirating the medium and the addition of 1 mL pre-warmed Accutase for 5 min. The reaction is stopped by 2-3 mL of DPBS or DMEM/F12 and the cell suspension is transferred into a 15 mL Falcon tube and centrifuged at 800 rpm for 5 min. The supernatant is aspirated and the cell pellet is resuspended in 5 mL DPBS or DMEM/F12 and 20 μL are mixed with 20 μL of Trypan Blue in a 1.5 mL Eppendorf cup and used for counting with the Neubauer Chamber. 2-3 mio cells are seeded into a well of 6-well-plate coated with Matrigel. $5\text{--}6 \times 10^6$ cells are used for freezing. The volume of cell suspension with the desired amount of cells is transferred into a new 15 mL Falcon tube and centrifuged down at 800 rpm for 5 min. NPCs used for cultivation are resuspended in NEM and seeded. NPCs that are being frozen are taken up into 1 mL of STEMdiff Neural Progenitor Freezing Medium, transferred in to a 2 mL cryo vial and stored at $-80\text{ }^\circ\text{C}$, respectively at $-196\text{ }^\circ\text{C}$.

NPCs are thawed by putting the cryo vial for maximal 5 min into the waterbath (37 °C) and transferring the cell suspension into 2-3 mL of DPBS or DMEM/F12. The cell suspension is centrifuged at 800 rpm for 5 min in order to remove the potentially cytotoxic residuals of the cryo storage medium. The cell pellet is resuspended in 2 mL NEM and the cell suspension is seeded onto one well of a 6-well-plate coated with Matrigel.

3.7 Immunocytochemical staining

For immunocytochemical staining, the cells are split and seeded onto cover slips, in low densities with approximately 60% confluence. The next day, the cover slips are transferred into a new plate and the cells are fixed with 4% PFA for 10 min. Subsequently, in each well 250 µL blocking buffer are added in order to prevent unspecific binding of the antibody. Afterwards, the first antibody is applied and left over night at 4 °C. The next day, the antibody is discarded and the coverslips are washed three times with 500 µL 1X PBS for 10 min. The second antibody is applied for 1 h at RT in the dark. The second antibody is discarded and the coverslips are washed again three times with 1X PBS for 10 min. The coverslips are mounted onto glass object slides with the help of a drop of Dako Fluorescing Mounting Medium and let to polymerize overnight.

3.8 Assessment of respiratory properties: Seahorse XFp Flux Analyzer

For respiratory experiments, the cells are being split and seeded as described beforehand the day before the experiment. 30,000 fibroblasts or 500,000 NPCs, respectively, are seeded into the wells of the XFp Seahorse Miniplate. The Wells B to G contain control cells respectively patient cells in triplicates. The wells A and H remain without cells as a blank control.

Additionally, an XFp Flux Cartridge is equilibrated with 200 µL in the wells A to H and 400 µL of Agilent Seahorse XF Calibrant solution in the outer chambers and left at 37 °C in a non-CO₂ incubator.

The following day, the XFp Seahorse Miniplate containing the cells is washed with 200 µL of Seahorse Assay Medium, finally filled with 180 µL of the Seahorse Assay Medium and left for 30 min to 1 h in a non-CO₂ incubator. Meanwhile, the reagents for the XFp Mito Stress Test are being prepared. Therefore, the component stocks are diluted 1:1000 in Seahorse Assay Medium and applied into the Seahorse XFp Flux Cartridge into different

volumes in order to get a final concentration of 1 μM Oligomycin, 2 μM FCCP and 0.5 μM Rotenone/Antimycin A.

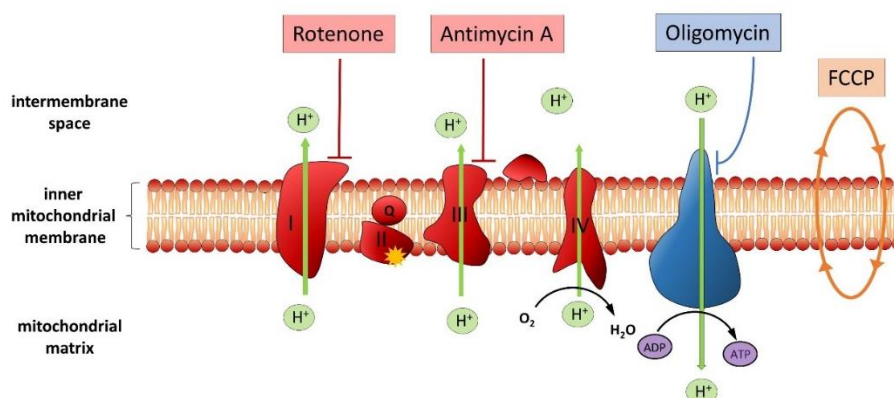


Figure 9 ETC inhibitors. Inhibition of the ETC is sequentially conducted in Seahorse XFp Flux experiments. Oligomycin acts on Complex V, the ATP synthase, and inhibits the degradation of the H^+ gradient. FCCP is an uncoupler of the ETC and enables an uninhibited flow of the H^+ . Rotenone and Antimycin A block Complex I and Complex III of the ETC and shut down OXPHOS.

20 μL Oligomycin are applied into all of the “A” ports, 22 μL FCCP are pipetted into ports “B” and 25 μL of the Rotenone/Antimycin A mixture are added into the ports “C” in all of the wells A to H of the Seahorse XFp Flux Cartridge.

The Seahorse XFp Flux Cartridge is placed into the XFp Flux Analyzer for calibration and afterwards, the cells are placed into the machine, according to the manufacturer’s instructions and the XFp Mito Stress Test is started. For the Mito Stress Test, four baseline measurements of the OCR and the ECAR are conducted and four measurements each are made after the sequential injection of the components (see figure 9). The assay output includes also an overall mean OCR value and mean ECAR value calculated from all 16 measured points.

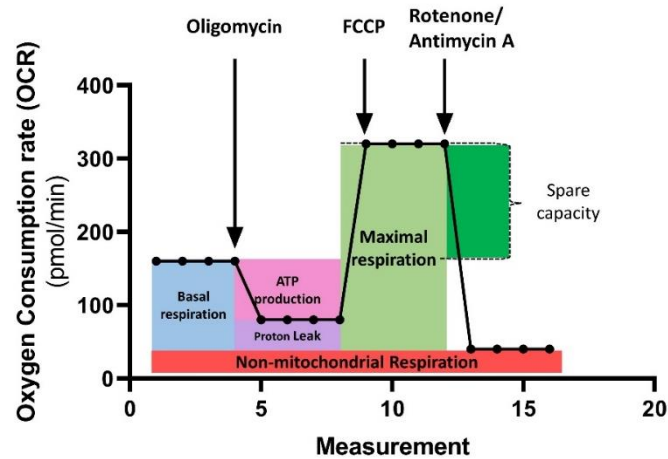


Figure 10 Mito Stress Test in the Seahorse XFp Flux Analyzer. Initially, the basal respiration is measured. By the inhibition of the ATP synthase by Oligomycin the OCR declines. The ATP production-related OCR and the proton leak can be determined. FCCP uncouples the ETC and OXPHOS can run at its maximum. The readout parameter of the maximal respiration can be assessed. Rotenone and Antimycin A block the ETC and the remaining OCR is related to non-mitochondrial processes that require oxygen. The spare capacity results out of the maximal respiration subtracted by the basal respiration.

After the measurement, the assay medium is aspirated and the fibroblasts are fixed with 4% PFA for 10 min for normalization purposes with Hoechst staining. The NPCs are stored at -20°C and normalized by determination of the protein content with the BCA Assay (see 3.10).

3.10 Normalization of respiratory experiments

3.10.1 Normalization by Hoechst staining

When XFp Mito Stress Test of fibroblasts is finished, the medium is aspirated and the cells are fixed with $100\ \mu\text{L}$ 4% PFA per XFp Seahorse Miniplate-well for 10 min. The cells are washed with $200\ \mu\text{L}$ PBS and stained with Hoechst (1:1000 in PBS) for 10 min in the dark and washed with $200\ \mu\text{L}$ PBS three times in order to remove residual dye. With the help of a fluorescence microscope pictures of the Miniplate-wells are taken that can be further used for cell counting with Image J. The cell numbers per Miniplate-well are entered into the Wave files that are created by the XFp Flux Analyzer.

3.10.2 Normalization by Bichinoic Acid Assay

Following the XFp Mito Stress Test of NPCs, the medium is aspirated and the cells are lysed in $20\ \mu\text{L}$ 1X Triton X-100 for 15 min at 4°C . Meanwhile, $10\ \mu\text{L}$ of BSA standards dissolved in 1X Triton X-100 with concentrations reaching from $100\ \mu\text{g}/\text{mL}$ to $2\ \text{mg}/\text{mL}$ BSA. The standards are applied onto a transparent 96-well-plate. The reagents A and B

are used in a ratio 1:50. 200 μL of the AB-reagent is applied to each Miniplate-well and the cells are resuspended properly. Twice 110 μL of the suspension are added to the 96-well-plate and 100 μL A-B-reagent are added to the cell suspension. 200 μL AB-reagent are added to the BSA standards. The plate is shaken for 5 min at RT and incubated for 30 min at 37 $^{\circ}\text{C}$ in a non- CO_2 incubator. The absorption is measured in a VarioScan plate reader and analyzed with the Software SkanIt. The protein content (mg/mL) is determined with the help of the BSA standards for each well and used for normalization of the respiratory experiments. The resulting protein amounts are added to the Wave files containing the results of the Mito Stress Test.

3.11 Luminescent assay for ATP content

For the determination of the ATP content, 1×10^5 fibroblasts and 1×10^6 NPCs cell pellets are collected in a 1.5 mL Eppendorf cup and stored at -20 $^{\circ}\text{C}$ if necessary. Untreated or previously treated fibroblasts with galactose (10 mM, 7 days) or dexamethasone (1 μM , 7 days) and untreated or previously with dexamethasone treated (1 μM , 7 days) NPCs are used for ATP content determination.

According to the manufacturer's advice, the CellTiter-Glo[®] Reagent containing CellTiter[®] Substrate and CellTiter[®] Buffer, is thawed on ice. As an ATP standard curve with concentrations of 10 μM , 100 nM, 10 nM and 10 pm ATP in PBS is used. The cell pellets are resuspended in 500 μL PBS and heated at 100 $^{\circ}\text{C}$ for 2 min in order to inactivate ATPases. Subsequently, the samples are stored on ice. 50 μL of each sample and each standard are applied to a black 96-well-plate in duplicates. 50 μL of the CellTiter-Glo[®] Reagent are added to the ATP standards and the samples and the 96-well-plate is shaken for 2 min in the dark. The absorption is measured at the VarioScan with an integration time of 1 s. The RLU generated by the SkanIT Software can be calculated to the actual ATP concentrations with the help of the ATP standard curve.

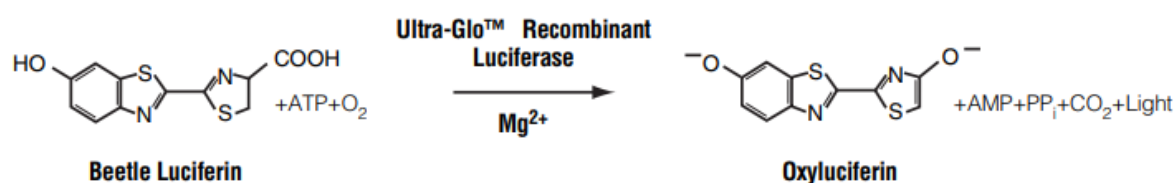


Figure 11 Luciferase reaction for ATP quantification. Mono-oxygenation of luciferin is catalyzed by luciferase in the presence of Mg^{2+} , ATP and molecular oxygen. Source: CellTiter-Glo[®] Assay Technical Manual, Promega

3.12 Live cell imaging

Live cell imaging experiments are conducted with a Zeiss Axio Observer Z.1 microscope equipped with Fluar 40/1.3 objective lens (Zeiss; Oberkochen, Germany) and a Lambda DG-4 excitation device (Sutter Instruments; Novato, California). All recordings are conducted at a magnification of 40X with oil and captured with an AxioCam MRm CCD camera (Zeiss; Oberkochen, Germany). Hardware control and measuring parameters are set with the help of ZEN 2012 Software. Fibroblasts and NPCs used in imaging experiments are either non-treated (N) or underwent metabolic (GAL) or hormonal stress (DEX) for one week.

3.12.1 Mitochondrial membrane potential measurements with JC-1

The cationic dye JC-1 allows the qualitative measurement of the MMP in different cell types. The dye exhibits a potential-dependent accumulation in mitochondria, indicated by a fluorescence emission shift from green (~529 nm) to red (~590 nm). Consequently, mitochondrial depolarization is indicated by a decrease in the red/green fluorescence intensity ratio. The potential-sensitive color shift from green fluorescing monomers of the dye is due to concentration-dependent formation of red fluorescent aggregates.

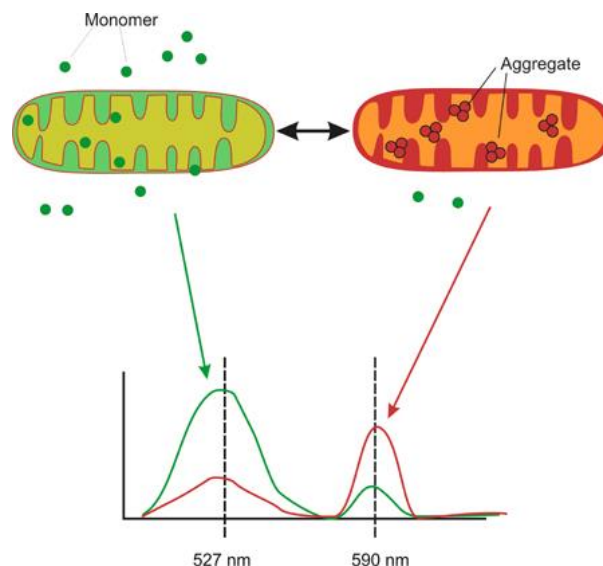


Figure 12 Emission spectra of the cationic dye JC-1. Depending on the mitochondrial membrane potential, JC-1 dye is present as monomers or forms aggregates. The monomers emit at 529 nm, whereas aggregates of the dye emit at 590 nm. The ratio between red/green is associated with the mitochondrial membrane potential. Source: <https://www.biotek.de/de/resources/application-notes/fluorescent-detection-of-drug-induced-mitochondrial-toxicity/>

The JC-1 dye is used at a final concentration of 300 nM in OptiMEM and the cells are incubated with the dye for 30 min. The cells are washed three times with Ringer's solution and the cover slip is placed in the measuring chamber. The cells are covered with 200 – 300 μ L of Ringer's solution. 5-10 visual fields are captured at a 40X magnification with oil. The exposure time is set to 150 ms. 5 cycles with 2s each are recorded. Data analysis is done with FIJI Image J by defining regions of interest per each picture and Ratio Plus Plugin for determination of the red/green ratios.

3.12.2 Analysis of intracellular Ca^{2+} with Fura-2 dye

For assessment of Ca^{2+} homeostasis, the fluorescent dye Fura-2/AM ("Fura-2") is used. The emission wavelength of Fura-2 is dependent on the free or Ca^{2+} -bound state of the dye. Free Fura-2 emits at 380 nm, Ca^{2+} -bound Fura-2 emits a wavelength of 340 nm. The ratio of 340 nm/380 nm is correlated with the amount of cytosolic Ca^{2+} in the cell.

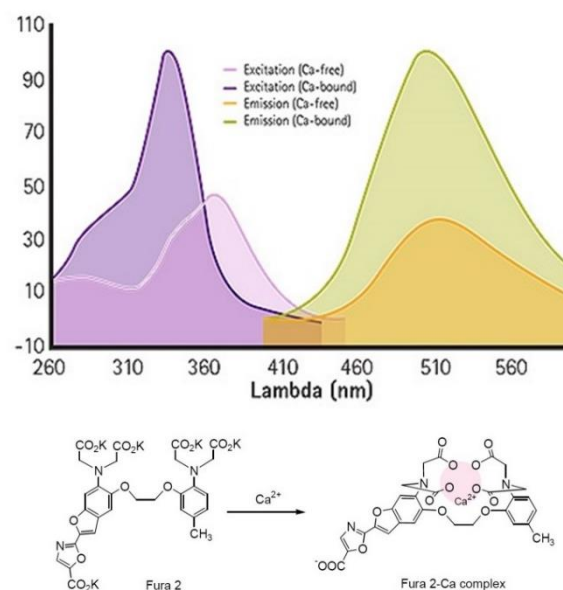


Figure 13. Emission spectra and complex forming of the ratio metric dye Fura-2. In the presence of Ca^{2+} Fura-2 forms a chelate complex and changes its conformation. Free Fura-2 is excited at 340 nm, whereas Ca^{2+} -bound Fura-2 is excited at 380 nm. Both forms emit at 510 nm. The ratio between 340 nm/380 nm is directly related to free cytosolic Ca^{2+} in the cell. Source: <https://www.moleculardevices.com/products/assay-kits/gpcrs/fura-2-qbt-calcium-kit#Technology>

Fibroblasts and NPCs are split and prepared for the measurements the previous day. The cells are plated onto 25mm cover slips. For NPCs coating with Matrigel is required as described before. 150,000 fibroblasts or 2.8 Mio NPCs are seeded. The following day 1 μ L

Fura-2 dye is mixed with 1 μL Pluronic 10% F127 and diluted in 1 mL OptiMEM (final concentration 2 μM). The cover slip is transferred into a 35 mm tissue dish, the solution with the dye is added and incubated for 30 mins. The cells are washed with Ringer's solution three times and the cover slip is applied onto the measuring chamber. The cells are covered with 200 – 300 μL Ringer solution. The measurements for Ca^{2+} are conducted at a Zeiss fluorescent microscope with the help of Zen software. For each cover slip 5 – 15 different sections with cells are measured. 5 cycles for 2 s each, with an exposure time of 300 ms (fibroblasts) or 150 ms (NPCs) for both channels are recorded at a 40X magnification with oil.

The analysis of the measurements is done with FIJI Image J, by manual definition of the regions of interest and building the 340 nm/380 nm ratio for each image.

3.13 Determination of the mitochondrial content

3.13.1 gDNA extraction

For each patient and control cell line gDNA was extracted from two biological replicates. The cell pellet of 1×10^6 cells is resuspended in 200 μL PBS and 20 μL QIAGEN Protease is added. Afterwards, 200 μL of AL buffer is added to each sample and vortexed for 15 s to ensure proper mixing. The samples are incubated at 56 $^{\circ}\text{C}$ for 10 min. 200 μL ethanol (100%) are added to the sample and again mixed by pulse-vortexing for 15 s. After mixing, the tube is briefly centrifuged to remove drops from the inside of the lid. Subsequently, the mixture is applied to the QIAamp Mini spin column placed in a 2 mL collection tube without wetting the rim. Cap closed, the samples are centrifuged at 8000 rpm for 1 min. The QIAamp Mini spin column is changed to a new collection tube and the tube with the filtrate is discarded. In the next step, 500 μL AW1 buffer is applied and the samples are centrifuged at 8000 rpm. Afterwards, the QIAamp Mini spin column is changed to a new 2 mL collection tube and the filtrate and the old collection tube can be discarded. The second washing AW2 buffer is applied to the sample (500 μL) and the QIAamp Mini Spin columns are centrifuged at full speed (14000 rpm for 5 min). In order to remove remaining washing buffer, the QIAamp Mini columns are placed into a fresh collection tube and centrifuged at full speed for 1 min. The QIAamp Mini Spin columns are then placed into a fresh 1.5 mL Eppendorf cup and to each sample 100 μL of distilled water are added. After an incubation time of one minute at RT (15-25 $^{\circ}\text{C}$) the gDNA is eluted at 8000 rpm for 1

min. The DNA concentration is determined at the Nano Drop and all the samples are adjusted to 50 ng/ μ L for RT-PCR measurements.

3.13.2 Quantitative Real-Time Poly Chain Reaction

3.13.2.1 Amplification efficiencies

For the quantification of the mtDNA content, the primers for the mitochondrial gene mt-TL1 and the nuclear gene B2M are used. Primer sequences are listed in table 19.

Table 19 Target genes, sequences, concentrations and manufacturer of the primers used for mtDNA quantification

Gene	Abbr.	direction	Sequence	Stock conc.	Manufacturer
Beta-2 microtubulin	B2M	forward	5'-	10 μ M	Metabion, Planegg, Germany
			TGCTGTCTCCA		
			TGTTTGATGTA		
		TCT			
reverse	5'-	TCTCTGCTCCC	CACCTCTAAGT		
mitochondrially encoded tRNA leucine 1	mt-TL1	forward	5'-	10 μ M	Metabion, Planegg, Germany
			CACCCAAGAAC		
			AGGGTTTGT		
		reverse	5'-	TGGCCATGGGT	

In order to test the primer efficiency first, five times a threefold serial dilution of one DNA sample in water is made. The dilutions are used to obtain a standard curve and the PCR efficiency (E) is determined. PCR efficiency is calculated from the slope of the standard curves using the equation formula:

$$E = 10^{-1/\text{slope}} - 1$$

In order to improve precision, the samples for the standard curve were pipetted in quadruplicates.

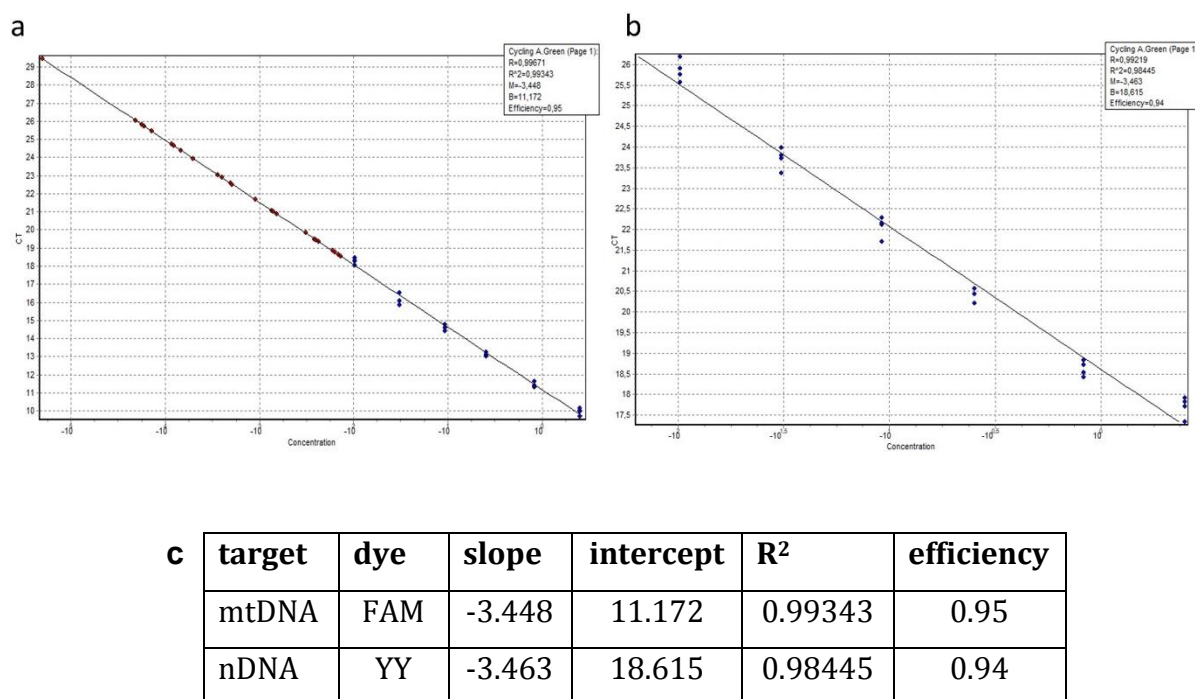


Figure 14 Graphs and values for primer efficiency for mtDNA copy number determination. Regression curve, R² and efficiency determination for (a) mtTL1 primer pair and (b) B2M primer pair. In the table (c) below, the values for slope, intercept, R² and efficiency for each target are listed.

The components and volumes for each single RT-PCR reaction is listed in table 20. The RT-PCR is run in an initial phase of 5 min at 95 °C, followed by 45 cycles of 95 °C for 15 s and 60 °C for 30 s. The melt curve is assessed from 65 °C to 95 °C.

Table 20 Reagents and volumes for RT-PCR

Reagent	Volume
gDNA 50 ng/ μL	0.5 μL
primer forward	0.5 μL
primer reverse	0.5 μL
H ₂ O	3.5 μL

3.13.2.2 mtDNA copy number calculation

Relative quantification was applied to calculate number of mtDNA per diploid nuclear (2n) cell:

$$2 \times E^{-\Delta\Delta Cq}$$

In this equation “Cq” is the quantification cycle, $\Delta\Delta Cq$ is $(Cq_{mt}-Cq_{nuc})$, “E” is the averaged mean efficiency of the PCR reactions of the two targets and “2” is to account for the two nDNA copies in a cell (Fazzini et al. 2018). The mtDNA copy number was assessed from two biological replicates for each cell line and each biological replicate was measured in two separate runs.

3.14 Data analysis and statistics

Data collection and calculations are done with Windows EXCEL (Microsoft Corporation; Redmond, Washington). Graphical depiction and statistical analysis is conducted with Graph Pad Prism 8.0.2 (GraphPad Software; San Diego, California).

For all analysis, the mean of two to three technical replicates is calculated and two or three biological replicates are averaged. All data is checked for normality and lognormality (Anderson-Darling test, D’Agostino & Pearson test, Shapiro Wilk test and Kolmogorov-Smirnov test). Consequently, the parametric test (Student’s paired t-test) or non-parametric test (Wilcoxon matched-pairs rank sum test) are applied. P-value limit for statistical significance is set to ≤ 0.05 . Values are given as means \pm standard error of the mean (SEM). Energy maps are statistically evaluated by ANOVA with repeated measures and Greenhouse Geisser as a Post Hoc Analysis respectively Bonferroni correction.

4 Results

4.1 Patient and control cohort

To exclude gender- and age-specific differences in mitochondrial and respiratory functions, for each patient a matching control was recruited. As depicted in Table 21, patients and controls do not differ in mean age or sex. The patients' age ranges from 21 to 50 with a mean age of 31 ± 3.12 and the controls are aged 19 to 49 with a mean age of 32 ± 2.81 . Eleven male patients and five female patients were paired with eleven male healthy controls and five healthy female controls. Moreover, physical parameters were assessed. Patients and controls do not differ in BMI (patients BMI = 23.0 ± 0.48 ; controls BMI = 24.2 ± 0.28). Whereas 94% of the MDD patients smoke, 25% of the controls exhibit a regular smoking habit. 56% of the patients drink regularly alcohol, whereas 94% of the healthy controls declared that they consume alcohol several times a week. 93% of the MDD patients and 83% of controls do not consume drugs. Drug abuse in controls was stated as "very seldom". Besides physiological examinations psychological health of the controls was confirmed by PD Dr. med. Caroline Nothdurfter (Bezirksklinikum Regensburg) to exclude possible mental diseases (HAM-D 0-3). The patient cohort for this study was selected according to their diagnosis at the Bezirksklinikum Regensburg. All patients were diagnosed according to ICD-10 with a medium severe or severe MDD (HAM-D 20-34, please see method section 3.1). All patients were treated with different combinations of ADs. The ADs given are listed in the table below.

Table 21 Mean and SEM of clinical characteristics of n=16 MDD patients and n=16 controls.

Variables	Groups	
	MDD (n=16)	Controls (n=16)
<i>ICD-10</i>		
F32.1	2	0
F32.2	10	0
F33.1	1	0
F33.3	3	0
Age (mean \pm SEM, years)	31 ± 3.12	32 ± 2.81
	11 (69%)/5 (31%)	11 (69%)/5 (31%)

Sex (male, n (%)/female, n (%))		
BMI (mean±SEM, kg m⁻²)	23.0 ± 0.48	24.2 ± 3.38
Smoker (yes, n (%))	9 (75%) [4 n/a]	4 (25%)
Alcohol (yes, n (%))	9 (75%) [4 n/a]	15 (94%)
Drugs (no, n (%))	11 (93%) [4 n/a]	13 (81%)
Medication		
Agomelatin	3	0
Bupropion	2	0
Duloxetine	1	0
Escitalopram	6	0
Mirtazapin	3	0
Olanzapin	2	0
Promethazin	1	0
Trimipramin	1	0
Venlafaxin	2	0

4.2 Differences in mitochondrial metabolism in peripheral cells: Fibroblasts show alterations in mitochondria-related functions

Human dermal fibroblasts are easily accessible, fast growing and simple to cultivate. Despite the fact, that the cells are not of neural origin, it already could be shown that peripheral cells (PBMCs, platelets or muscle cells) from people suffering from psychiatric disorders - like MDD and PTSD - harbor alterations in their cellular metabolism (Garbett et al. 2015; Gardner et al. 2003; Hroudová et al. 2013; Karabatsiakakis et al. 2014). Therefore, experiments with human dermal fibroblast are the initial approach to investigate mitochondria-related changes in association with MDD. The results regarding the patient cohort and experiments with fibroblasts - including respiration, energy maps, ATP levels as well as imaging experiments (JC-1 and cytosolic Ca²⁺ levels) and mtDNA content - have previously been published in Kuffner et al. (Kuffner et al. 2020).

4.2.1 Mito Stress Test: ETC function and glycolysis

4.2.1.1 Respiration of fibroblasts

In order to test the mitochondrial function in fibroblasts, each patient cell line was examined in comparison to the control cell line. In total, 16 patient cell lines were compared to 16 gender- and age-matched cell lines. The cells were measured under standard culturing conditions (non-treated), but also after the exposure to one week of either hormonal stress induced by DEX or metabolic stress which is evoked by the exchange of glucose to galactose in the culture medium. The cellular respiration in form of OCR and the measure for the function of the glycolysis, the ECAR, was assessed in the XFp Flux Analyzer. The Mito Stress Test allows a readout of various parameters linked to the function of the ETC. By the application of compounds interacting with the ETC, the basal respiration, the maximum respiration, the spare capacity, the non-mitochondrial respiration, the ATP production-related oxygen consumption and the proton leak were determined.

The assessment of the respiratory parameters resulted in significant differences in peripheral cells (figure 15). Fibroblasts derived from MDD patients compared to fibroblasts from healthy controls have a significantly lower basal respiration under basal conditions (MDD 16.09 ± 0.88 , CON 18.53 ± 0.95 , Student's t-test, paired, two-tailed, * $p > 0.05$, $p = 0.0200$, mean \pm SEM). The differences that were detected under basal conditions are reversed after one week of stress. The basal respiration after hormonal stress induced by DEX does not show differences between MDD cells and cells from controls (MDD 22.96 ± 1.14 , CON 23.25 ± 1.12 , Student's t-test, paired, two-tailed, $p = 0.7392$, mean \pm SEM, figure 15 a). The application of galactose medium for one week, which demonstrates metabolic stress for the cells, also abolished the significant differences between cells from patients and healthy subjects (MDD 22.31 ± 1.70 , CON 22.64 ± 1.58 , Student's t-test, paired, two-tailed, $p = 0.7899$, mean \pm SEM, figure 15 a). The maximum respiration is an important measure to determine how much the cells could respire in case of an energetic challenge or a high energetic demand. In the Mito Stress Test it is induced by the ETC uncoupler FCCP. For the maximal respiration similar observations are made. Whereas cells from healthy controls reach significantly higher OCRs than MDD cells under non-treated conditions (MDD 32.20 ± 2.23 , CON 37.01 ± 2.40 , Student's t-test, paired, two-tailed, *** $p < 0.001$, $p = 0.0003$, mean \pm SEM, figure 15 b), the detected differences are not present after DEX stress (MDD 48.76 ± 3.88 , CON 45.03 ± 2.32 , Student's t-test, paired, two-tailed,

$p = 0.4514$, mean \pm SEM, figure 15 b) neither after galactose stress (MDD 57.86 ± 2.64 , CON 60.04 ± 3.51 , Wilcoxon matched-pairs signed rank test, $p = 0.2769$, mean \pm SEM, figure 15 b). A parameter that is closely related to the basal respiration and the maximal respiration is the spare respiratory capacity. The spare respiratory capacity is a measure for the cells flexibility and ability to react to an excess energetic need. Theoretically, the higher the spare capacity the more reserves the cells have in case of an energetic challenge. Accompanying the results from basal respiration and the maximal respiration, the MDD cells also show significant differences in the spare respiratory capacity under normal, non-treated conditions (MDD 16.11 ± 1.81 , CON 18.95 ± 2.29 , Student's t-test, paired, two-tailed, * $p < 0.05$, $p = 0.0257$, mean \pm SEM, figure 15 c). The spare respiratory capacity did not differ between MDD fibroblasts and fibroblasts derived from healthy controls after hormonal stress (DEX, MDD 25.28 ± 3.15 , CON 27.72 ± 3.92 , Wilcoxon matched-pairs signed rank test, $p = 0.2769$, mean \pm SEM) or after metabolic stress (GAL, MDD 35.91 ± 3.19 , CON 37.33 ± 3.65 , Wilcoxon matched-pairs signed rank test, $p = 0.2078$, mean \pm SEM, figure 15 c). Furthermore, the non-mitochondrial respiration was determined after the application of Rotenone and Antimycin A that block the Complex I and III of the ETC and therefore inhibit mitochondrial respiration. The non-mitochondrial respiration is caused by other enzymatic reactions in the cell or oxygenases outside the mitochondria. MDD fibroblasts exhibit a significantly lower non-mitochondrial respiration under normal conditions in comparison with control fibroblasts (MDD 7.90 ± 0.71 , CON 9.65 ± 0.91 , Student's t-test, paired, two-tailed, * $p < 0.05$, $p = 0.0115$, mean \pm SEM), indicating an overall decreased cellular metabolism. These alterations are cancelled out after one week of DEX stress (MDD 11.08 ± 0.95 , CON 11.84 ± 0.79 , Student's t-test, paired, two-tailed, $p = 0.2134$, mean \pm SEM) but not by metabolic stress (MDD 15.43 ± 1.34 , CON 18.05 ± 1.60 , Student's t-test, paired, two-tailed, * $p < 0.05$, $p = 0.0818$, mean \pm SEM, figure 15 d).

Oligomycin blocks the ATP synthase and allows the proton leak and the ATP-related OCR as readout parameters in the Mito Stress Test. Oligomycin prevents the increase in mitochondrial respiration induced by ADP without inhibiting uncoupling-stimulated respiration. NADH remains high and NAD⁺ is too low for the citric acid cycle to operate (O. Lee, P.J. O'Brien, 2010). The proton leak describes the flux of H⁺ across the mitochondrial membrane independently from the ETC, but through transporters, for example (Cheng et al. 2017). No significant differences were detected in the proton leak-associated OCR neither under non-treated conditions (MDD 2.38 ± 0.20 , CON 2.80 ± 0.22 , Student's t-test,

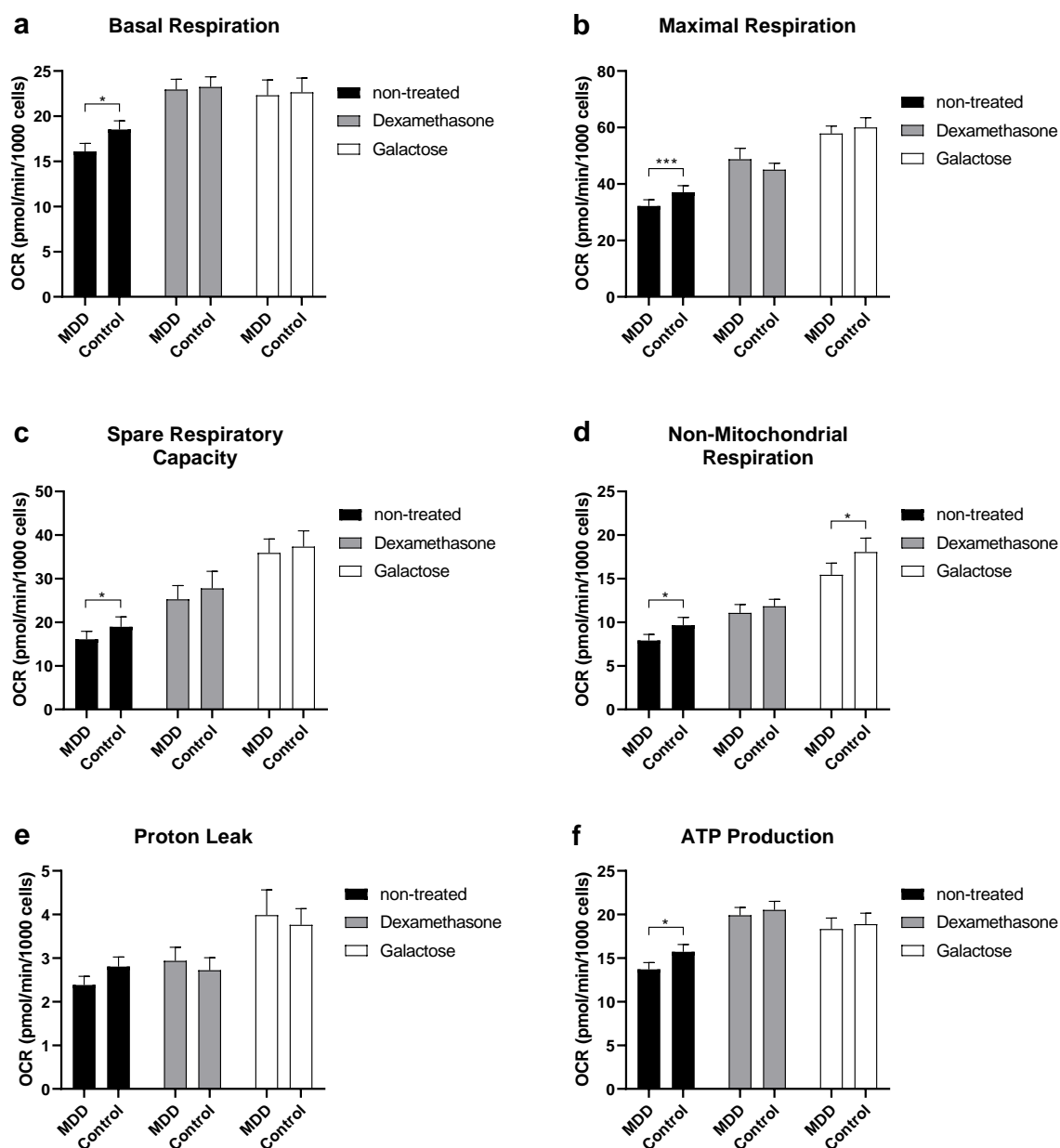


Figure 15 Seahorse XFp Flux Analyzer results of fibroblasts. (a) Shown is the basal respiration in fibroblasts of MDD and control cell lines under non-treated conditions and after one week of 1 μ M DEX or 10 mM GAL stress. Significant differences were found for MDD vs. control, non-treated (* $p < 0.05$, compared with control, Student's t-test, paired, two-tailed). (b) Shown is the maximal respiration in fibroblasts of MDD and control cell lines under non-treated conditions and after one week of 1 μ M DEX or 10 mM GAL stress. Significant differences were found for MDD vs. control, non-treated (*** $p < 0.001$, compared with control, Student's t-test, paired, two-tailed). (c) Shown is the spare respiratory capacity in fibroblasts of MDD and control cell lines under non-treated conditions and after one week of 1 μ M DEX or 10 mM GAL stress. Significant differences were found for MDD vs. control, non-treated (* $p < 0.05$, compared with control, Student's t-test, paired, two-tailed). (d) Shown is the non-mitochondrial respiration in fibroblasts of MDD and control cell lines under non-treated and after one week of 1 μ M DEX or 10 mM GAL stress. Significant differences were found for MDD vs. control, non-treated (* $p < 0.05$, compared with control, Student's t-test, paired, two-tailed) and GAL (* $p < 0.05$, compared with control, Wilcoxon matched-pairs signed rank test). (e) Shown is the proton leak in fibroblasts of MDD and control cell lines under non-treated conditions and after one week of 1 μ M DEX or 10 mM GAL stress. No significant differences were found. (f) Shown is the ATP production in fibroblasts of MDD and control cell lines under non-treated conditions and after one week of 1 μ M DEX or 10 mM GAL stress. Significant differences were found for MDD vs. control, non-treated (* $p < 0.05$, compared with control, Student's t-test, paired, two-tailed). Bar graphs show normalized mean OCR values + SEM; MDD $n=16$, control $n=16$.

paired, two-tailed, $p = 0.2041$, mean \pm SEM, figure 15 e), nor under DEX stress (MDD 2.94 ± 0.31 , CON 2.72 ± 0.29 , Student's t-test, paired, two-tailed, $p = 0.2415$ mean \pm SEM, figure 15 e) neither GAL stress (MDD 3.99 ± 0.58 , CON 3.76 ± 0.37 , Student's t-test, paired, two-tailed, $p = 0.5415$ mean \pm SEM, figure 15 e). Nevertheless, control fibroblasts show under normal conditions a higher ATP-related OCR compared to MDD fibroblasts (MDD 13.71 ± 0.76 , CON 15.72 ± 0.82 , Student's t-test, paired, two-tailed, * $p < 0.05$, $p = 0.0257$, mean \pm SEM, figure 15 f), but not subsequent to exposure of DEX (MDD 19.91 ± 0.90 , CON 20.52 , Student's t-test, paired, two-tailed, $p = 0.4110$, mean \pm SEM, figure 15 f) or GAL (MDD 18.32 ± 1.26 , CON 18.88 ± 1.27 , Student's t-test, paired, two-tailed, $p = 0.5847$, mean \pm SEM, figure 15 f).

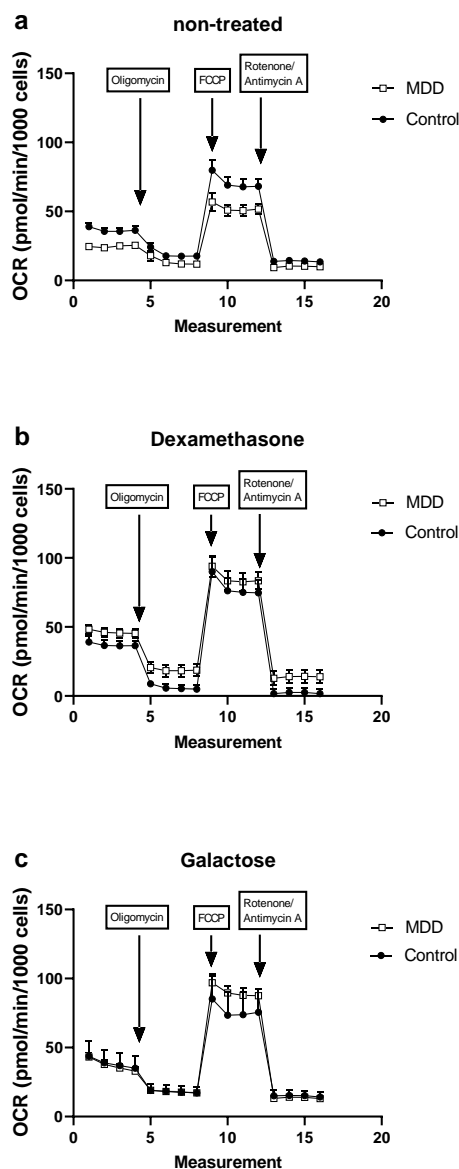


Figure 16 Mito Stress Test in fibroblasts. Exemplary curves for OCR measurement during the Mito Stress Test for MDD (white squares) and control (black dots) fibroblast lines (pair #6). Sequential injection of Oligomycin, FCCP and Rotenone/Antimycin A causes by interaction with the complexes of the ETC changes in the OCR. Figure (a) depicts graphically the differences in basal respiration and maximal respiration after injection of FCCP. The lower basal and maximal respiration of MDD cells is rescinded after one week of (b) 1 μ M DEX stress or (c) 10 mM GAL stress.

4.2.1.2 Energy profile of fibroblasts

Besides the OCR, the Seahorse XFp Flux Analyzer assesses the secretion of H^+ , the ECAR, which is a measure for glycolysis. The OCR values in dependence of the ECAR values across the entire Mito Stress Test describes the general energetic state of the fibroblasts and gives a hint whether the cells metabolism is more driven towards a glycolytic state or OXPHOS activity.

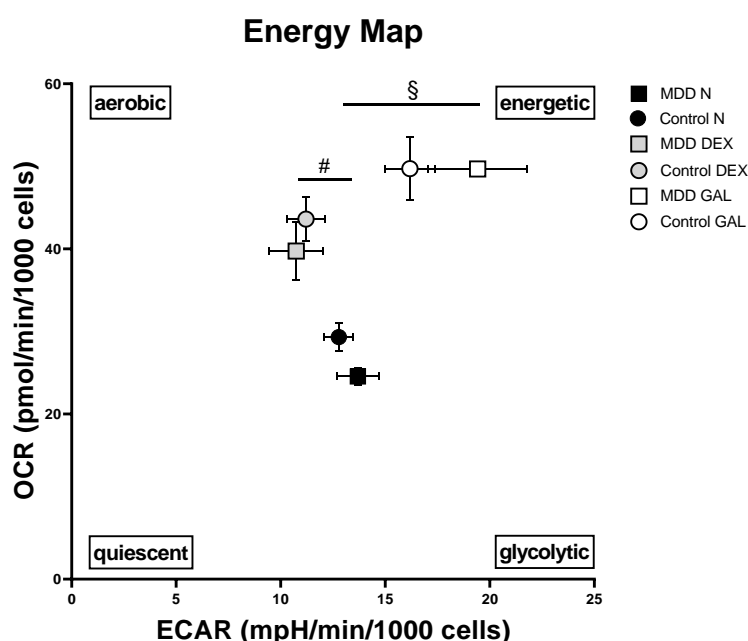


Figure 17 Energy map of fibroblasts. Mean OCR in dependence of mean ECAR are shown for MDD and control fibroblasts for non-treated, after one week of 1 μ M DEX and 10 mM GAL stress. Significant effects of treatment were found for DEX (# $p < 0.05$, compared with non-treated, ANOVA with repeated measures, Greenhouse-Geisser correction, Post-Hoc Analysis with Bonferroni) and GAL (§ $p < 0.05$, compared with non-treated, ANOVA with repeated measures, Greenhouse-Geisser correction, Post-Hoc Analysis with Bonferroni), Data are shown as mean OCR \pm SEM vs. mean ECAR \pm SEM; MDD $n=16$, control $n=16$.

In fibroblasts, the three conditions non-treated (MDD OCR 24.55 \pm 1.00 vs. CON OCR 29.32 \pm 1.70 vs. MDD ECAR 13.68 \pm 0.99 vs. CON ECAR 12.78 \pm 0.7, mean \pm SEM), DEX (MDD OCR 39.74 \pm 3.57 vs. CON OCR 43.62 \pm 2.66 vs. MDD ECAR 10.74 \pm 1.28 vs. CON ECAR 11.21 \pm 0.9, mean \pm SEM) and GAL (MDD OCR 49.69 \pm 4.58 vs. CON OCR 49.72 \pm 3.83 vs. MDD ECAR 19.42 \pm 2.38 vs. CON ECAR 16.18 \pm 1.21, mean \pm SEM, figure 17) compared to each other had significantly different effects (ANOVA with repeated measures, Greenhouse-Geisser correction, $F_{(2, 64)} = 32.904$, $p < 0.05$, $df = 2$). In particular, DEX had a significant effect on OCR and ECAR (N vs. DEX for MDD and CON, Post-Hoc Analysis, Bonferroni correction $p < 0.05$) and GAL stress changed OCR and ECAR significantly (N vs. GAL for

MDD and CON, Post-Hoc Analysis, Bonferroni correction $p \ll 0.05$). However, the conditions with DEX (MDD OCR DEX 39.74 ± 3.57 vs. MDD OCR N 24.55 ± 1.00 vs. CON OCR DEX 43.62 ± 2.66 vs. CON OCR N 29.32 ± 1.70 , MDD ECAR DEX 10.74 ± 1.28 vs. MDD ECAR N 13.68 ± 0.99 vs. CON ECAR DEX 11.21 ± 0.97 vs. CON ECAR N 12.78 ± 0.77 , mean \pm SEM, figure 18 b) and GAL (MDD OCR GAL 49.69 ± 4.58 vs. MDD OCR N 24.55 ± 1.00 vs. CON OCR GAL 49.72 ± 3.83 vs. CON OCR N 29.32 ± 1.70 , MDD ECAR GAL 19.42 ± 2.38 vs. MDD ECAR N 13.68 ± 0.99 vs. CON ECAR GAL 16.18 ± 1.21 vs. CON ECAR N 12.78 ± 0.77 , mean \pm SEM, figure 18 c) did not have significantly different effects on the groups (ANOVA with repeated measures Greenhouse-Geisser correction, $F_{(2, 64)} = 0.788$, $p = 0.457$). The shift towards a more aerobic state for DEX and the shift towards a more energetic state is similar in the MDD and the control group. The treatment with DEX (MDD OCR 39.74 ± 3.57 , MDD ECAR 10.74 ± 1.28 ; CON OCR 43.62 ± 2.66 , CON ECAR 11.21 ± 0.97 ; mean \pm SEM) compared to GAL (MDD OCR 49.69 ± 4.58 , MDD ECAR 19.42 ± 2.38 ; CON OCR 49.72 ± 3.83 , CON ECAR 16.18 ± 1.21 ; mean \pm SEM) did not have the same effect on OCR respectively ECAR (ANOVA with repeated measures Greenhouse-Geisser correction, $F_{(2, 64)} = 18.215$, $p \ll 0.05$, $df = 1.664$), which describes that DEX treatment leads to an increase in OCR and therefore OXPHOS, but a reduction of ECAR and therefore a decrease in glycolytic activity. GAL treatment caused a rise in both, OCR and ECAR and therefore fueled OXPHOS and glycolysis.

Overall, there is no significant difference between the MDD group and the control group (ANOVA with repeated measures, Greenhouse-Geisser correction, $F_{(1, 32)} = 0.340$, $p = 0.562$, $df = 1.664$). Moreover, the MDD and the control group do not differ significantly regarding their OCR (MDD N 24.55 ± 1.00 vs. CON N 29.32 ± 1.70 ; MDD DEX 39.74 ± 3.57 vs. CON DEX 43.62 ± 2.66 ; MDD GAL 49.69 ± 4.58 vs. CON GAL 49.72 ± 3.83) and their ECAR (MDD N 13.68 ± 0.99 vs. CON N 12.78 ± 0.77 ; MDD DEX 10.74 ± 1.28 vs. CON DEX 11.21 ± 0.97 ; MDD GAL 19.42 ± 2.38 vs. CON GAL 16.18 ± 1.21 , mean \pm SEM) values (ANOVA with repeated measures Greenhouse-Geisser correction, $F_{(1, 32)} = 2.024$, $p = 0.160$, $df = 1$).

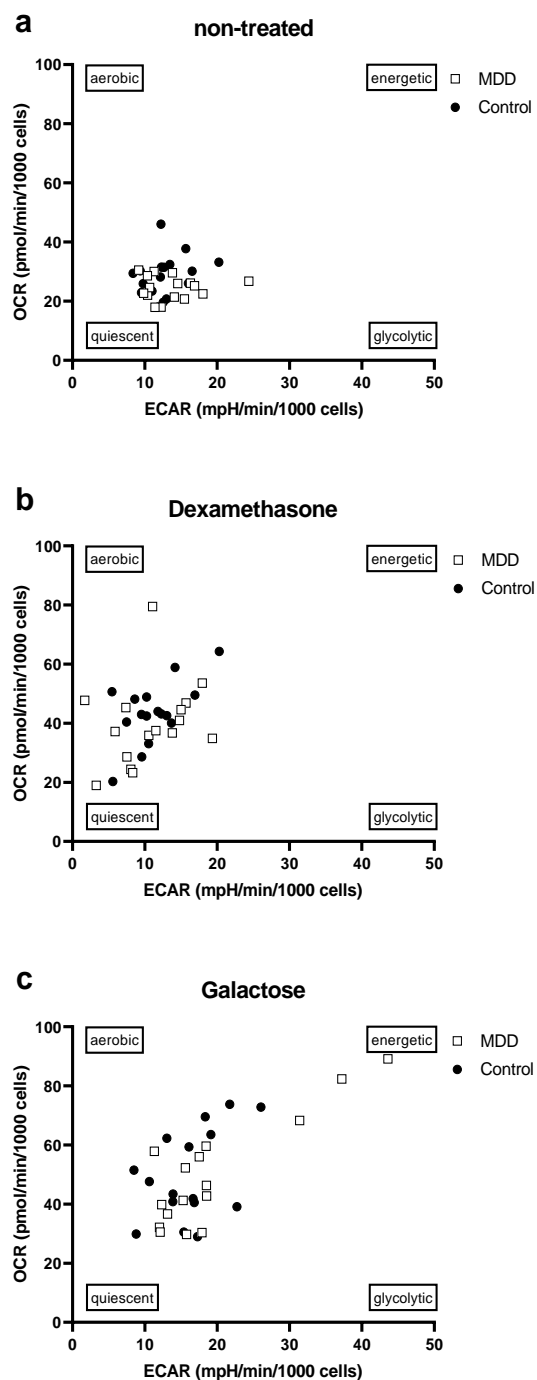


Figure 18 Energy maps of fibroblasts for the three conditions. Single OCR values in dependence of single ECAR values are shown of 16 MDD and control pairs for the three different conditions (a) non-treated (b) after one week of 1 μ M dexamethasone stress and (c) after one week of galactose stress. Due to the induction of either hormonal or metabolic stress OXPHOS and glycolysis are fueled, which can be seen in an increase in OCR and ECAR values. MDD and control fibroblast lines do not significantly differ in their OCR and ECAR values for any of the conditions (ANOVA with repeated measures, Greenhouse-Geisser correction, $p > 0.05$). However, both stressors had significant effects on the energetic parameters OCR and ECAR in MDD and control fibroblast lines (ANOVA with repeated measures, Greenhouse-Geisser correction, $p < 0.05$). After (b) dexamethasone stress fibroblasts are mainly driven towards a more aerobic state (shift along the y-axis), whereas (c) galactose induces a more energetic state (shift along the x-axis and y-axis). The lack of glucose inhibits energy provision through glycolysis and forces the fibroblasts towards meeting their energetic needs by OXPHOS. MDD fibroblast lines are indicated by white squares, black dots represent control fibroblast lines; MDD $n=16$, control $n=16$.

4.2.2 ATP content

Since differences in the respiration of fibroblasts from MDD patients compared to control fibroblasts were unraveled, the energy production of mitochondria was examined in detail. The main function of mitochondria is the production of energy in form of ATP. In the last step of the ETC, the ATP synthase converts ADP and inorganic phosphate to ATP. Hence, to test a direct readout parameter of the mitochondrial function and function of

the Complex V of the ETC, the ATP content was determined in the 16 patient and control fibroblast cell lines by a luminescence assay.

As shown in figure 19, there are statistically significant differences in the ATP content between MDD patient fibroblasts and control fibroblasts under non-treated conditions. Control cells contain more ATP than MDD cells (MDD 59908 ± 11595 , CON 73315 ± 12402 , Wilcoxon matched-pairs signed rank test, * $p < 0.05$, $p = 0.036$, mean \pm SEM). Moreover, ATP contents significantly differ between MDD fibroblasts and control fibroblasts after DEX stress. Patient cells contain a significantly lower amount of ATP than cells of healthy subjects (MDD 52419 ± 10382 , CON 58836 ± 11328 , Wilcoxon matched-pairs signed rank test, ** $p < 0.01$, $p = 0.0052$, mean \pm SEM). These differences could not be detected under GAL stress (MDD 89158 ± 15043 , CON 99162 ± 14537 , Wilcoxon matched-pairs signed rank test, $p = 0.463$, mean \pm SEM), indicating that only hormonal stress in the cellular model leads to an altered provision of ATP in MDD patient cells, but not metabolic stress. The differences detected under non-treated conditions correlate with the reduced OCR values in various parameters in Seahorse XFp Analyzer measurements in MDD cells.

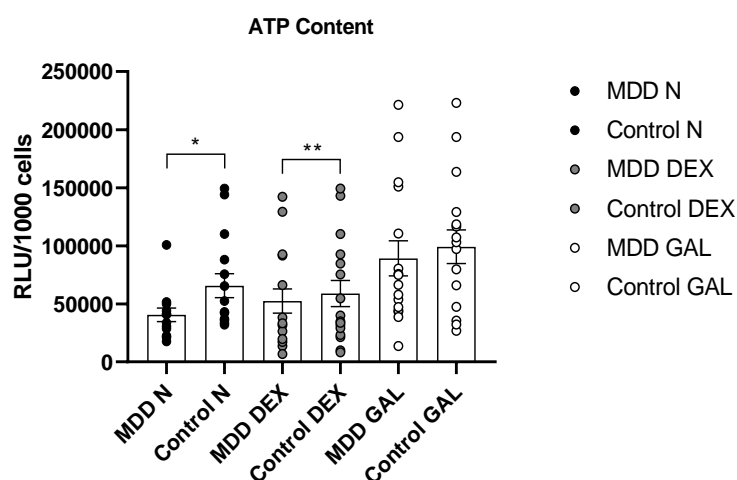


Figure 19 ATP content in fibroblasts. Shown is the ATP content in MDD and control fibroblast lines under non-treated conditions and after one week of 1 μ M DEX or 10 mM GAL stress. Significant differences were found for MDD vs. control, non-treated (* $p < 0.05$, Wilcoxon matched-pairs signed rank test) and DEX (** $p < 0.01$, compared with control, Wilcoxon matched-pairs signed rank test). Bar graphs show normalized mean RLU values \pm SEM. Dots show the distribution of single RLU values for MDD and control fibroblast lines; MDD $n=16$, control $n=16$.

4.2.3 Bioenergetic properties and mitochondria-related homeostasis in fibroblasts

The function of the ETC is directly associated with other measurable parameters which are linked to crucial functions of the mitochondria and therefore for the viability, survival

and homeostasis of the cell. Besides the transport of electrons along the Complexes I-IV, a gradient of protons is built across the inner mitochondrial membrane. This gradient is decisive for the drive of the ATP synthase and therefore the production of ATP. This electro-chemical gradient across the IMM is defined as the MMP. In addition, the mitochondria's function of serving as buffer for the positively charged Ca^{2+} , underlies the negative MMP. With the help of fluorescent dyes and live cell imaging those two parameters were determined in viable fibroblasts.

4.2.3.1 Mitochondrial Membrane Potential

The MMP in fibroblasts was measured by loading the mitochondria with the cationic dye JC-1 (see figure 20).

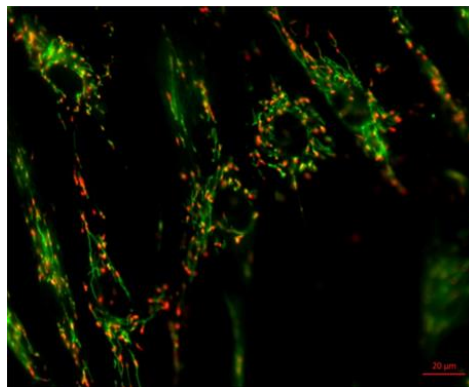


Figure 20 Fibroblasts loaded with the cationic dye JC-1. Aggregates of the dye fluoresce red, monomers fluoresce green. Scale bar indicates 20 μm .

Depending on the MMP, the dye fluoresces red or green. The ratio between the two signals is directly associated with the MMP. Higher red/green ratios indicate a more negative MMP.

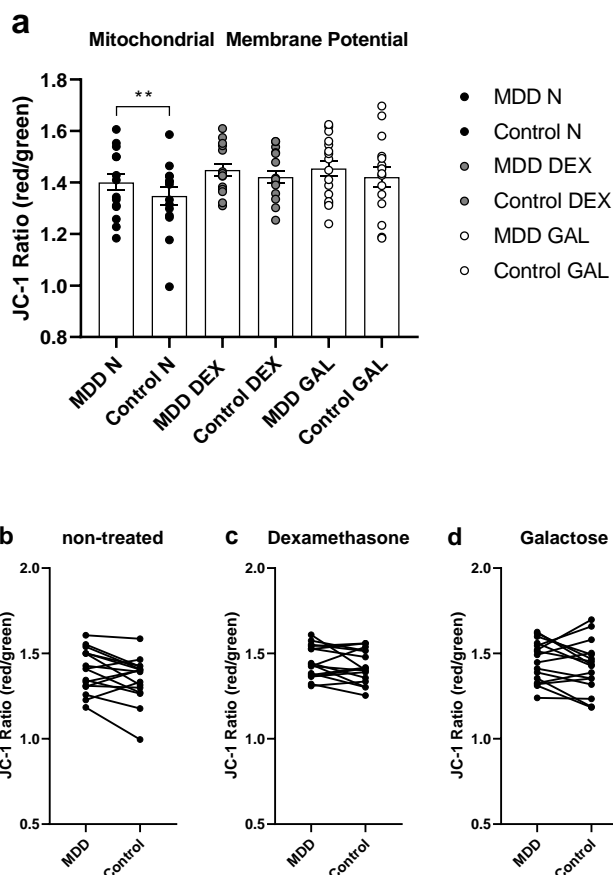


Figure 21 Mitochondrial membrane potential of fibroblasts. **(a)** Shown are the red/green ratios of MDD and control fibroblast lines under non-treated conditions and after one week of 1 μ M DEX or 10 mM GAL stress. Significant differences were found for MDD vs. control, non-treated (* $p < 0.05$, compared with control, Student's t-test, paired, two-tailed). Bar graphs show mean red/green ratios \pm SEM, MDD $n=16$, control $n=16$). Dots show the distribution of single red/green values for MDD and control fibroblast lines under non-treated conditions and after one week of 1 μ M DEX or 10 mM GAL stress; MDD $n=16$, control $n=16$. **b-d** Graphs show the pairwise red/green ratios for each MDD and control fibroblast line under **(b)** non-treated conditions and **(c)** after one week of 1 μ M DEX stress or **(d)** 10 mM GAL stress.

In fibroblasts, there are detectable significant differences in the MMP between MDD cells and control cells (figure 21 a). MDD cells under non-treated conditions show a higher red/green ratio suggesting that the MMP is more negative in MDD cells than in control cells (MDD 1.40 ± 0.0008 , CON 1.35 ± 0.0008 , Student's t-test, paired, two-tailed, ** $p < 0.01$, $p = 0.419$, mean \pm SEM). Considering the results of the respiratory experiments, where MDD cells show a lower OCR and the fact that MDD contain less ATP, it might be assumed that the ATP synthase itself is less active in MDD cells. If the ATP synthase is less active, the MMP is not degraded by a reflux of H^+ into the mitochondrion as much as in control fibroblasts and therefore MDD fibroblasts harbor lower ATP levels compared to healthy control cells under non-treated conditions.

These alterations are not present under both stress conditions (DEX, MDD 1.46 ± 0.006 , CON 1.42 ± 0.006 , Student's t-test, paired, two-tailed, $p = 0.1874$; GAL, MDD 1.46 ± 0.008 , CON 1.42 ± 0.009 , Student's t-test, paired, two-tailed, $p = 0.2443$; mean \pm SEM, figure 21 a). Figure 21 a also depicts that the single values within the groups show only little variation, also indicated by the small error bars. When comparing the individual pairs, the difference between the MDD cells and the control cells vary from pair to pair (figure 21 c-d). Some of the gender- and age-matched cell line pairs show bigger differences in the MMP, whereas other paired cell lines display smallest or almost no differences in their MMP.

4.2.3.2 Calcium Homeostasis

The capability of mitochondria to store Ca^{2+} and to serve as a buffer for the important second messenger molecule is dependent on the MMP. Cytosolic Ca^{2+} concentrations were assessed by loading viable fibroblasts with the ratiometric dye Fura-2/AM ("Fura-2"). The two excitation spectra of Fura-2 in a Ca^{2+} -bound (380 nm) or Ca^{2+} -free (340 nm) state are directly related to the cytosolic amount of Ca^{2+} . The ratio between the emission 340 nm/380 nm reflect the Ca^{2+} homeostasis in the cell. High 340 nm/380 nm ratios indicate higher Ca^{2+} concentrations in the cytosol.

Overall, there are no statistically significant differences between cells derived from depressed patients and healthy controls in their Ca^{2+} homeostasis (figure 22 a). The 340 nm/380 nm ratio, which reflects the Ca^{2+} amount in the cytosol of the cell, is roughly the same und MDD cells and control cells (MDD 0.67 ± 0.013 , CON 0.67 ± 0.009 , Wilcoxon matched-pairs signed rank test, $p = 0.4954$, mean \pm SEM). Measurements after one week of stress did not result in any statistically significant differences either (DEX, MDD 0.64 ± 0.005 , CON 0.64 ± 0.006 Student's t-test, paired, two-tailed, $p = 0.2285$; GAL, MDD 0.62 ± 0.005 , CON 0.62 ± 0.006 Student's t-test, paired, two-tailed, $p = 0.6648$; mean \pm SEM). Figure 22 a also depicts that the values within one group do not vary strongly. Nonetheless, in some pairs there are bigger intra-pair-individual differences than in other pairs. These pairwise comparisons are shown in figure 22 (b-d). It is obvious that pairs with higher differences in the Fura-2 ratio do not show these high differences after one week of hormonal or metabolic stress. Interestingly, these effects were evened out after the application of the stress protocol.

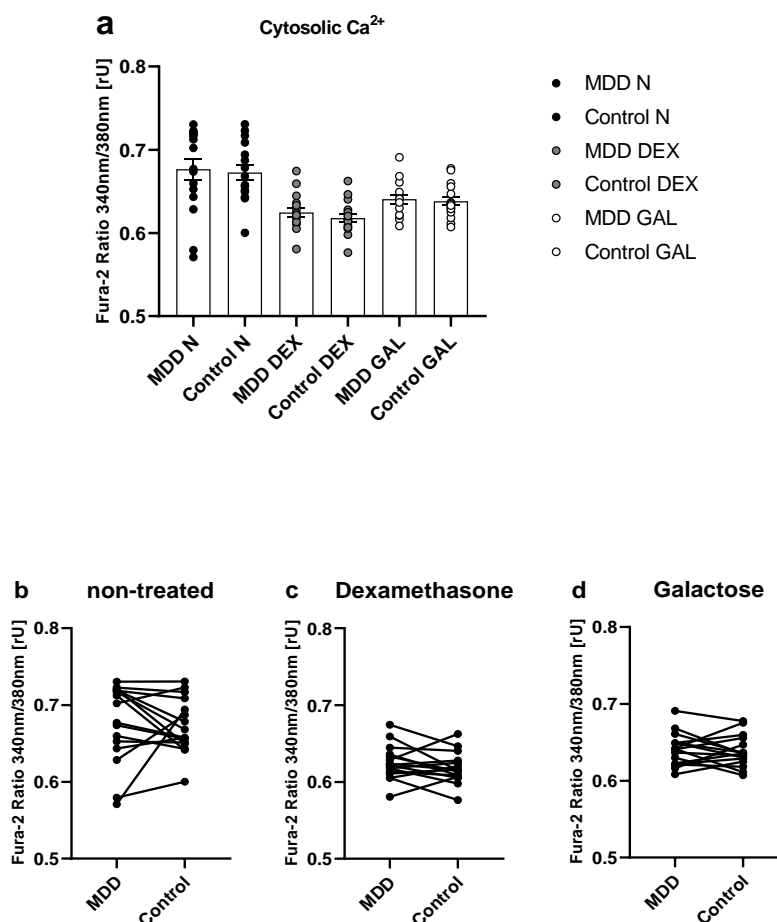


Figure 22 Cytosolic Ca²⁺ homeostasis in fibroblasts. **(a)** Shown are the 340nm/380nm ratios of MDD and control fibroblast lines under non-treated conditions and after one week of 1 µM DEX or 10 mM GAL stress. No significant differences were found. Bar graphs show mean 340nm/380nm ratios ± SEM. Dots show the distribution of single 340 nm/380 nm values for MDD and control fibroblast lines under non-treated conditions and after one week of 1 µM DEX or 10 mM GAL stress; MDD n=16, control n=16. **b-d** Graphs show the pairwise 340 nm/380 nm ratios for each MDD and control fibroblast line under **(b)** non-treated conditions and **(c)** after one week of 1 µM DEX stress or **(d)** 10 mM GAL stress.

4.3 Mitochondrial content: mtDNA copy number in fibroblasts

In the present study, it could be shown that there are deficiencies in respiratory parameters. Additionally, there are differences in the ATP production and the MMP. In the literature it has been shown that a reduced energy metabolism is correlated with reduced number in mtDNA, whereas higher mtDNA copy number is associated with a lower level of depression (Kim et al. 2001). MtDNA replication does not coincide with the cell cycle and occurs independently of nuclear DNA replication (Clayton and Bogenhagen 1977). Consequently, the mtDNA copy number was determined in relation to the diploid nuclear genome in 16 MDD and control fibroblast cell lines.

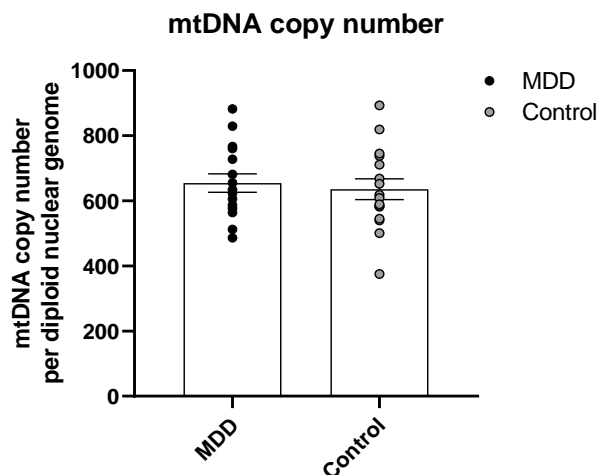


Figure 23 MtDNA copy number in 16 MDD and patient fibroblast cell lines. Shown are the mtDNA copy numbers per nDNA of MDD and control fibroblast lines. No significant differences were found. Bar graph show mean mtDNA copy number \pm SEM. Dots show the single values of mtDNA copy numbers for MDD and control fibroblast lines; MDD n=16, control n=16.

As depicted in figure 23, there are no significant differences in the mtDNA copy number when MDD and control cell lines are compared (MDD 654 ± 28.04 , CON 636 ± 31.68 , Student's t-test, paired, two-tailed, $p = 0.6540$, mean \pm SEM).

MtDNA copy numbers are, besides the telomere length, part of the "biological clock" and studies prove that there are significant correlations between mtDNA copy number and chronological age (Fries et al. 2017; Mengel-From et al. 2014). In this case we cannot detect a correlation between age and mtDNA copy number (Linear Regression Analysis, $R^2 = 0.01742$, $p = 0.4714$). Single values of the mtDNA copy numbers can be taken from Table 35 (see Appendix), the age of MDD patients and controls are listed in Table 16.

4.4 Successful reprogramming of fibroblasts into iPSCs and induction of NPCs

4.4.1 Cultivation and reprogramming of human dermal fibroblasts

A few days after taking the skin biopsies and cultivation of the skin pieces, primary human dermal fibroblasts were growing out of the skin piece. Every cell line could be successfully cultivated and cryo-stored. Early passages of the primary fibroblast lines were successfully reprogrammed in to iPSCs. By episomal (Epi 5) reprogramming with the Yamanka factors stem cell formation was observed after 21-33 days (Takahashi and

Yamanaka 2006). Stem cell colonies were successfully isolated and cultivated. With immunocytochemistry, staining, markers for pluripotency were detected and labelled.

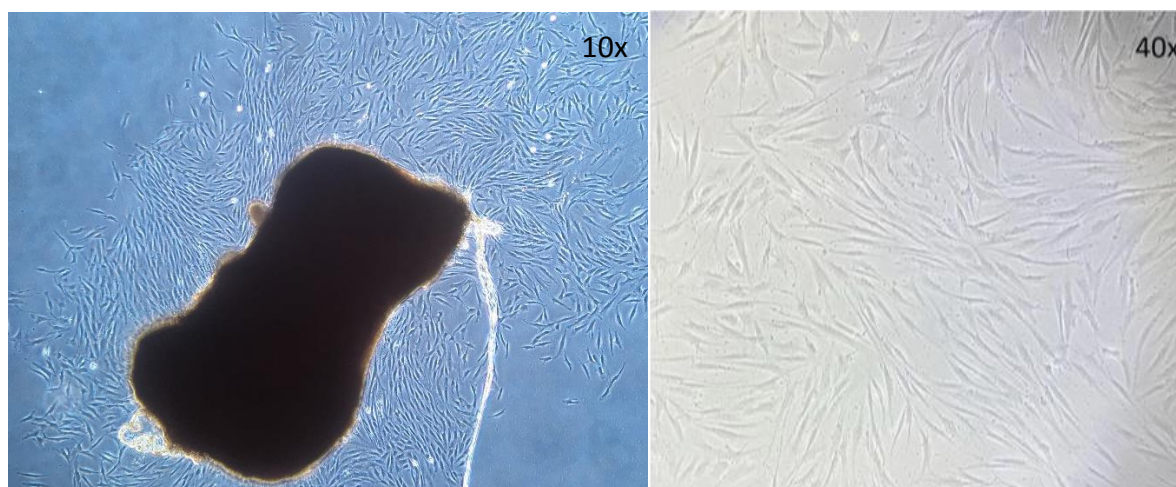


Figure 24 Fibroblasts in cell culture. **(left)** Shown is a piece of skin with primary human dermal fibroblasts growing out. 10X magnification. **(right)** Primary Human dermal fibroblasts in culture. 40X magnification.

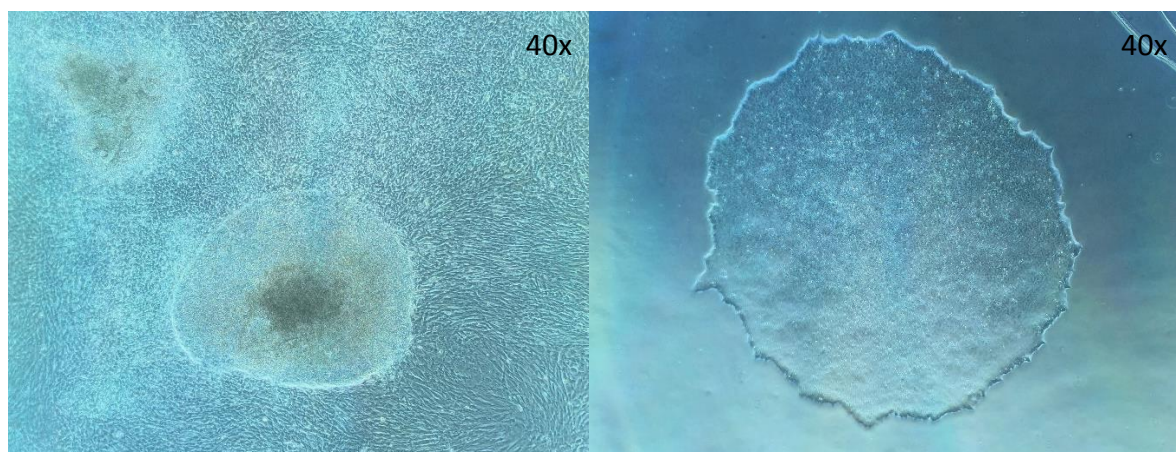


Figure 25 Reprogramming and iPSC clone separation. **(left)** iPSC clone formation after 21 days of episomally induced reprogramming of primary human fibroblasts. 40X magnification. **(right)** selected iPSC clone in culture. 40X magnification.

4.4.2 Quality control for pluripotency

The quality control of the iPSCs was conducted by a collaborating laboratory (Prof. Dr. Riemenschneider, Neuropathology, University Hospital of Regensburg, Regensburg, Germany). By PluriTest analysis the first 8 patient and 7 control cell lines were examined (Schulze et al., 2016). For 8 of the 15 iPSC lines pluripotency could be confirmed. One probe is still pending. The 7 cell lines are close to threshold values. Most likely, the cell lines did not pass the PluriTest not because of a lack of pluripotency, but most likely

because improper iPSC sample collecting with insufficient cleaning of iPSCs colonies and therefore fibroblast contamination.

Table 22 Results of the PluriTest for pluripotency of iPSC lines.

Cell line	result	remarks
CON2	not pluripotent	threshold for pluripotency: 1424, reached value: 1277.0
CON3	not pluripotent	threshold for pluripotency: 1424, reached value 1330.2
CON4	pluripotent	---
CON5	pluripotent	---
CON6	not pluripotent	threshold for pluripotency: 1424, reached value 1330.2
CON7	pluripotent	---
CON8	pluripotent	---
MDD1	not pluripotent	threshold for pluripotency: 1424, reached value: 1358.5
MDD2	not pluripotent	threshold for pluripotency: 1424, reached value: 1336.6
MDD3	not pluripotent	threshold for pluripotency: 1424, reached value: 1306.5
MDD4	pluripotent	---
MDD5	pluripotent	---
MDD6	pluripotent	---
MDD7	pluripotent	---
MDD8	not pluripotent	threshold for pluripotency: 1424, reached value: 1404.9

4.4.3 Differentiation of neural progenitor cells

For each iPSC cell line one clone was used to obtain NPCs. Neural induction from iPSC cells took 7 days to transform iPSC colonies to early neural progenitor cells.

NPCs were passaged until p5 in order to reach a higher maturity. Then they were stained for neural progenitor markers PAX6 and SOX2 (figure 26). Positive staining for a percentage higher than 70% is considered as successful differentiation. Table 23 shows that all the differentiated cell lines are > 70% positive for both markers and the differentiation was successful.

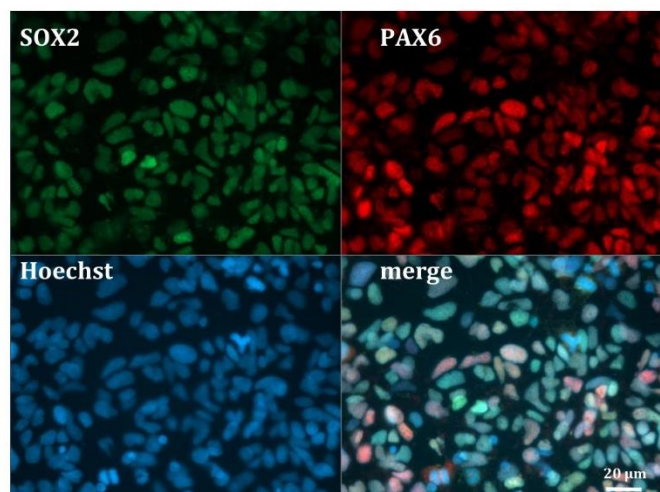


Figure 26 Immunostaining of NPC line MDD4. Staining against (**top left**) SOX2 (green, 488 rat), (**top right**) PAX6 (red, Cy3) and (**bottom left**) nuclei (blue). (**bottom right**) merge picture. Scale bar indicates 20 μm .

Table 23 Percentage of PAX6/SOX2 positively stained NPCs

cell line	clone	PAX6-positiv (%)	SOX2-positiv (%)
CON1	k 6	87.61	86.00
MDD1	k 4	90.81	96.25
CON2	k 12	90.67	89.96
MDD2	k 12	82.22	85.35
CON3	k 2	84.64	85.60
MDD3	k 5	91.73	91.41
CON4	k 4	86.44	90.76
MDD4	k 12	84.31	86.94
CON5	k 1	90.43	93.01
MDD5	k 4	87.76	89.58
CON6	k 17	93.14	92.85
MDD6	k 13	91.78	89.16
CON7	k 13	91.71	91.71
MDD7	k 6	89.12	90.38
CON8	k 2	88.56	89.67
MDD8	k 13	88.26	90.16
CON12	k 5	90.67	87.93
MDD12	k 4	75.34	77.89

4.5 Alterations of the mitochondrial metabolism in cells of the CNS: Neural progenitor cells depict changes in energy supply

Despite that fact that fibroblasts are a suitable model to investigate mitochondria function, since differences in the OXPHOS, MMP could be determined in this study and by others (Garbett et al. 2015; Karabatsiakakis et al. 2014), neural cells are of large interest. MDD is a disease of the body and the brain and therefore we extended our studies to

investigate mitochondrial function in neural cells. Moreover, the NPCs depend on glycolysis to a higher extent when compared to fibroblasts. NPCs were exposed to hormonal (DEX) stress, but not to metabolic stress induced by galactose, since NPCs still mainly rely on glycolysis like iPSCs and do not survive without glucose over one week (Lorenz et al. 2017).

NPCs are an attractive cellular model since they are an intermediate state between iPSCs and neurons and could hint at the impact of mitochondrial dysfunction in the neural development (Mlody et al. 2016; Zheng et al. 2016). The developing brain is highly dynamic and dependent on proper energetic supply (Edmond 1992). Deficiencies in energy supply could therefore influence neuron growth and renewal.

4.5.1 Mito Stress Test: ETC and glycolysis

4.5.1.1 Respiration of NPCs

Differentiated NPCs were examined pairwise with the Mito Stress Test protocol in the Seahorse Flux XFp Flux Analyzer. After the serial application of four inhibitors of the ETC – Oligomycin, FCCP and Rotenone/Antimycin A – the respiratory parameters, namely the basal and maximal respiration, the non-mitochondrial respiration, the proton leak, the ATP-related oxygen consumption and the spare respiratory capacity were determined.

Under normal conditions, NPCs from patients exhibit a significantly lower basal respiration compared to NPCs from controls (MDD 88.49 ± 3.42 , CON 103.72 , Student's t-test, paired, two-tailed, ** $p > 0.01$, $p = 0.0098$, mean \pm SEM, figure 27 a).

However, when the NPCs undergo one week of hormonal stress, the differences in the basal respiration are repealed. There are no significant differences between MDD and controls after DEX stress in basal respiration (MDD 94.53 ± 5.94 , CON 107.26 ± 6.49 , Student's t-test, paired, two-tailed, * $p > 0.05$, $p = 0.0658$, mean \pm SEM, figure 27 a). NPCs exhibit in comparison to fibroblasts a lower rise in OCR after the application of FCCP. Whereas fibroblasts can double their OCR, the maximal respiration of NPCs is only about one third higher compared to the NPCs basal respiration. The main source of energy of NPCs is not OXPHOS but glycolysis which results in lower maximal respiratory abilities.

The maximal respiration of MDD NPCs and controls NPCs does not differ under non-treated conditions (MDD 114.94 ± 5.55 , CON 131.15 ± 11.54 , Student's t-test, paired, two-tailed, $p = 0.1540$, mean \pm SEM, figure 27 b) neither after DEX stress (MDD 114.61 ± 9.84 , CON 121.34 ± 2.96 , Student's t-test, paired, two-tailed, $p = 0.4294$, mean \pm SEM, figure 27 b).

Closely related to the maximal and the basal respiration, is the spare respiratory capacity. The spare respiratory capacity is important for the cells' survival in case of an energetic challenge and is a measure for the cell's energetic reserves. In general, NPCs possess a lower spare respiratory capacity than fibroblasts, since OXPHOS is not their main source of ATP production. In case of an energetic demand NPCs rely on other energetic sources like glycolysis, most probably. In NPCs the spare respiration capacity does not result in

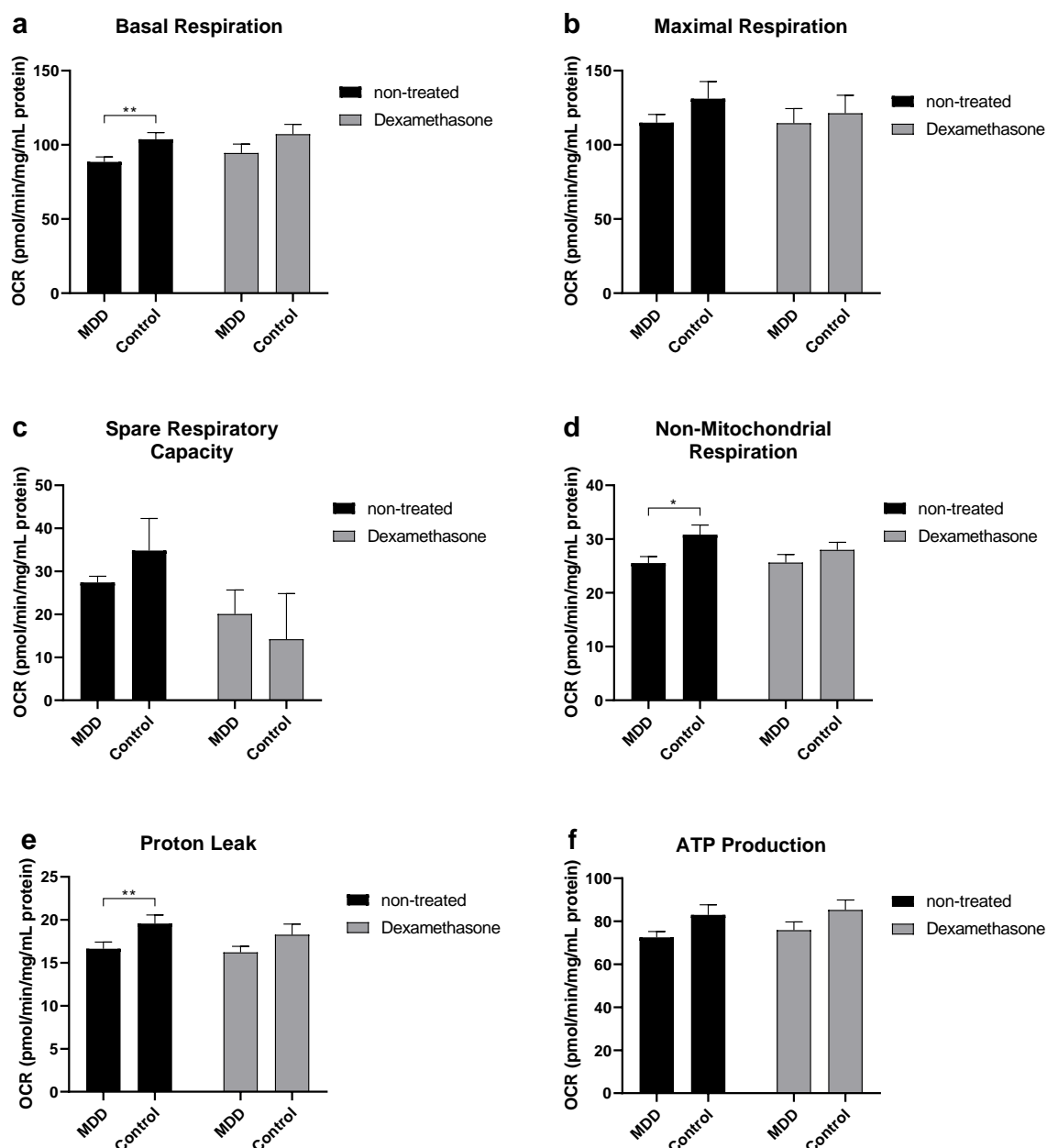


Figure 27 Seahorse XFp Flux analyzer results of NPCs. (a) Shown is the basal respiration in NPCs of MDD and control cell lines under non-treated conditions and after one week of 1 μ M DEX stress. Significant differences were found for MDD vs. control, non-treated (** $p < 0.01$, compared with control, Student's t-test, paired, two-tailed). (b) Shown is the maximal respiration of NPCs of MDD and control cell lines under non-treated conditions and after one week of 1 μ M DEX stress. No significant differences were found. (c) Shown is the spare respiratory capacity in NPCs of MDD and control cell lines under

non-treated conditions and after one week of 1 μM DEX stress. No significant differences were found. (d) Shown is the non-mitochondrial respiration in NPCs of MDD and control cell lines under non-treated conditions and after one week 1 μM DEX stress. Significant differences were found for MDD vs. control, non-treated (* $p < 0.05$, compared with control, Wilcoxon matched-pairs signed rank test). (e) Shown is the proton leak in NPCs of MDD and control cell lines under non-treated conditions and 1 μM DEX. Significant differences were found for MDD vs. control, non-treated (* $p < 0.05$, compared with control, Wilcoxon matched-pairs signed rank test). (g) ATP production in NPCs of MDD and control cell lines under non-treated conditions and after one week of 1 μM DEX stress. No significant differences were found. Bar graphs show normalized mean OCR values + SEM; MDD $n=9$, control $n=9$.

any significant differences between patients and controls under normal conditions (MDD 27.04 ± 1.44 , CON 34.81 ± 7.46 , Student's t-test, paired, two-tailed, $p = 0.5256$, mean \pm SEM, figure 27 c). Likewise, it does not significantly alter between MDD subjects and healthy subjects after the cells were exposed to DEX (MDD 20.08 ± 5.59 , CON 14.21 ± 10.62 , Wilcoxon matched-pairs signed rank test, $p = 0.4258$, mean \pm SEM, figure 27 c). Another parameter that is determined in the Mito Stress Test is the non-mitochondrial OCR. Non-mitochondrial OCR has usually been attributed to inefficient mitochondrial electron transport, or to other cellular oxidative reactions not linked to energy metabolism (Herst et al. 2004).

NPCs from controls have a significantly higher non-mitochondrial respiration compared to MDD patients at normal culturing conditions (MDD 25.54 ± 1.20 , CON 30.82 ± 1.81 , Wilcoxon matched-pairs signed rank test, * $p < 0.05$, $p = 0.0195$, mean \pm SEM, figure 27 d). Similar to the observation for the basal respiration, the non-mitochondrial respiration is of no significant difference after hormonal stress exposure (25.62 ± 1.52 , CON 28.00 ± 1.40 , Wilcoxon matched-pairs signed rank test, two-tailed, $p = 0.2659$, mean \pm SEM, figure 27 d). As proton leak depicts the protons that migrate into the matrix without producing ATP, it makes the coupling of substrate oxygen and ATP generation incomplete. Proton leak is the principal, but not the only, mechanism that incompletely couples substrate oxygen to ATP generation (Cheng et al. 2017). In this parameter NPCs from MDD patients significantly differ. The proton leak-associated OCR is significantly higher in control cells under normal conditions (MDD 16.63 ± 0.79 , CON 19.56 ± 1.01 , Student's t-test, paired, two-tailed, ** $p < 0.01$, $p = 0.0078$, mean \pm SEM, figure 26 e). However, after DEX stress there are no significant aberrations between MDD cells and control cells (MDD 16.22 ± 0.70 , CON 21.02 ± 2.96 , Student's t-test, paired, two-tailed, $p = 0.0771$, mean \pm SEM, figure 27 e). Regarding the ATP-related OCR, there are no differences between MDD NPCs and control NPCs, neither under non-treated conditions (MDD 72.55 ± 2.70 , CON 82.94 ± 4.77 , Student's t-test, paired, two-tailed, $p = 0.0537$, mean \pm SEM, figure 27 f) nor after one week of

hormonal stress (MDD 75.87 ± 3.83 , CON 85.27 ± 4.64 , Student's t-test, paired, two-tailed, $0.1368m$, , mean \pm SEM, figure 27 f).

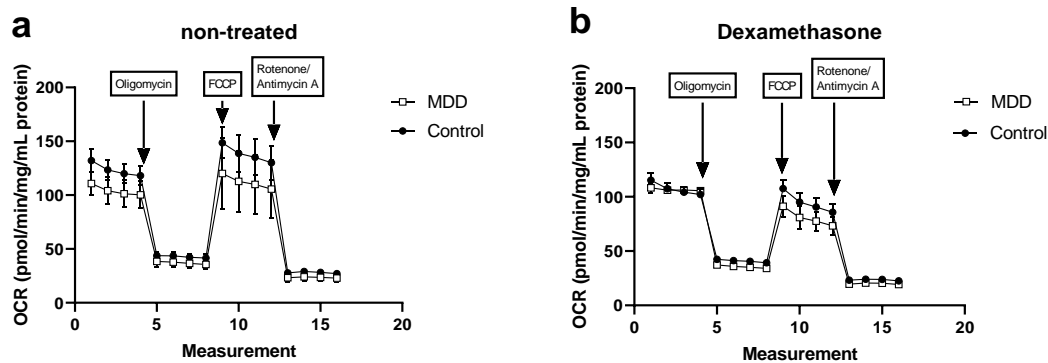


Figure 28 Mito Stress Test in NPCs. Typical course for OCR values during a stress protocol in the Seahorse XFp Flux Analyzer before compound injection and after application of Oligomycin, FCCP and Rotenone/Antimycin A for MDD NPCS (white squares) and control NPC cell line (pair #9). Figure (a) depicts the differences in basal and maximal respiration, which are erased respectively diminished after (b) one week of $1 \mu\text{M}$ DEX stress. Characteristic is also the lowered rise in maximal respiration – and the resulting reduction in spare respiratory capacity – after FCCP injection due to hormonal stress.

4.5.1.2 Energy profile of NPCs

OCR and ECAR can be used to describe the energetic state of NPCs, as well (figure 29). OCR in dependence of ECAR values across the Mito Stress Test can describe the energy states MDD and controls for the two different conditions.

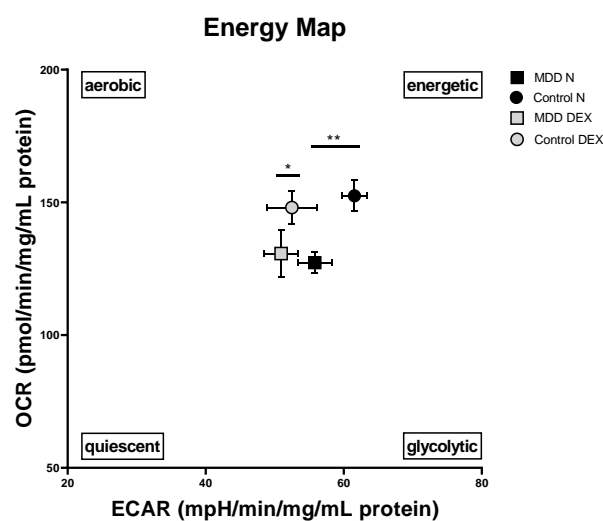


Figure 29 Energy map of NPCs. Mean OCR in dependence of mean ECAR are shown for MDD and control NPCs for non-treated conditions and after one week of $1 \mu\text{M}$ DEX stress. No significant effects of treatment were found. Significant differences were found for MDD vs. control for the non-treated condition (* $p < 0.05$, compared to control, ANOVA with repeated measures Greenhouse-Geisser correction) and after one week of $1 \mu\text{M}$ DEX stress (** $p <$

0.05, compared to control, ANOVA with repeated measures, Greenhouse-Geisser correction). Data are shown as mean OCR \pm SEM vs. mean ECAR \pm SEM; MDD n=9, control n=9.

The treatment with DEX (MDD OCR 130.74 \pm 8.74 vs. CON OCR 148.07 \pm 6.19 vs. MDD ECAR 50.92 \pm 2.50 vs. CON ECAR 52.49 \pm 3.65, mean \pm SEM, figure 30 b) compared to non-treated (MDD OCR 127.26 \pm 4.02 vs. CON OCR 152.46 \pm 5.90 vs. MDD ECAR 55.84 \pm 2.40 vs. CON ECAR 61.55 \pm 1.84, mean \pm SEM, figure 30 a) did not have significantly different effects on MDD and control NPCs, since the shift towards a less glycolytic state and more energetic state is similar (ANOVA with repeated measures, Greenhouse-Geisser correction, $F_{(1,32)} = 1.037$, $p = 0.316$, $df = 1$, figure 29). Overall, the DEX treatment did not alter OCR (MDD OCR DEX 130.74 \pm 8.74 vs. MDD OCR N 127.26 \pm 4.02; CON OCR DEX 148.07 \pm 6.19 vs. CON OCR N 152.46 \pm 5.90) compared to ECAR (MDD ECAR DEX 50.92 \pm 2.50 vs. MDD ECAR N 55.84 \pm 2.40, CON ECAR DEX 52.49 \pm 3.65 vs. CON ECAR N 61.55 \pm 1.84, mean \pm SEM) significantly different across both groups (ANOVA with repeated measures, Greenhouse-Geisser correction, $F_{(1,32)} = 1.232$, $p = 0.275$). The treatment with DEX did also not have a different effect within the groups on the parameters OCR and ECAR (ANOVA with repeated measures, Greenhouse-Geisser correction, $F_{(1,32)} = 0.101$, $p = 0.753$, $df = 1$). The treatment with the hormonal stressor causes a slight reduction in OXPHOS in control cells as well as a drop in glycolytic activity for MDD and control cells.

However, when comparing the groups themselves, there is a significant difference between MDD and control NPCs (ANOVA with repeated measures, Greenhouse-Geisser correction, $F_{(1,32)} = 10.677$, $p = 0.003$). MDD and control NPCs significantly differ regarding their OCR (MDD N 127.26 \pm 4.02 vs. CON N 152.46 \pm 5.90, MDD DEX 130.74 \pm 8.74 vs. CON DEX 148.07 \pm 6.19) and ECAR (MDD N 55.84 \pm 2.40 vs. CON N 61.55 \pm 1.84, MDD DEX 50.92 \pm 2.50 vs. CON DEX 52.49 \pm 3.65, mean \pm SEM) values (ANOVA with repeated measures Greenhouse-Geisser correction, $F_{(1,32)} = 5.343$, $p = 0.27$). The MDD group has significantly lower OCR and ECAR values for non-treated as well as for DEX conditions. Conclusively, MDD NPCs show a lower overall metabolism compared to control NPCs, under non-treated conditions and after DEX stress.

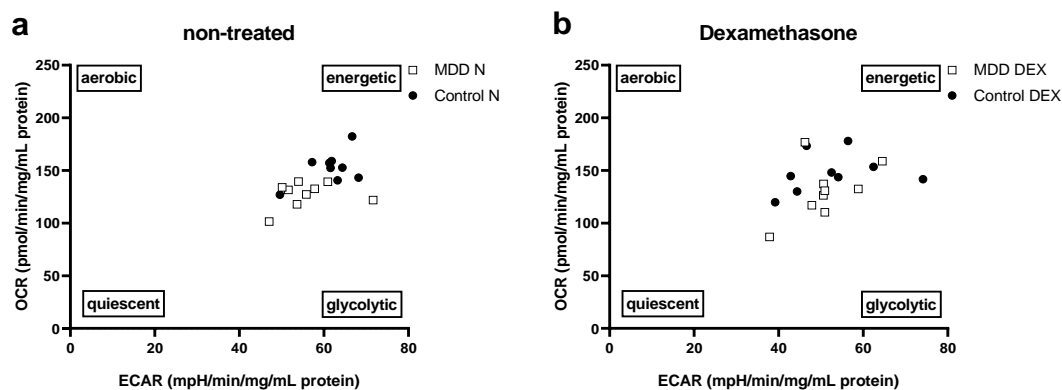


Figure 30 Energy map for NPCs for the two conditions. OCR values in dependence of the ECAR values are shown for (a) non-treated conditions and (b) after one week of 1 μM DEX stress. DEX stress caused predominantly a reduction in overall metabolism for both groups, which is indicated by a shift towards more glycolytic (y-axis) state and a shift towards more quiescent (x-axis) state. However, this effect is not statistically significant (ANOVA with repeated measures, Greenhouse-Geisser correction, $p > 0.05$). Nevertheless, there are significant differences between MDD and control NPC lines, since OCR and ECAR values are lower in MDD NPCs. Significant differences were found for both conditions (compared to control group, ANOVA with repeated measures, Greenhouse-Geisser correction, $p < 0.05$). MDD NPC lines are indicated by white squares, black dots represent control NPC lines; MDD $n=9$, control $n=9$.

4.5.2 ATP content

The main function and the crucial task also of mitochondria in NPCs is to generate ATP out of ADP and P_i . In the last step of the ETC the ATP synthase is driven by the proton gradient over the membrane that is built up by the previous reactions at the Complexes I-V. Inasmuch as in this study we have seen differences in the ATP production in fibroblasts of MDD patients and controls, the differentiated neural cells were also measured separately in their ATP contents. Since NPCs of patients show a lower basal respiration, it might be possible that the ETC does not function properly and this could therefore result in differences in the drive of the ATP synthase and lower ATP contents. Nevertheless, there are overall no differences in the ATP levels of MDD NPCs and control NPC. As depicted in the figure below, cells from MDD patients do not harbor a significantly distinct amount of ATP compared to cells from healthy subjects (MDD 341064 ± 49780 , CON 324275 ± 47085 , Student's t-test, paired, two-tailed, $p = 0.7939$, mean \pm SEM, figure 31). DEX stress does also not cause a difference between MDD subjects and healthy controls (MDD 362357 ± 65367 , CON 369576 ± 57303 , Student's t-test, paired, two-tailed, $p = 0.8317$, mean \pm SEM, figure 31). Possibly, the defects in basal respiration and hence potential deficits of ETC transport function do not have an impact on the overall ATP

levels. NPCs are highly reliant on glycolysis and they can assumedly compensate for deficits of the ETC.

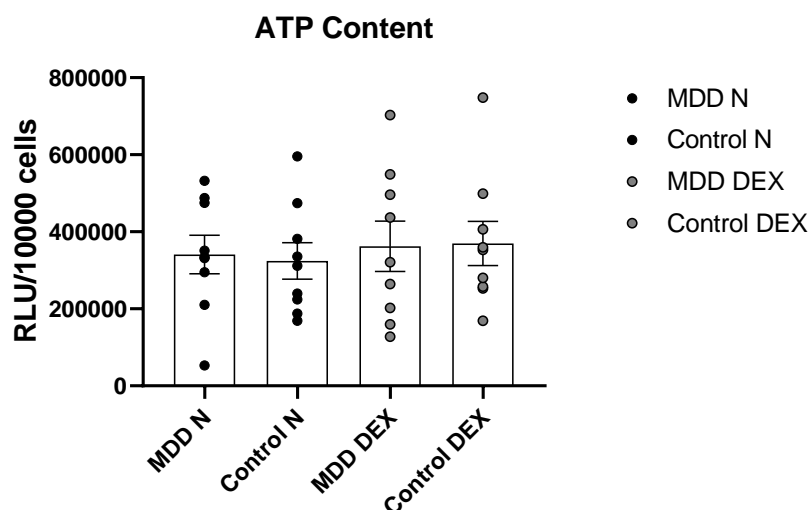


Figure 31 ATP content in NPCs. Shown is the ATP content in MDD and control NPC lines under non-treated conditions and after one week of 1 μ M DEX stress. No significant differences were found for MDD vs. control NPCs, neither for non-treated and 1 μ M DEX stress. Bar graphs show normalized mean RLU values \pm SEM. Dots show the distribution of single RLU values for MDD and control NPC lines under non-treated conditions and after one week of 1 μ M DEX stress; MDD n=9, control n=9.

4.5.3 Bioenergetics and mitochondria-related homeostasis in NPCs

Besides the assessment of respiratory parameters in neural cells and the determination of the ATP content, the nine differentiated cell lines derived from MDD patients and control were observed with the help of fluorescent dyes in order to determine the MMP and the cytosolic Ca^{2+} homeostasis. Since the NPCs from MDD patients exhibited lowered OCR values in respiratory parameters, the MMP and the Ca^{2+} homeostasis, respectively the Ca^{2+} buffer function of the mitochondria, might be also affected. The NPCs are likely to show changes in other mitochondria-related properties.

4.5.3.1 Mitochondrial Membrane Potential

JC-1 measurements in nine NPC cell lines resulted in significant differences. NPCs derived from controls show a higher JC-1 red/green ratio compared to NPCs from MDD patients (MDD 1.70 ± 0.065 , CON 1.84 ± 0.092 , Student's t-test, paired, two-tailed, * $p < 0.05$, $p = 0.0286$, mean \pm SEM, figure 32 a). Higher red/green ratios indicate a lower – more negative – MMP. After one week of DEX stress, MDD and control cell lines do not exhibit

any significant differences in their MMP (MDD 1.96 ± 0.079 , CON 2.04 ± 0.128 , Student's t-test, paired, two-tailed, $p = 0.1843$, mean \pm SEM, Figure 32 a). These observations might be related to the change of the ETC function in MDD NPCs. There is a low variance in the single values of the JC-1 ratios for all groups, also indicated by small error bars. As figures 32 b and c show, seven of the nine MDD cell lines show a lower MMP than the control cell lines as well as after DEX stress the majority of MDD cells exhibits a lower MMP. However, depending on the pair, the differences in MMP vary in size.

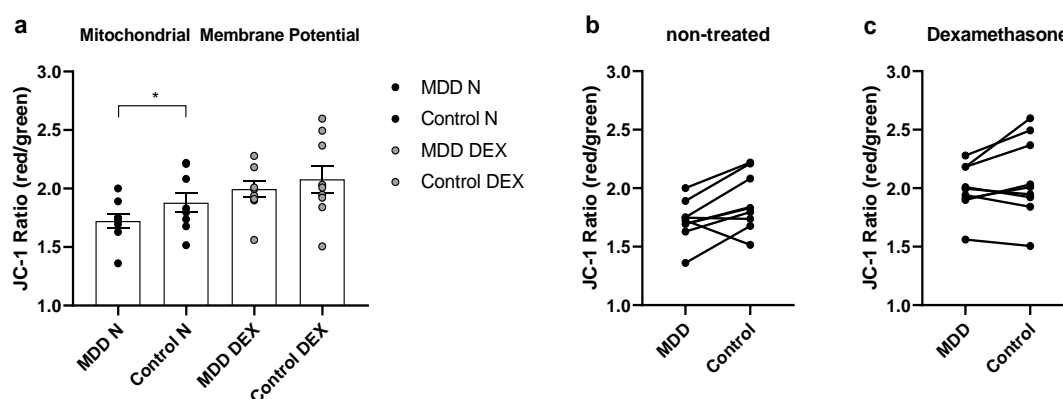


Figure 32 Mitochondrial membrane potential measurements of NPCs. Shown are the red/green ratios of MDD and control NPC lines under non-treated conditions and after one week of $1 \mu\text{M}$ DEX stress. Significant differences were found for MDD vs. control, non-treated ($* p < 0.05$, compared with control, Student's t-test, paired, two-tailed). Bar graphs show mean red/green ratios \pm SEM. Dots show the distribution of single red/green values for MDD and control NPC lines under non-treated conditions and after one week of $1 \mu\text{M}$ DEX stress; MDD $n=9$, control $n=9$. **b-c** Graphs show the pairwise red/green ratios for each MDD and control NPC line under (**b**) non-treated conditions, (**c**) after one week of $1 \mu\text{M}$ DEX.

4.5.3.2 Cytosolic Ca^{2+} homeostasis

Changes in the MMP are closely related to changes in the Ca^{2+} homeostasis in the cell. Therefore, in this study the cytosolic Ca^{2+} homeostasis was examined with the fluorescent dye Fura-2 in nine paired NPC cell lines. Higher Fura-2 ratios are directly related to higher amounts of cytosolic Ca^{2+} . Overall, the measurement of Fura-2 ratios did not result in any significant differences in NPCs. Statistically, there is no difference between MDD patients cell lines compared to the control cell line (non-treated, MDD 0.62 ± 0.01 , CON 0.60 ± 0.01 , Student's t-test, paired, two-tailed, $p = 0.0705$; DEX, MDD 0.62 ± 0.01 , CON 0.061 ± 0.00 , Student's t-test, paired, two-tailed, $p = 0.1977$; mean \pm SEM, figure 33 a). Generally, there is a low variation in the values in each group, also indicated by small error bars. Despite

the fact that MDD patients show a slightly higher Fura-2 ratio for both conditions, the values of each pair are of individual differences (figure 33 b-c).

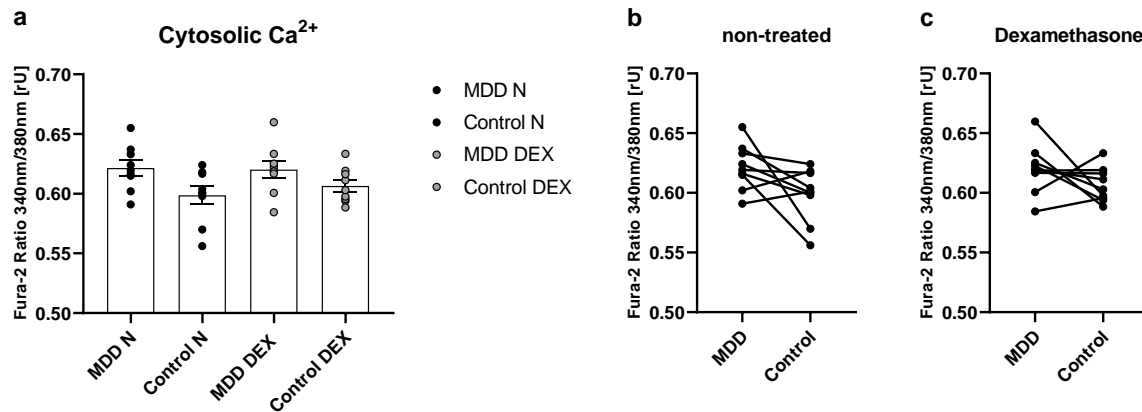


Figure 33 Cytosolic Ca²⁺ homeostasis in NPCs. Shown are the 340 nm/380 nm ratios of MDD and control NPC lines under non-treated conditions and after one week of 1 μ M DEX stress. No significant differences were found. Bar graphs show mean 340 nm/380 nm ratios \pm SEM. Dots show the distribution of single 340 nm/380 nm values for MDD and control NPC lines under non-treated conditions and after one week of 1 μ M DEX stress; MDD n=9, control n=9. **b-c** Graphs show the pairwise 340 nm/380 nm ratios for each MDD and control NPC line under (b) non-treated conditions and (c) after one week of 1 μ M DEX stress.

5 Discussion

5.1 Fibroblasts from MDD patients show lower respiratory rates and altered bioenergetic functions

In the present study, it could be demonstrated that there are differences in the mitochondria-related functions in MDD fibroblasts compared to the fibroblasts from gender- and age-matched healthy controls. Fibroblasts from MDD patients show lower OCR values for basal and maximal respiration, the spare respiratory capacity, the non-mitochondrial respiration and the ATP-turnover related respiration. Lower basal respiration and a reduced ATP-related OCR rate could either be a consequence of a diminished activity of the mitochondrial respiratory chain or a restricted substrate or enzyme availability. In case of a restricted availability of the substrates glucose or fatty acids or the improper functioning of enzymes in their metabolic breakdown (e.g. the hexokinase or the Acyl-CoA Dehydrogenase), the availability of the reduction equivalents NADH/H⁺ and FADH₂ is limited. Moreover, those reduction equivalents have to be shuttled into the mitochondrion, which also can be a limiting factor for the function of the ETC (Leverve 2007). The levels of reduction equivalents in MDD and control cells were not determined in this study. In order to draw a conclusion if the reduced respiration is because of a reduced presence of NADH/H⁺ or FADH₂ further measurements are needed. However, a lower basal respiration can also result from a reduced function of the ETC itself, meaning that the Complexes I – IV might exhibit a lower activity in MDD fibroblasts. The inhibition of Complex I by rotenone was shown to cause an inhibition of Complex II since the TCA cycle stops succinate production when NADH/H⁺ is not oxidized since there are no succinate sources in the cytosol (Steinlechner-Maran et al. 1997). Complex I produces most of the superoxide. A defect of Complex I activity, therefore, can be considered as a potential cause for altered ROS levels (Paradies et al. 2004). It cannot be excluded that the reduced respiration in MDD fibroblasts originates from a reduced mitochondrial mass. An estimation of the mitochondrial content in permeabilized PBMCs of acutely depressed patients resulted in increased levels and Karabatsiakakis et al. therefore concluded the lowered respiration is actually attributable to a lower ETC function (Karabatsiakakis et al. 2014). However, for this study, the mitochondrial content definition by CS activity – as is was determined in the study of Karabatsiakakis et al. – is remaining to be done.

Non-mitochondrial oxygen consumption is observed at low levels in a variety of cells and tissues. This has been linked to an inefficient ETC or to other cellular oxidative reactions which are not linked to energy metabolism (Herst et al. 2004). MDD fibroblasts exhibit a lower non-mitochondrial respiration compared to control fibroblasts, which could be either point at a reduced activity of the ETC or a generally decreased metabolism.

Moreover, the reduced maximal uncoupled respiration and the lower spare respiratory capacity indicate that the fibroblasts of MDD patients exhibit a reduced capacity of mitochondrial respiration. This decreased capacity might result in a lack of energy in times of higher energy demand (Buttgereit, Burmester, and Brand 2000).

Similar observations to those in the present study were made in PBMCs of acutely depressed patients. Karabatsiakos et al. also observed a reduction in routine respiration, ATP turnover-related respiration and uncoupling efficiency (Karabatsiakos et al. 2014). These findings are in line with those from Hroudová et al. . They revealed that the physiological respiratory rate and the maximal capacity of the ETC are significantly decreased in intact blood platelets of patients with a current depressive episode – regardless of a partial or complete remission of the mild to severe depressive symptoms (Hroudová et al. 2013). Another study demonstrated that muscle cells of depressed patients show an impaired activity of Complex I+III and II+III. They also discovered a significant decreases of mitochondrial ATP production rates (Gardner et al. 2003). In the present study significantly lower ATP levels in MDD fibroblasts could also be measured. This finding is in line with the overall decreased respiration of MDD fibroblasts and the reduced ATP-related turnover in particular.

The electron flow at each complex of the ETC is used to pump protons into the IMS and the MMP is build up over the IMM. The flux of protons down their electrochemical gradient through the ATP synthase to generate ATP (Spinelli and Haigis 2018). The MMP is more negative in MDD fibroblasts whereas they harbor lower ATP levels. This observation might be related to a reduced function of the ATP synthase and therefore a preserved proton gradient causing the more negative MMP. The general assumption is that the electrochemical gradient regulates the activity of the ETC complexes. At high potentials further proton pumping is inhibited. A decrease of the MMP due to proton utilization, e.g. by the ATP synthase, allows the ETC to rebuild the MMP. Thus, mitochondria in intact cells respire between the extreme energetic states, state 3 in the presence of ADP and state 4 when ADP has been converted into ATP (Hüttemann et al. 2008). Studies of fibroblasts with primary defects in mitochondrial ATP synthase show that the MMP at state 4 is

normal, but ADP-induced discharge of the MMP is impaired as ATP synthesis at state 3 is decreased. Increased MMP and low ATP synthesis is also found when the ATP synthase content is diminished by altered biogenesis of the enzyme complex (Vojtíšková et al. 2004).

Although the ER is considered to be the main intracellular Ca^{2+} store, mitochondria essentially contribute to the cellular Ca^{2+} homeostasis. Mitochondria are able to accumulate Ca^{2+} in an energy-dependent way and they release Ca^{2+} through antiporters. Mitochondrial key functions – in particular the matrix dehydrogenases – are strongly influenced by the cytosolic Ca^{2+} level (Denton 2009). Cytosolic Ca^{2+} also influences the activity of other mitochondrial enzymes at the IMM such as the glycerophosphate dehydrogenase or the malate-aspartate shuttle (Satrústegui, Pardo, and Del Arco 2007). The examination of cytosolic Ca^{2+} in MDD fibroblasts and fibroblasts from controls did not reveal any significant differences. Mitochondrial Ca^{2+} concentrations were not assessed in the present study. However, the more negative MMP in MDD fibroblasts could cause a higher uptake of Ca^{2+} into the mitochondrion. Exceeded Ca^{2+} uptake by mitochondria triggers a bioenergetic failure of the organelle through the opening of the permeability transition pore, the release of Cyt c and other pro-apoptotic factors which cause cellular death by apoptosis or necrosis (Kroemer, Galluzzi, and Brenner 2007). Whether the more negative MMP in MDD fibroblasts also results in higher mitochondrial Ca^{2+} remains elusive in this case and will be part of further measurements.

5.2 Enhanced metabolism in fibroblasts due to hormonal and metabolic stressors

Besides the basal, non-treated state, the fibroblasts were investigated after one week of 1 μM DEX stress or after one week of 10 mM GAL stress.

Glucocorticoid hormones play an important role in times of stress by regulating salt and water metabolism, blood pressure, immune function, and carbohydrate, protein and fat metabolism (Schäcke, Döcke, and Asadullah 2002). However, chronic glucocorticoid treatment induces side effects, including insulin resistance, a catabolic effect on the skeletal muscle and an increased risk of osteoporosis (Schäcke, Döcke, and Asadullah 2002). Chronic exposure to either endogenously released or synthetic GC is related to numerous physical diseases, but also mental disorders (Björntorp and Rosmond 2000;

Pufall 2015b; Steckler, Holsboer, and Reul 1999; Strüber, Strüber, and Roth 2014b). Long-term GC presence causes ETC dysfunction, increased ROS, mitochondrial abnormalities, apoptosis and cell death (Manoli et al. 2007).

In this study, the overall analysis of the Mito Stress Test by ANOVA with repeated measures revealed a significant enhancement of OXPHOS, but not glycolysis, due to DEX exposure. DEX stress induced in both groups – MDD and controls – a rise of the OCR in all parameters of the Mito Stress Test. The differences in the OCR detected in the Mito Stress Test between MDD fibroblasts and control fibroblasts for the non-treated state could not be measured after the DEX condition. It is known that chronic injection of glucocorticoids over 3 to 7 days decreases the rate of oxygen consumption and lowers phosphate/oxygen-ratio (the ATP produced per oxygen atom reduced by the respiratory chain) of liver mitochondria, but not in mitochondria from skeletal muscle (Bullock et al. 1972; Kerppola 1959; Kimberg, Loud, and Wiener 1968; Peter, Verhaag, and Worsfold 1970).

A 48 h treatment with 1 μM of dexamethasone in adipocytes caused an impaired insulin-induced glucose uptake and a mitochondrial dysfunction. The mitochondrial dysfunction was supported by decreased intracellular ATP and MMP, increased intracellular and mitochondrial ROS and mtDNA damage. Changes in the mitochondrial dynamics and biogenesis were suggested by decreased Drp1, increased Mfn2, and decreased PGC-1 α , NRF1, and TFam levels (Guangxiang et al. 2019). Although the application of DEX resulted in a higher activity of the ETC and OXPHOS, MDD and control fibroblasts exhibit slightly lower ATP levels. The exposure of fibroblasts to 1 μM DEX seems to have rather adverse effects on the energy supply. MDD fibroblasts exhibit significantly lower ATP levels compared to control fibroblasts. The enhancement of the ETC machinery through DEX might have caused, that the MMP is not significantly different between MDD fibroblasts and controls. Yet, MDD fibroblasts exhibit significantly lower ATP levels, suggesting a restricted substrate or enzyme availability also under hormonal exposure.

Besides hormonal stress induced by DEX, metabolic stress was induced by 10 mM galactose instead of glucose in the culture medium. The production of pyruvate via glycolytic metabolism yields 2 net ATP, whereas the production via glycolytic metabolism of galactose yields no net ATP. Therefore, the cells are forced to have an increased reliance on OXPHOS for their energy supply (Marroquin et al. 2007; Robinson et al. 1992; Rossignol et al. 2004). Different types of cells, e.g. cancer cells or primary fibroblasts, grown in a medium in which glucose is replaced with galactose show a significantly increased OCR compared to cells grown in medium containing a high

concentration of glucose. Cells grown in galactose exhibit a more aerobic state due to a diminished ATP production via anaerobic glycolysis (Bustamante and Pedersen 1977). It is also suggested that galactose modulated mitochondrial structure and the oxidative capacity is risen by increased OXPHOS protein expression and enzymatic activities (Rossignol et al. 2004). The study by Robinson et al. showed that primary skin fibroblasts isolated from patients with mitochondrial deficiency including cytochrome oxidase deficiency, complex I deficiency, pyruvate dehydrogenase complex deficiency or with multiple respiratory chain defects, were not able to survive when cultured in a galactose-based medium (Robinson et al. 1992). Aguer et al. assessed the mitochondrial respiration in human primary muscle cells after 7 day and acute (24 h) 10 mM galactose incubation and they discovered higher OCR rates after chronic but not after acute exposure. Moreover they confirmed a lower aerobic metabolism proofed by a diminished generation of lactate (Aguer et al. 2011).

In the present study of MDD fibroblasts and control fibroblasts the GAL treatment resulted in an overall significant heightened metabolism compared to the non-treated state. However, not only OCR was fueled, but also ECAR. Although the acidification rate is widely used to describe glycolytic events, glycolysis is not the sole contributor to the production of H^+ . Extracellular acid produced by cells is derived from both lactate, produced by anaerobic glycolysis, and CO_2 , produced in the citric acid cycle during respiration. The export of CO_2 , the hydration to H_2CO_3 and the dissociation to $HCO_3^- + H^+$ is the reason for respiratory acidification (Mookerjee et al. 2015). This phenomenon might explain the elevated ECAR levels in fibroblasts despite of glucose deprivation. The higher respiratory rate causes a higher extracellular acidification.

The respiratory parameters of the Mito Stress test do not result in significant differences between patients and controls due to GAL exposure, except the non-mitochondrial respiration. The ATP levels are higher for both groups compared to non-treated conditions and there are no significant differences between MDD fibroblasts and controls. The measurements of MMP and cytosolic Ca^{2+} did also not result in any significant differences between MDD and control fibroblasts subsequent to GAL exposure. A study by Garbett et al. has shown that metabolic challenges evoked by substitution of glucose with GAL or reducing the abundance of lipids in the growth media of fibroblasts from MDD patients result in changes of mRNA and miRNA expression. These stress-induced changes are suggested to be MDD-related. The impairments in molecular pathways involved in the control of metabolism and energy production, cell survival, proliferation and migration

were found in MDD fibroblasts due to GAL and reduced-lipid challenges, but not in control fibroblasts (Garbett et al. 2015).

5.3 Similar mitochondrial densities in MDD and control fibroblasts

Mitochondrial volume or content is an important quantitative indicator, since the mitochondrial mass is dependent on intact mitochondrial dynamics and therefore proper mitochondrial bioenergetics (Chen, McCaffery, and Chan 2007; Detmer and Chan 2007). The mitochondrial content is most commonly defined by the measurement of the Citrate Synthase (CS) activity, the mtDNA copy number, cardiolipin or the activity of the Cyt c oxidase (Boushel et al. 2007; Karabatsiakos et al. 2014; Mogensen et al. 2006; Picard, Taivassalo, Ritchie, et al. 2011; Ritov, Menshikova, and Kelley 2006). In the present study the mitochondrial content was determined by mtDNA copy number. Using this method, there are no significant differences in mtDNA copy number between MDD fibroblasts and control fibroblasts. This observation suggests that the differences detected in respiratory parameters and bioenergetic properties are not due to differences in the mitochondrial mass. Hroudová et al. determined mitochondrial content by CS activity in blood platelets. Although they did not mention absolute CS values, they reported that after CS normalization the significant differences in respiration were sustained (Hroudová et al. 2013). Other studies report contrary results. The mitochondrial content definition, by the analysis of CS activity, in PBMCs from depressed subjects revealed higher densities, suggesting that this increase in mitochondrial mass is an attempt of the body to compensate for the reduced efficiency in mitochondrial ATP production (Karabatsiakos et al. 2014). This finding is in line with a study by Cai et al. . They revealed that the amount of mtDNA alters in response to external stress: there was significantly more mtDNA in the saliva and blood of people with MDD than in controls. Besides that, chronic stress also altered the amount of mtDNA in mouse tissues. The stressed mice also showed a lowered mitochondrial respiratory activity (Cai et al. 2015).

Furthermore, Wang et al. proposed elevated mtDNA copy numbers in MDD as a compensatory mechanism for energetic deficiencies (Wang et al. 2017).

Nonetheless, Larsen et al. published a study, examining the different biomarkers and their correlation to cristae surface area determined by TEM. The goal was to evaluate the association and validity of CS activity, cardiolipin content, mtDNA, Complex I-V protein

content and Complex I-IV activity to muscle mitochondria content and OXPHOS in skeletal muscle cells from healthy subjects. Cardiolipin content, followed by CS activity and Complex I activity, were the biomarkers exhibiting the strongest association with mitochondrial content, whereas mtDNA was supposed to be a possibly less suitable method to estimate the mitochondrial content in skeletal muscle cells (Larsen et al. 2012). Considering those contrasting findings for mitochondrial mass determination, a future quantification of the mitochondrial mass in MDD fibroblasts and controls in terms of cardiolipin determination or CS activity measurement is suggested.

5.4 Decreased mitochondria-related metabolism in MDD NPCs

MDD fibroblast and control cell lines were reprogrammed into iPSCs by the ectopic overexpression of the transcription factors including Oct3/4, Sox2, Klf4, c-Myc and differentiated into NPCs that express the neural stem cell markers PAX6 and SOX2 (Takahashi and Yamanaka 2006; Yan et al. 2013). Several studies reported that following the reprogramming of iPSCs, the epigenetic memory is inherited from the parental cells (Doi et al. 2009; Kim et al. 2010; Lister et al. 2011; Ohi et al. 2011; Polo et al. 2010).

In the first part of this study, it could be shown that there are detectable bioenergetic alterations in the somatic cells. In the second part could be shown that, despite of the whole progress of reprogramming to iPSCs and the differentiation process, there are also measurable differences in the bioenergetics of mitochondria in NPCs.

The Mito Stress Test revealed that NPCs from MDD patients exhibit a significantly lower basal respiration, a lowered non-mitochondrial respiration and a significantly lower OCR for the proton leak under standard culturing conditions. However, MDD NPCs do not exhibit a lower maximal respiration as it could be measured for MDD fibroblasts. There are also no statistically different levels in the ATP production determined by the bioluminescence assay. This observation could be due to the slightly distinct metabolism in NPCs compared to fibroblasts. Whereas fibroblasts are highly reliant on OXPHOS, NPCs gain a large part of their energy via glycolytic pathways (Lorenz et al. 2017; Zheng et al. 2016). Therefore, it is suggested that potential deficits in ETC activity – indicated by the lowered basal respiration - in MDD NPCs can be compensated by the generation of energy through glucose metabolism. In accordance with the lower basal respiration, the MMP in MDD NPCs is less negative.

The proton circuit across the IMM optimally drives the OXPHOS, where substrate oxidation and ADP phosphorylation are coupled. The oxidation of substrates releases electrons to NADH or FADH₂. These electrons are passed through electron carriers in respiratory chain complexes with increasing oxidation potentials. This exergonic reactions transports protons from the matrix to the IMS, eventually creating an electrochemical gradient and the proton motive force driving the ATP synthase (Alberts et al. 2002). However, this proton motive force is incompletely converted into ATP, since the coupling is only about 50–80 %. This loss of energy is due to protons that return to the matrix independently of ATP synthase (Buttgereit, Burmester, and Brand 2000). The proton leak, and also the electron leak, have an impotent impact on mitochondrial coupling efficiency and production of reactive oxygen species. The OCR values assigned to the proton leak in MDD NPCs are significantly lower compared to those of control NPCs. This observation could indicate that the uncoupling in control NPCs is actually less efficient. Taken together, these findings point towards a lower substrate or enzyme availability in MDD NPCs.

The cytosolic Ca²⁺ levels do not significantly alter between MDD and control NPCs. However, unlike in fibroblasts, in MDD NPCs there is a trend towards a higher cytosolic Ca²⁺ level. This observation is in accordance with the measurement of a significantly less negative MMP in MDD NPCs. Mitochondria have important buffer functions since they sequester – due to their negative MMP – large amounts of Ca²⁺ (Ernster and Schatz 1981). Especially in neuronal cells, the cytosolic Ca²⁺ concentration is critical. Elevated cytosolic Ca²⁺ would stimulate glutamate release which causes an activation of N-methyl-D-aspartate receptors. This in turn would result in massive Ca²⁺ influx and cell damage and death (Kannurpatti, Joshi, and Joshi 2000). Elevated Ca²⁺ levels in NPCs due to a disturbance of the sequestration of Ca²⁺ by their mitochondria therefore might induce apoptosis and hence this might cause a reduced cellular mass that could give rise to neurons or astrocytes, for example. Cytosolic Ca²⁺ in iN of two MDD patient and control pairs of this study were already shown to be significantly altered and will depict an important objective in future investigations (Röhrl 2019).

5.5 Effects of the synthetic hormonal stressor dexamethasone in NPCs

GC levels are elevated in neuropsychiatric disorders and it is known that their chronic administration causes a loss of memory and impaired logical thinking, disrupted HPA axis function and alterations in calcium homeostasis in neurons (Chen et al. 2011; Lajic, Nordenström, and Hirvikoski 2011; Young et al. 1999). The effects of a glucocorticoid – dexamethasone – were also tested in this cellular model. Besides the evaluation of the bioenergetic properties of NPCs under standard culturing-conditions, the cells were exposed to a synthetic hormonal stressor for one week. After the NPCs were treated with DEX, they do not exhibit any significant differences in the Mito Stress Test. The significant differences between MDD NPCs and control NPCs in basal respiration, non-mitochondrial respiration or proton leak are not detectable under stressed conditions. After 1 week of 1 μM DEX stress there are no significant differences in the MMP between control and MDD NPCs. One possible explanation could be, that, as the overall analysis of the metabolism revealed, MDD NPCs exhibit slightly heightened OCR values consequently to hormonal stress. However, DEX did not cause a significant effect on overall metabolism – considering OCR and ECAR together – in MDD and control NPCs as it did in fibroblasts. However, the analysis of the overall metabolism, respectively OCR in the dependence of ECAR, revealed that also MDD NPCs show a significantly lower metabolism under standard culturing conditions but also after DEX stress. Generally, the exposure to chronic (hormonal) stress is considered to be detrimental to mitochondrial metabolism. The adverse effects include a lowered OXPHOS function, disruptions of the MMP and Ca^{2+} homeostasis, damage of mtDNA and elevated ROS levels (Manoli et al. 2007). In this study, possibly the exposure of 1 μM DEX for 7 days was too short to induce deficiencies in the OXPHOS. Similar to the effects in fibroblasts, NPCs exhibited rather the beneficial effects of an acute exposure to stress than the adverse consequences. An important regulator for mitochondrial biogenesis is PGC-1 α . Balanced levels of this master regulator are crucial for driving OXPHOS and energy expenditure (Michael et al. 2001; Wu et al. 2006). PGC-1 α levels were not determined in the present study. The measurement of PGC-1 α by qPCR will be considered as a future objective.

Suwanjan et al. examined the mitochondrial dynamics underlying dexamethasone-induced toxicity in the human neuroblastoma SH-SY5Y cells. The treatment with DEX for 24 h of those neuronal cells resulted in a marked decrease in cell proliferation. DEX-induced neurotoxicity also caused upregulation of mitochondrial fusion. Unlike in the present study with NPCs, in the study of Suwanjang et al. a reduced ATP production could

be detected due to DEX treatment. Furthermore they reported increased ROS levels (Suwanjang et al. 2019). Morin et al. tested the effects of four different glucocorticoids – hydrocortisone, triamcinolone, prednisolone and dexamethasone – on isolated rat brain mitochondria. The application of 1 μ M DEX caused a reduction of respiratory rates due to an inhibition of oxidative phosphorylation (state 3 respiration) and of Complex V activity and a modification of the proton-fluxes through the mitochondrial inner membrane. Moreover, DEX also inhibited the CCCP-induced rise in the OCR in a concentration-dependent manner. Morin et al. suggested therefore an adverse effect of glucocorticoids on brain mitochondria and a limited capacity to increase OCR upon ETC stimulation (Morin et al. 2000). Nonetheless, DEX stimulation in NPCs did exhibit neither significantly negative nor significantly beneficial effects in the present study. The possibly differential effects on mitochondria of iN from MDD and controls remain elusive and will be part of further studies.

6 Conclusion and future perspectives

The aim of this study was to investigate the association of mitochondrial function and underlying psychopathological mechanisms in MDD.

This study shows that cells from MDD patients and healthy controls exhibit differences in mitochondria-associated functions. In this explorative approach the mitochondrial key functions in fibroblasts were assessed and differences between MDD patients and healthy controls could actually be demonstrated. Mitochondria in fibroblasts of MDD patients appear to have reduced oxidative capacities and therefore a reduced energy availability. These alterations in the somatic cells were in line with those from other groups (Hroudová et al. 2013; Karabatsiakos et al. 2014). Nonetheless, an indispensable objective for the future will be the verification of the mitochondrial mass with a second method. In order to know if the respiratory differences originate from a lower density of mitochondria, a measurement of the CS activity is suggested.

Moreover, mitophagy is an important aspect with regard to mitochondrial mass. Mitophagy, as well as fission and fusion, are the cells' major mitochondria quality control mechanisms and ensure a whole mitochondrial genome turnover and proper mitochondrial functioning (Dombi, Mortiboys, and Poulton 2018). The recycling and engulfment of mitochondria by acidic lysosomes can be visualized by transfection of cells with mt-Rosella, which is a dual-emission biosensor sensitive to pH changes (Sargsyan et al. 2015). Therefore, mitophagy is strongly suggested to be assessed also in MDD fibroblasts to control for a functional restoring of mitochondria.

A regulator of mitochondrial dynamics is OPA1 and it is – among many others – one of many targets of human sirtuins (SIRT) that coordinate a variety of molecules involved in certain aspects of cellular metabolism (Dombi, Mortiboys, and Poulton 2018). SIRT are transcription regulators and may act as metabolic sensors, since they are dependent on NAD⁺ levels. NAD⁺ links transcriptional events and changes in cellular signaling to cellular metabolism. NAD⁺ has a pivotal role in mitochondrial metabolism: NAD⁺ accepts H⁺ equivalents to form reduced NADH, which then provides reducing equivalents to the mitochondrial ETC and to fuel OXPHOS (Cantó, Menzies, and Auwerx 2015). Therefore, a crucial objective for future investigations is the assessment of NAD⁺/NADH ratios. The determination of NAD⁺/NADH ratios allow a more detailed statement about the reduction equivalent availability and the redox state in MDD cells versus control cells.

The redox potential of a cell is widely defined by GSH. The majority of GSH is found in the cytosol. However, a small but significant percentage is also found in the mitochondria. Mitochondrial GSH is of huge importance protecting the organelle from ROS produced during coupled mitochondrial electron transport and OXPHOS (Buttke and Sandstrom 1994). A lack of antioxidant defenses, e.g. GSH, leads to a generation of high ROS levels, which is suggested to act as a signal for the induction of apoptosis (Langer, Jürgensmeier, and Bauer 1996). In the context of the present study, the investigation of GSH levels depicts an interesting future approach to determine the capability of scavenging superoxide in MDD cells.

To my knowledge, this is the first study to investigate bioenergetics in neural cells derived from iPSCs of MDD patients. It could be shown that differences in respiration and the MMP in peripheral cells are also present at neuronal cell level, despite the process of reprogramming and differentiation. These novel observations highlight the importance of further investigations of mitochondria – especially in neurons. Neural cells require in comparison to peripheral cells higher amounts of energy: The brain with its high metabolic rate consumes 20% of the whole-body oxygen uptake (Vergara et al. 2019). Neurons might be even more sensitive to potential improper mitochondrial functioning and insufficient energy provision.

First experiments with iN of selected patient and control pairs showed that neurons from MDD patients exhibit altered properties including Ca^{2+} homeostasis and spontaneous activity (Röhrl 2019; Triebelhorn, *in preparation*). Cytosolic Ca^{2+} was measured with the help of Fura-2. However, mitochondrial Ca^{2+} levels will also be in focus of future investigations. Mitochondrial Ca^{2+} levels can be assessed by the use of the fluorescent dye Rhod-2, for instance. However, synthetic fluorescent indicators targeted to mitochondria have blunted responses to repetitive increases in mitochondrial Ca^{2+} and disrupt mitochondrial morphology. Moreover, indicators like Rhod-2 tends to leak out of mitochondria over several hours which makes them unsuitable for long-term experiments (Nagai et al. 2001). Ratiometric mt-Pericam though, which is an indicator based on a fusion of circularly permuted yellow fluorescent protein and calmodulin, is genetically encoded and allows the measurement of rapid changes in and long-term measurements of mitochondrial Ca^{2+} concentrations (Akimzhanov and Boehning 2011). Moreover, first experiments with the treatment of cells with the particular ADs the patients received were conducted. Mitochondrial respiration, MMP and Ca^{2+} homeostasis

was assessed after 24 h, 3 days and 7 days of ADs treatment of fibroblasts. MMP and cytosolic Ca^{2+} homeostasis were assessed in consequence to ADs treatment. It could be shown that the ADs have different effects on the MDD patient cells compared to the matched control (Röhrl 2019). Since the MDD patients of this study responded to AD treatment, the inclusion of non-responder is proposed for future investigation in order to gain more detailed insight into potential pathologic changes and the association to mitochondrial (dys-)function in MDD.

However, the importance of respiratory deficiencies and the energy supply in MDD patients is unresolved. The effect of stress and the impact of ADs on OXPHOS activity in MDD remain widely elusive and depict a future direction of research.

List of references

- Aguer, C., Gambarotta, D., Mailloux, R. J., Moffat, C., Dent, R., McPherson, R., & Harper, M. E. (2011). Galactose enhances oxidative metabolism and reveals mitochondrial dysfunction in human primary muscle cells. *PLoS ONE*, *6*(12). <https://doi.org/10.1371/journal.pone.0028536>
- Akimzhanov, A. M., & Boehning, D. (2011). Monitoring dynamic changes in mitochondrial calcium levels during apoptosis using a genetically encoded calcium sensor. *Journal of Visualized Experiments*, (50), 2–5. <https://doi.org/10.3791/2579>
- Alberts, B., Brey, D., Lewis, J., Raff, M., Roberts, K., & Walter, P. (2002). *The Molecular Biology of the cell* (4th ed.).
- Amodeo, G., Allegra Trusso, M., & Fagiolini, A. (2018). Depression and Inflammation: Disentangling a Clear Yet Complex and Multifaceted Link. *Neuropsychiatry*, *07*(04), 448–457. <https://doi.org/10.4172/neuropsychiatry.1000236>
- Anacker, C., Zunszain, P. A., Carvalho, L. A., & Pariante, C. M. (2001). The glucocorticoid receptor: Pivot of depression and of antidepressant treatment? *Psychoneuroendocrinology*, *36*(3), 415–425.
- Anandatheerthavarada, H. K., Biswas, G., Robin, M. A., & Avadhani, N. G. (2003). Mitochondrial targeting and a novel transmembrane arrest of Alzheimer's amyloid precursor protein impairs mitochondrial function in neuronal cells. *Journal of Cell Biology*, *161*(1), 41–54. <https://doi.org/10.1083/jcb.200207030>
- Bartl, J., Müller, T., Grünblatt, E., Gerlach, M., & Riederer, P. (2014). Chronic monoamine oxidase-B inhibitor treatment blocks monoamine oxidase-A enzyme activity. *Journal of Neural Transmission*, *121*(4), 379–383. <https://doi.org/10.1007/s00702-013-1120-z>
- Barton, C., Sklenicka, J., Sayegh, P., Yaffe, K., Schubert, C. C., Boustani, M., ... Samuel, M. J. (2003). A double-blind trial of bupropion versus desipramine for bipolar depression. *Journal of Clinical Psychiatry*, *55*(2), 391–393. <https://doi.org/10.1002/hup>
- Beluche, I., Chaudieu, I., Norton, J., Carrière, I., Boulenger, J., Ritchie, K., ... Boulenger, J. (2009). Persistence of abnormal cortisol levels in elderly persons after recovery from major depression. *43*(8), 777–783.
- Belvederi Murri, M., Pariante, C., Mondelli, V., Masotti, M., Atti, A. R., Mellacqua, Z., ... Amore, M. (2014). HPA axis and aging in depression: Systematic review and meta-analysis. *Psychoneuroendocrinology*, *41*, 46–62. <https://doi.org/10.1016/j.psyneuen.2013.12.004>
- Bersani, F. S., Morley, C., Lindqvist, D., Epel, E. S., Picard, M., Yehuda, R., ... Mellon, S. H. (2016). Mitochondrial DNA copy number is reduced in male combat veterans with PTSD. *Progress in Neuro-Psychopharmacology and Biological Psychiatry*, *64*, 10–17. <https://doi.org/10.1016/j.pnpbp.2015.06.012>
- Bertholet, A. M., Delerue, T., Millet, A. M., Moulis, M. F., David, C., Daloyau, M., ... Belenguer, P. (2016). Mitochondrial fusion/fission dynamics in neurodegeneration and neuronal plasticity. *Neurobiology of Disease*, *90*, 3–19. <https://doi.org/10.1016/j.nbd.2015.10.011>
- Bilello, J. A. (2016). Seeking an objective diagnosis of depression. *Biomarkers in Medicine*, *10*(8), 861–875. <https://doi.org/10.2217/bmm-2016-0076>
- Björntorp, P., & Rosmond, R. (2000). Obesity and cortisol. *Nutrition*, *16*(10), 924–936. [https://doi.org/10.1016/S0899-9007\(00\)00422-6](https://doi.org/10.1016/S0899-9007(00)00422-6)
- Borthwick, G. M., Johnson, M. A., Ince, P. G., Shaw, P. J., & Douglass, M. (2001). Mitochondrial enzyme activity in amyotrophic lateral sclerosis: Implications for the

- role of mitochondria in neuronal cell death. *Annals of Neurology*, 46(5), 787–790.
- Boushel, R., Gnaiger, E., Schjerling, P., Skovbro, M., Kraunsøe, R., & Dela, F. (2007). Patients with type 2 diabetes have normal mitochondrial function in skeletal muscle. *Diabetologia*, 50(4), 790–796. <https://doi.org/10.1007/s00125-007-0594-3>
- Brand, M. D., & Esteves, T. C. (2005). Physiological functions of the mitochondrial uncoupling proteins UCP2 and UCP3. *Cell Metabolism*, 2(2), 85–93. <https://doi.org/10.1016/j.cmet.2005.06.002>
- Bullock, G. R., Carter, E. E., Elliott, P., Peters, R. F., Simpson, P., & White, A. M. (1972). Relative changes in the function of muscle ribosomes and mitochondria during the early phase of steroid-induced catabolism. *The Biochemical Journal*, 127(5), 881–892. <https://doi.org/10.1042/bj1270881>
- Bustamante, E., & Pedersen, P. L. (1977). High aerobic glycolysis of rat hepatoma cells in culture: Role of mitochondrial hexokinase. *Proceedings of the National Academy of Sciences of the United States of America*, 74(9), 3735–3739. <https://doi.org/10.1073/pnas.74.9.3735>
- Buttgereit, F., Burmester, G. R., & Brand, M. D. (2000). Bioenergetics of immune functions: Fundamental and therapeutic aspects. *Immunology Today*, 21(4), 194–199. [https://doi.org/10.1016/s0167-5699\(00\)01593-0](https://doi.org/10.1016/s0167-5699(00)01593-0)
- Buttke, T. M., & Sandstrom, P. A. (1994). Oxidative stress as a mediator of apoptosis. *Immunology Today*, 15(1), 7–10. [https://doi.org/10.1016/0167-5699\(94\)90018-3](https://doi.org/10.1016/0167-5699(94)90018-3)
- Cai, N., Chang, S., Li, Y., Li, Q., Hu, J., Liang, J., ... Flint, J. (2015). Molecular signatures of major depression. *Current Biology*, 25(9), 1146–1156. <https://doi.org/10.1016/j.cub.2015.03.008>
- Cantó, C., Menzies, K., & Auwerx, J. (2015). NAD⁺ metabolism and the control of energy homeostasis - a balancing act between mitochondria and the nucleus. *Cell Metabolism*, 22(1), 31–53.
- Charmandari, E., Tsigos, C., & Chrousos, G. (2005). Endocrinology of the Stress Response. *Annual Review of Physiology*, 67(1), 259–284. <https://doi.org/10.1146/annurev.physiol.67.040403.120816>
- Chen, H., Chomyn, A., & Chan, D. C. (2005). Disruption of fusion results in mitochondrial heterogeneity and dysfunction. *Journal of Biological Chemistry*, 280(28), 26185–26192. <https://doi.org/10.1074/jbc.M503062200>
- Chen, H., McCaffery, J. M., & Chan, D. C. (2007). Mitochondrial Fusion Protects against Neurodegeneration in the Cerebellum. *Cell*, 130(3), 548–562. <https://doi.org/10.1016/j.cell.2007.06.026>
- Chen, S., Wang, X. H., Zhang, X. Z., Wang, W. C., Liu, D. W., Long, Z. Y., ... Zhou, J. H. (2011). High-dose glucocorticoids induce decreases calcium in hypothalamus neurons via plasma membrane Ca²⁺ pumps. *NeuroReport*, 22(13), 660–663. <https://doi.org/10.1097/WNR.0b013e32834a282a>
- Cheng, J., Nanayakkara, G., Shao, Y., Ramon, C., Wang, L., Wang, Y. Y., ... Yang, X. (2017). Mitochondrial Proton Leak Plays a Critical Role in Pathogenesis of Cardiovascular Diseases. *Advances in Experimental Medicine and Biology*, 982, 982–370.
- Chrousos, G. P. (2000). The role of stress and the hypothalamic–pituitary–adrenal axis in the pathogenesis of the metabolic syndrome: Neuro-endocrine and target tissue-related causes. *International Journal of Obesity*, 24, 50–55. <https://doi.org/10.1038/sj.ijo.0801278>
- Cipolat, S., De Brito, O. M., Dal Zilio, B., & Scorrano, L. (2004). OPA1 requires mitofusin 1 to promote mitochondrial fusion. *Proceedings of the National Academy of Sciences of the United States of America*, 101(45), 15927–15932. <https://doi.org/10.1073/pnas.0407043101>

- Clapham, D. E. (2007). Calcium Signaling. *Cell*, *131*(6), 1047–1058.
<https://doi.org/10.1016/j.cell.2007.11.028>
- Clayton, D., & Bogenhagen, D. (1977). Mouse L cell mitochondrial DNA molecules are selected randomly for replication throughout the cell cycle. *Cell Press*, *11*(4), 719–727.
- Cogswell, P. C., Kashatus, D. F., Keifer, J. A., Guttridge, D. C., Reuther, J. Y., Bristow, C., ... Baldwin, A. S. (2003). NF- κ B and I κ B α are found in the mitochondria. Evidence for regulation of mitochondrial gene expression by NF- κ B. *Journal of Biological Chemistry*, *278*(5), 2963–2968. <https://doi.org/10.1074/jbc.M209995200>
- Colombini, M. (2004). VDAC: The channel at the interface between mitochondria and the cytosol. *Molecular and Cellular Biochemistry*, *256/257*, 107–115. Retrieved from <http://www.life.umd.edu/biology/colombini/pubs/review04.pdf%5Cnpapers3://publication/uuid/30544E36-806E-4797-9F1F-8621C9A64B96>
- Comi, G. P., Bordoni, A., Salani, S., Franceschina, L., Sciacco, M., Prella, A., ... Scarlato, G. (1998). Cytochrome c oxidase subunit I microdeletion in a patient with motor neuron disease. *Annals of Neurology*, *43*(1), 110–116.
<https://doi.org/10.1002/ana.410430119>
- Corral-Debrinski, M., Horton, T., Lott, M. T., Shoffner, J. M., Beal, M. F., & Wallace, D. C. (1992). Mitochondrial DNA deletions in human brain: Regional variability and increase with advanced age. *Nature Genetics*, *2*(4), 324–329.
<https://doi.org/10.1038/ng1292-324>
- De Brito, O. M., & Scorrano, L. (2008). Mitofusin 2 tethers endoplasmic reticulum to mitochondria. *Nature*, *456*(7222), 605–610. <https://doi.org/10.1038/nature07534>
- Dejean, L., Cámara, Y., Sibille, B., Solanes, G., & Villarroya, F. (2004). Uncoupling protein-3 sensitizes cells to mitochondrial-dependent stimulus of apoptosis. *Journal of Cellular Physiology*, *201*(2), 294–304. <https://doi.org/10.1002/jcp.20048>
- Demonacos, C., Djordjevic-Markovic, R., Tsawdaroglou, N., & Sekeris, C. E. (1995). The mitochondrion as a primary site of action of glucocorticoids: the interaction of the glucocorticoid receptor with mitochondrial DNA sequences showing partial similarity to the nuclear glucocorticoid responsive elements. *Journal of Steroid Biochemistry and Molecular Biology*, *55*(1), 43–55. [https://doi.org/10.1016/0960-0760\(95\)00159-W](https://doi.org/10.1016/0960-0760(95)00159-W)
- Denton, R. M. (2009). Regulation of mitochondrial dehydrogenases by calcium ions. *Biochimica et Biophysica Acta - Bioenergetics*, *1787*(11), 1309–1316.
<https://doi.org/10.1016/j.bbabi.2009.01.005>
- Detmer, S. A., & Chan, D. C. (2007). Functions and dysfunctions of mitochondrial dynamics. *Nature Reviews Molecular Cell Biology*, *8*(11), 870–879.
<https://doi.org/10.1038/nrm2275>
- DiMauro, S., & Moraes, C. T. (1993). Mitochondrial Encephalomyopathies. *Archives of Neurology*, *50*(11), 1197–1208.
<https://doi.org/10.1001/archneur.1993.00540110075008>
- Dimmock, D. P., Zhang, Q., Dionisi-Vici, C., Carrozzo, R., Shieh, J., Tang, L. Y., ... Wong, L. J. (2008). Clinical and molecular features of mitochondrial DNA depletion due to mutations in deoxyguanosine kinase. *Human Mutation*, *29*(2), 330–331.
<https://doi.org/10.1002/humu.9519>
- Doi, A., Park, I., Wen, B., Murakami, P., Aryee, M. J., Herb, B., ... Feinberg, A. P. (2009). Differential methylation of tissue- and cancer-specific CpG island shores distinguishes human induced pluripotent stem cells, embryonic stem cells and fibroblasts. *Nature Genetics*, *41*(12), 1350–1353.
<https://doi.org/10.1038/ng.471>.Differential

- Dombi, E., Mortiboys, H., & Poulton, J. (2018). Modulating Mitophagy in Mitochondrial Disease. *Current Medicinal Chemistry*, 25(40), 5597–5612. <https://doi.org/10.2174/0929867324666170616101741>
- Dutta, A., McKie, S., & Deakin, J. F. W. (2015). Ketamine and other potential glutamate antidepressants. *Psychiatry Research*, 225(1–2), 1–13. <https://doi.org/10.1016/j.psychres.2014.10.028>
- Edmond, J. (1992). Energy metabolism in developing brain cells. *Canadian Journal Of Physiology and Pharmacology*, 70(1), 118–129.
- Eisenhofer, G., Kopin, I. J., & Goldstein, D. S. (2004). Catecholamine metabolism: A contemporary view with implications for physiology and medicine. *Pharmacological Reviews*, 56(3), 331–349. <https://doi.org/10.1124/pr.56.3.1>
- Epel, E. S., Blackburn, E. H., Lin, J., Dhabhar, F. S., Adler, N. E., Morrow, J. D., & Cawthon, R. M. (2004). Accelerated telomere shortening in response to life stress. *Proceedings of the National Academy of Sciences of the United States of America*, 101(49), 17312–17315. <https://doi.org/10.1073/pnas.0407162101>
- Ernster, L., & Schatz, G. (1981). Mitochondria: a historical review. *The Journal of Cell Biology*, 91(3 Pt 2), 227s–255s. <https://doi.org/10.1083/jcb.91.3.227s>
- Fazzini, F., Schöpf, B., Blatzer, M., Coassin, S., Hicks, A. A., Kronenberg, F., Fendt, L. (2018). Plasmid-normalized quantification of relative mitochondrial DNA copy number. *Scientific Reports* 8, 15347. <https://doi.org/10.1038/s41598-018-33684-5>
- Felger, J. C. (2018). *Role of Inflammation in Depression and Treatment Implications*.
- Ferrer, I., Martinez, A., Boluda, S., Parchi, P., & Barrachina, M. (2008). Brain banks: Benefits, limitations and cautions concerning the use of post-mortem brain tissue for molecular studies. *Cell and Tissue Banking*, 9(3), 181–194. <https://doi.org/10.1007/s10561-008-9077-0>
- Finsterer, J. (2004). Mitochondriopathies. *European Journal of Neurology*, 11(3), 163–186. <https://doi.org/10.1046/j.1351-5101.2003.00728.x>
- Forlenza, M. J., & Miller, G. E. (2006). Increased serum levels of 8-hydroxy-2'-deoxyguanosine in clinical depression. *Psychosomatic Medicine*, 68(1), 1–7. <https://doi.org/10.1097/01.psy.0000195780.37277.2a>
- Fries, G. R., Bauer, I. E., Scaini, G., Wu, M. J., Kazimi, I. F., Valvassori, S. S., ... Quevedo, J. (2017). Accelerated epigenetic aging and mitochondrial DNA copy number in bipolar disorder. *Translational Psychiatry*, 7(12). <https://doi.org/10.1038/s41398-017-0048-8>
- Garbett, K. A., Vereczkei, A., Kálmán, S., Wang, L., Korade, Z., Shelton, R. C., & Mirnics, K. (2015). Fibroblasts from patients with major depressive disorder show distinct transcriptional response to metabolic stressors. *Translational Psychiatry*, 5(3), 1–11. <https://doi.org/10.1038/tp.2015.14>
- Gardner, A., Johansson, A., Wibom, R., Nennesmo, I., Von Döbeln, U., Hagenfeldt, L., & Hällström, T. (2003). Alterations of mitochondrial function and correlations with personality traits in selected major depressive disorder patients. *Journal of Affective Disorders*, 76(1–3), 55–68. [https://doi.org/10.1016/S0165-0327\(02\)00067-8](https://doi.org/10.1016/S0165-0327(02)00067-8)
- Gold, P. W., Gabry, K. E., Yasuda, M. R., & Chrousos, G. P. (2002). Divergent endocrine abnormalities in melancholic and atypical depression: Clinical and pathophysiologic implications. *Endocrinology and Metabolism Clinics of North America*, 31(1), 37–62. [https://doi.org/10.1016/S0889-8529\(01\)00022-6](https://doi.org/10.1016/S0889-8529(01)00022-6)
- Goldenthal, M. J., & Marin-Garcia, J. (2004). Mitochondrial signaling pathways: a receiver/integrator organelle. *Molecular and Cellular Biochemistry*, 262(1–2), 1–16.
- Graier, W. F., Trenker, M., & Malli, R. (2004). Mitochondrial Ca²⁺, the secret behind the function of uncoupling proteins 2 and 3? *Nature Cell Biology*, 44(1), 36–50.

- <https://doi.org/10.1038/ncb1556>
- Guangxiang, L., Gang, L., Xiao, M., Youcai, J., Na, H., Li, J., ... Honglun, W. (2019). Dexamethasone-induced mitochondrial dysfunction and insulin resistance-study in 3T3-L1 adipocytes and mitochondria isolated from mouse liver. *Molecules*, *24*(10), 1–16. <https://doi.org/10.3390/molecules24101982>
- Gurney, M. E., Pu, H., Chiu, A. Y., Dal Canto, M. C., Polchow, C. Y., Alexander, D. D., ... Siddique, T. (1994). Motor neuron degeneration in mice that express a human Cu,Zn superoxide dismutase mutation. *Science*, *264*(5166), 1772–1775. <https://doi.org/10.1126/science.8209258>
- Gururajan, A., Clarke, G., Dinan, T. G., & Cryan, J. F. (2016). Molecular biomarkers of depression. *Neuroscience and Biobehavioral Reviews*, *64*, 101–133. <https://doi.org/10.1016/j.neubiorev.2016.02.011>
- Hammen, C. (2005). Stress and Depression. *Annual Review of Clinical Psychology*, *1*, 293–319.
- Harper, M.-E., Dent, R., Monemdjou, S., Bezaire, V., Wyck, L., Wells, G., ... Mcpherson, R. (2002). Decreased Mitochondrial Proton Leak and Reduced Expression of Uncoupling Protein 3 in Skeletal Muscle of Obese Diet-Resistant Women. *Diabetes*, *51*, 2459–2466. <https://doi.org/10.2337/diabetes.51.8.2459>
- Hashimoto, K. (2009). Emerging role of glutamate in the pathophysiology of major depressive disorder. *Brain Research Reviews*, *61*(2), 105–123. <https://doi.org/10.1016/j.brainresrev.2009.05.005>
- Herst, P. M., Tan, A. S., Scarlett, D. J. G., & Berridge, M. V. (2004). Cell surface oxygen consumption by mitochondrial gene knockout cells. *Biochimica et Biophysica Acta - Bioenergetics*, *1656*(2–3), 79–87. <https://doi.org/10.1016/j.bbabi.2004.01.008>
- Hroudová, J., Fišar, Z., Kitzlerová, E., Zvěřová, M., & Raboch, J. (2013). Mitochondrial respiration in blood platelets of depressive patients. *Mitochondrion*, *13*(6), 795–800. <https://doi.org/10.1016/j.mito.2013.05.005>
- Hüttemann, M., Lee, I., Pecinova, A., Pecina, P., Przyklenk, K., & Doan, J. W. (2008). Regulation of oxidative phosphorylation, the mitochondrial membrane potential, and their role in human disease. *Journal of Bioenergetics and Biomembranes*, *40*(5), 445–456. <https://doi.org/10.1007/s10863-008-9169-3>
- Iosifescu, D. V., Bolo, N. R., Nierenberg, A. A., Jensen, J. E., Fava, M., & Renshaw, P. F. (2008). Brain Bioenergetics and Response to Triiodothyronine Augmentation in Major Depressive Disorder. *Biological Psychiatry*, *63*(12), 1127–1134. <https://doi.org/10.1016/j.biopsych.2007.11.020>
- Kannurpatti, S. S., Joshi, P. G., & Joshi, N. B. (2000). Calcium sequestering ability of mitochondria modulates influx of calcium through glutamate receptor channel. *Neurochemical Research*, *25*(12), 1527–1536. <https://doi.org/10.1023/A:1026602100160>
- Karabatsiakos, A., Böck, C., Salinas-Manrique, J., Kolassa, S., Calzia, E., Dietrich, D. E., & Kolassa, I. T. (2014). Mitochondrial respiration in peripheral blood mononuclear cells correlates with depressive subsymptoms and severity of major depression. *Translational Psychiatry*, *4*. <https://doi.org/10.1038/tp.2014.44>
- Kato, N., & Kato, T. (2000). Mitochondrial dysfunction in Bipolar Disorder. *Bipolar Disorder*, *2*(3), 180–190.
- Kendler, K. S., Karkowski, L. M., & Prescott, C. A. (1998). Stressful life events and major depression: risk period, long-term contextual threat and diagnostic specificity. *The Journal of Nervous and Mental Disease*, *186*, 661–669.
- Kerppola, W. (1959). Uncoupling of the oxidative phosphorylation with cortisone in liver mitochondria. *Endocrinology*, *67*, 252–263.

- Kessler, R. C., & Bromet, E. J. (2013). Annu Rev Public Health. *The Epidemiology of Depression across Cultures.*, 34, 119–138. <https://doi.org/10.1146/annurev-publhealth-031912-114409>
- Kim, J. H., Kim, H. K., Ko, J. H., Bang, H., & Lee, D. C. (2013). The Relationship between Leukocyte Mitochondrial DNA Copy Number and Telomere Length in Community-Dwelling Elderly Women. *PLoS ONE*, 8(6), 1–8. <https://doi.org/10.1371/journal.pone.0067227>
- Kim, K., Doi, A., Wen, B., Ng, K., Zhao, R., Cahan, P., ... Daley, G. Q. (2010). Epigenetic memory in induced pluripotent stem cells performed CHARM and guided analysis of methylation HHS Public Access. *Nature*, 467(7313), 285–290. <https://doi.org/10.1038/nature09342>
- Kim, M.-Y., Lee, J.-W., Hee-Cheol, K., Kim, E., & Lee, D.-Ch. (2001). Leukocyte mitochondrial DNA (mtDNA) content is associated with depression in old women. *Archives of Gerontology and Geriatrics*, 53(2), 218–221.
- Kimberg, D. V., Loud, A. V., & Wiener, J. (1968). Cortisone-induced alterations in mitochondrial function and structure. *Journal of Cell Biology*, 37(1), 63–79. <https://doi.org/10.1083/jcb.37.1.63>
- Klein Gunnewiek, T. M., Hugte, E. J. H. Van, Frega, M., Guardia, G. S., Foreman, K. B., Panneman, D., ... Kozicz, T. (2019). Mitochondrial dysfunction impairs human neuronal development and reduces neuronal network activity and synchronicity. *BioRxiv*, 720227. <https://doi.org/10.1101/720227>
- Klinedinst, N. J., & Regenold, W. T. (2014). A mitochondrial bioenergetic basis of depression. *Journal of Bioenergetics and Biomembranes*, 47(1–2), 155–171. <https://doi.org/10.1007/s10863-014-9584-6>
- Krauss, S., Zhang, C. Y., Scorrano, L., Dalgaard, L. T., St-Pierre, J., Grey, S. T., & Lowell, B. B. (2003). Superoxide-mediated activation of uncoupling protein 2 causes pancreatic β cell dysfunction. *Journal of Clinical Investigation*, 112(12), 1831–1842. <https://doi.org/10.1172/JCI200319774>
- Krempler, F., Esterbauer, H., Weitgasser, R., Ebenbichler, C., Patsch, J. R., Miller, K., ... Patsch, W. (2002). A functional polymorphism in the promoter of UCP2 enhances obesity risk but reduces type 2 diabetes risk in obese middle-aged humans. *Diabetes*, 51(11), 3331–3335. <https://doi.org/10.2337/diabetes.51.11.3331>
- Kroemer, G., Galluzzi, L., & Brenner, C. (2007). Mitochondrial membrane permeabilization in cell death. *Physiological Reviews*, 87(1), 99–163. <https://doi.org/10.1152/physrev.00013.2006>
- Krystal, J. H., Sanacora, G., & Duman, R. S. (2013). Rapid-acting glutamatergic antidepressants: the path to ketamine and beyond. *Biological Psychiatry*, 73(12), 1133–1141. <https://doi.org/10.1161/CIRCULATIONAHA.110.956839>
- Kuffner, K., Triebelhorn, J., Meindl, K., Benner, C., Sudria, D., Siebert, R., Manook, A., Nothdurfter, C., Drexler, K.; Berneburg, M., Rupprecht, R., Milenkovic, V., Wetzels, C.H. (2020). Major depressive disorder is associated with impaired mitochondrial function in skin fibroblasts. *Cells*, 9(4), 884. <https://doi.org/10.3390/cells9040884>
- Kumar, P., Efsthathopoulos, P., Millischer, V., Olsson, E., Bin Wei, Y., Brüstle, O., ... Lavebratt, C. (2018). Mitochondrial DNA copy number is associated with psychosis severity and anti-psychotic treatment. *Scientific Reports*, 8(1), 1–13. <https://doi.org/10.1038/s41598-018-31122-0>
- Kupfer, D. J., Frank, E., & Phillips, M. L. (2012). Major depressive disorder: new clinical, neurobiological and treatment perspectives. *The Lancet Psychiatry*, 379(9820), 1045–1055. [https://doi.org/10.1016/S0140-6736\(11\)60602-8](https://doi.org/10.1016/S0140-6736(11)60602-8)
- Kyrou, I., Chrousos, G. P., & Tsigos, C. (2006). Stress, visceral obesity, and metabolic

- complications. *Annals of the New York Academy of Sciences*, 1083, 77–110. <https://doi.org/10.1196/annals.1367.008>
- Lajic, S., Nordenström, A., & Hirvikoski, T. (2011). Long-Term Outcome of Prenatal Dexamethasone Treatment of 21-Hydroxylase Deficiency. *Endocrine Development*, 20, 96–105. <https://doi.org/10.1159/000321228>
- Langer, C., Jürgensmeier, J. M., & Bauer, G. (1996). Reactive oxygen species act at both TGF- β -dependent and -independent steps during induction of apoptosis of transformed cells by normal cells. *Experimental Cell Research*, 222(1), 117–124. <https://doi.org/10.1006/excr.1996.0015>
- Larsen, S., Nielsen, J., Hansen, C. N., Nielsen, L. B., Wibrand, F., Stride, N., ... Hey-Mogensen, M. (2012). Biomarkers of mitochondrial content in skeletal muscle of healthy young human subjects. *Journal of Physiology*, 590(14), 3349–3360. <https://doi.org/10.1113/jphysiol.2012.230185>
- Lee, H., & Yoon, Y. (2016). Mitochondrial fission and fusion. *Biochemical Society Transactions*, 44(6), 1725–1735. <https://doi.org/10.1042/BST20160129>
- Leonard, B. E. (2007). Psychopathology of depression. *Drugs Today*, 43(10), 705–716.
- Lépine, J. P., & Briley, M. (2011). The increasing burden of depression. *Neuropsychiatric Disease and Treatment*, 7(1), 3–7. <https://doi.org/10.2147/NDT.S19617>
- Leverve, X. M. (2007). Mitochondrial function and substrate availability. *Critical Care Medicine*, 35(9). <https://doi.org/10.1097/01.CCM.0000278044.19217.73>
- Liang, H., Balas, B., Tantiwong, P., Dube, J., Goodpaster, B. H., O'Doherty, R. M., ... Ward, W. F. (2009). Whole body overexpression of PGC-1 α has opposite effects on hepatic and muscle insulin sensitivity. *American Journal of Physiology - Endocrinology and Metabolism*, 296(4). <https://doi.org/10.1152/ajpendo.90292.2008>
- Lister, R., Pelizzola, M., Hwankins, R. D., Nery, J. R., Hon, G., Antosiewicz-Bourget, J., ... Ecker, J. R. (2011). Hotspots of aberrant epigenomic reprogramming in human induced pluripotent stem cells. *Nature*, 471(7336), 68–73.
- Lorenz, C., Lesimple, P., Bukowiecki, R., Zink, A., Inak, G., Mlody, B., ... Prigione, A. (2017). Human iPSC-Derived Neural Progenitors Are an Effective Drug Discovery Model for Neurological mtDNA Disorders. *Cell Stem Cell*, 20(5), 659–674. <https://doi.org/10.1016/j.stem.2016.12.013>
- Luscher, B., Shen, Q., & Sahir, N. (2011). The GABAergic deficit Hypothesis of Major Depressive Disorder. *Molecular Psychiatry*, 16(4), 383–406. <https://doi.org/10.1038/mp.2010.120>
- Maes, M. (1999). Major depression and activation of the inflammatory response system. *Advances in Experimental Medicine and Biology*, 461, 25–46.
- Maes, M., Lambrecht, J., Bosmans, E., Jacobs, J., Suy, E., Vandervorst, C., ... Raus, J. (1992). Evidence for a systemic immune activation during depression: results of leukocyte enumeration by flow cytometry in conjunction with monoclonal antibody staining. *Psychological Medicine*, 22(1), 45–53.
- Manoli, I., Alesci, S., Blackman, M. R., Su, Y. A., Rennert, O. M., & Chrousos, G. P. (2007). Mitochondria as key components of the stress response. *Trends in Endocrinology and Metabolism*, 18(5), 190–198. <https://doi.org/10.1016/j.tem.2007.04.004>
- Marroquin, L. D., Hynes, J., Dykens, J. A., Jamieson, J. D., & Will, Y. (2007). Circumventing the crabtree effect: Replacing media glucose with galactose increases susceptibility of hepG2 cells to mitochondrial toxicants. *Toxicological Sciences*, 97(2), 539–547. <https://doi.org/10.1093/toxsci/kfm052>
- Meeusen, S., DeVay, R., Block, J., Cassidy-Stone, A., Wayson, S., McCaffery, J. M., & Nunnari, J. (2006). Mitochondrial Inner-Membrane Fusion and Crista Maintenance Requires the Dynamin-Related GTPase Mgm1. *Cell*.

- <https://doi.org/10.1016/j.cell.2006.09.021>
- Mengel-From, J., Thinggaard, M., Dalgård, C., Kyvik, K. O., Christensen, K., & Christiansen, L. (2014). Mitochondrial DNA copy number in peripheral blood cells declines with age and is associated with general health among elderly. *Human Genetics*, *133*(9), 1149–1159. <https://doi.org/10.1007/s00439-014-1458-9>
- Mertens, J., Wang, Q. W., Kim, Y., Yu, D. X., Pham, S., Yang, B., ... Yao, J. (2015). Differential responses to lithium in hyperexcitable neurons from patients with bipolar disorder. *Nature*, *527*(7576), 95–99. <https://doi.org/10.1038/nature15526>
- Michael, L. F., Wu, Z., Cheatham, R. B., Puigserver, P., Adelmant, G., Lehman, J. J., ... Spiegelman, B. M. (2001). Restoration of insulin-sensitive glucose transporter (GLUT4) gene expression in muscle cells by the transcriptional coactivator PGC-1. *Proceedings of the National Academy of Sciences of the United States of America*, *98*(7), 3820–3825. <https://doi.org/10.1073/pnas.061035098>
- Micheau, O., & Tschopp, J. (2003). Induction of TNF receptor I-mediated apoptosis via two sequential signaling complexes. *Cell*, *114*(2), 181–190. [https://doi.org/10.1016/S0092-8674\(03\)00521-X](https://doi.org/10.1016/S0092-8674(03)00521-X)
- Mikes, Z., Ku, J., Weber, K., Bru, P., Klingenspor, M., Wiesner, R. J., ... Pathology, M. (2002). Biogenesis Specifically in Skeletal Muscle. *Endocrinology*, *143*(1), 177–184.
- Mlody, B., Lorenz, C., Inak, G., & Prigione, A. (2016). Energy metabolism in neuronal/glia induction and in iPSC models of brain disorders. *Seminars in Cell and Developmental Biology*, *52*, 102–109. <https://doi.org/10.1016/j.semcd.2016.02.018>
- Mogensen, M., Bagger, M., Pedersen, P. K., Fernström, M., & Sahlin, K. (2006). Cycling efficiency in humans is related to low UCP3 content and to type I fibres but not to mitochondrial efficiency. *Journal of Physiology*, *571*(3), 669–681. <https://doi.org/10.1113/jphysiol.2005.101691>
- Mookerjee, S. A., Divakuruni, A. S., Jastroch, M., & Brand, M. D. (2010). Mitochondrial uncoupling and lifespan. *Mechanisms of Ageing and Development*, *13*(7–8), 463–472. <https://doi.org/10.1038/jid.2014.371>
- Mookerjee, S. A., Goncalves, R. L. S., Gerencser, A. A., Nicholls, D. G., & Brand, M. D. (2015). The contributions of respiration and glycolysis to extracellular acid production. *Biochimica et Biophysica Acta - Bioenergetics*, *1847*(2), 171–181. <https://doi.org/10.1016/j.bbabi.2014.10.005>
- Moreno, J., Gaspar, E., López-Bello, G., Juárez, E., Alcázar-Leyva, S., González-Trujano, E., ... Alvarado-Vásquez, N. (2013). Increase in nitric oxide levels and mitochondrial membrane potential in platelets of untreated patients with major depression. *Psychiatry Research*, *209*(3), 447–452. <https://doi.org/10.1016/j.psychres.2012.12.024>
- Morgan-Hughes, J. A. (1996). Mitochondrial disorders. *Current Opinion in Neurology*, *9*, 269–374.
- Morin, C., Zini, R., Simon, N., Charbonnier, P., Tillement, J. P., & Le Louet, H. (2000). Low glucocorticoid concentrations decrease oxidative phosphorylation of isolated rat brain mitochondria: An additional effect of dexamethasone. *Fundamental and Clinical Pharmacology*, *14*(5), 493–500. <https://doi.org/10.1111/j.1472-8206.2000.tb00432.x>
- Nagai, T., Sawano, A., Park, E. S., & Miyawaki, A. (2001). Circularly permuted green fluorescent proteins engineered to sense Ca²⁺. *Proceedings of the National Academy of Sciences of the United States of America*, *98*(6), 3197–3202. <https://doi.org/10.1073/pnas.051636098>
- Oakley, R. H., & Cidlowski, J. A. (2013). The Biology of the Glucocorticoid Receptor: New Signaling Mechanisms in Health and Disease. *Journal of Allergy and Clinical*

- Immunology*, 132(5), 1033–1044.
- Oexle, K., & Zwirner, A. (1997). Advanced telomere shortening in respiratory chain disorders. *Human Molecular Genetics*, 6(6), 905–908. <https://doi.org/10.1093/hmg/6.6.905>
- Ohi, Y., Qin, H., Hong, C., Blouin, L., Polo, J. M., Guo, T., ... Ramalho-Santos, M. (2011). Incomplete DNA methylation underlies a transcriptional memory of somatic cells in human iPS cells. *Nature Cell Biology*, 13(5), 541–549. <https://doi.org/10.1038/ncb2239>
- Ostergaard, E., Hansen, F. J., Sorensen, N., Duno, M., Vissing, J., Larsen, P. L., ... Schwartz, M. (2007). Mitochondrial encephalomyopathy with elevated methylmalonic acid is caused by SUCLA2 mutations. *Brain*, 130(3), 853–861. <https://doi.org/10.1093/brain/awl383>
- Ozcan, M. E., Gulec, M., Ozerol, E., Polat, R., & Akyol, O. (2004). Antioxidant enzyme activities and oxidative stress in affective disorders. *International Clinical Psychopharmacology*, 19(2), 89–95. <https://doi.org/10.1097/00004850-200403000-00006>
- Paradies, G., Petrosillo, G., Pistolese, M., Di Venosa, N., Federici, A., & Ruggiero, F. M. (2004). Decrease in Mitochondrial Complex I Activity in Ischemic/Reperfused Rat Heart: Involvement of Reactive Oxygen Species and Cardiolipin. *Circulation Research*, 94(1), 53–59. <https://doi.org/10.1161/01.RES.0000109416.56608.64>
- Patti, M. E., Butte, A. J., Crunkhorn, S., Cusi, K., Berria, R., Kashyap, S., ... Mandarino, L. J. (2003). Coordinated reduction of genes of oxidative metabolism in humans with insulin resistance and diabetes: Potential role of PGC1 and NRF1. *Proceedings of the National Academy of Sciences of the United States of America*, 100(14), 8466–8471. <https://doi.org/10.1073/pnas.1032913100>
- Peter, J. B., Verhaag, D. A., & Worsfold, M. (1970). Studies of steroid myopathy. *Biochemical Pharmacology*, 19(5), 1627–1636. [https://doi.org/10.1016/0006-2952\(70\)90151-6](https://doi.org/10.1016/0006-2952(70)90151-6)
- Picard, M., Taivassalo, T., Gouspillou, G., & Hepple, R. T. (2011). Mitochondria: Isolation, structure and function. *Journal of Physiology*, 589(18), 4413–4421. <https://doi.org/10.1113/jphysiol.2011.212712>
- Picard, M., Taivassalo, T., Ritchie, D., Wright, K. J., Thomas, M. M., Romestaing, C., & Hepple, R. T. (2011). Mitochondrial structure and function are disrupted by standard Isolation methods. *PLoS ONE*, 6(3), 1–12. <https://doi.org/10.1371/journal.pone.0018317>
- Pittenger, C., & Duman, R. S. (2008). Stress, depression, and neuroplasticity: A convergence of mechanisms. *Neuropsychopharmacology*, 33(1), 88–109. <https://doi.org/10.1038/sj.npp.1301574>
- Polo, J. M., Liu, S., Figueroa, M. E., Kulalaert, W., Eminli, S., Tan, K. Y., ... Hochedlinger, K. (2010). Cell type of origin influences the molecular and functional properties of mouse induced pluripotent stem cells. *Nature Biotechnology*, 28(8), 848–855.
- Prayson, R. A., & Wang, N. (1998). Mitochondrial myopathy, encephalopathy, lactic acidosis, and strokelike episodes (MELAS) syndrome: an autopsy report. *Archives of Pathology & Laboratory Medicine*, 122(11), 978–981.
- Pufall, M. A. (2015a). Glucocorticoids and Cancer. *Advances in Experimental Medicine and Biology*, 872, 253–278. <https://doi.org/10.1007/978-1-4939-2895-8>
- Pufall, M. A. (2015b). Glucocorticoids and Cancer. *Advances in Experimental Medicine and Biology*, 872, 253–278. <https://doi.org/10.1007/978-1-4939-2895-8>
- Rantamaki, T., & Yalcin, I. (2016). Antidepressant drug action - From rapid changes on network function to network rewiring. *Progress in Neuro-Psychopharmacology and Biological Psychiatry*, 64, 285–292. <https://doi.org/10.1016/j.pnpbp.2015.06.001>

- Réus, G. Z., Titus, S. E., Abelaira, H. M., Freitas, S. M., Tuon, T., Quevedo, J., & Budni, J. (2016). Neurochemical correlation between major depressive disorder and neurodegenerative diseases. *Life Sciences*, *158*, 121–129. <https://doi.org/10.1016/j.lfs.2016.06.027>
- Ricquier, D., & Bouillaud, F. (2000). The uncoupling protein homologues: UCP1, UCP2, UCP3, StUCP and AtUCP. *Biochemical Journal*, *345*(2), 161–179. <https://doi.org/10.1042/0264-6021:3450161>
- Ritov, V. B., Menshikova, E. V., & Kelley, D. E. (2006). Analysis of cardiolipin in human muscle biopsy. *Journal of Chromatography B: Analytical Technologies in the Biomedical and Life Sciences*, *831*(1–2), 63–71. <https://doi.org/10.1016/j.jchromb.2005.11.031>
- Robin, E. D., & Wong, R. (1988). Mitochondrial DNA molecules and virtual number of mitochondria per cell in mammalian cells. *Journal of Cellular Physiology*, *136*(3), 507–513. <https://doi.org/10.1002/jcp.1041360316>
- Robinson, B. H., Petrova-Benedict, R., Buncic, J. R., & Wallace, D. C. (1992). Nonviability of cells with oxidative defects in galactose medium: A screening test for affected patient fibroblasts. *Biochemical Medicine and Metabolic Biology*, *48*(2), 122–126. [https://doi.org/10.1016/0885-4505\(92\)90056-5](https://doi.org/10.1016/0885-4505(92)90056-5)
- Roma, P., Rinker, L., Peng, J., & Chilian, W. M. (2017). *Reactive Oxygen Species: The Good and the Bad*. <https://doi.org/DOI:10.5772/intechopen.71547>
- Rossignol, R., Gilkerson, R., Aggeler, R., Yamagata, K., Remington, S. J., & Capaldi, R. A. (2004). Energy Substrate Modulates Mitochondrial Structure and Oxidative Capacity in Cancer Cells. *Cancer Research*, *64*(3), 985–993. <https://doi.org/10.1158/0008-5472.CAN-03-1101>
- Russell, L. K., Mansfield, C. M., Lehman, J. J., Kovacs, A., Courtois, M., Saffitz, J. E., ... Kelly, D. P. (2004). Cardiac-Specific Induction of the Transcriptional Coactivator Peroxisome Proliferator-Activated Receptor γ Coactivator-1 α Promotes Mitochondrial Biogenesis and Reversible Cardiomyopathy in a Developmental Stage-Dependent Manner. *Circulation Research*, *94*(4), 525–533. <https://doi.org/10.1161/01.RES.0000117088.36577.EB>
- Sargsyan, A., Cai, J., Fandino, L. B., Labasky, M. E., Forostyan, T., Colosimo, L. K., ... Graham, T. E. (2015). Rapid parallel measurements of macroautophagy and mitophagy in mammalian cells using a single fluorescent biosensor. *Scientific Reports*, *5*(July), 1–11. <https://doi.org/10.1038/srep12397>
- Sarzi, E., Goffart, S., Serre, V., Chrétien, D., Slama, A., Munnich, A., ... Rötig, A. (2007). Twinkle helicase (PEO1) gene mutation causes mitochondrial DNA depletion. *Annals of Neurology*, *62*(6), 579–587. <https://doi.org/10.1002/ana.21207>
- Satrústegui, J., Pardo, B., & Del Arco, A. (2007). Mitochondrial transporters as novel targets for intracellular calcium signaling. *Physiological Reviews*, *87*(1), 29–67. <https://doi.org/10.1152/physrev.00005.2006>
- Schäcke, H., Döcke, W.-D., & Asadullah, K. (2002). Mechanisms involved in the side effects of glucocorticoids. *Pharmacology & Therapeutics*, *96*, 23–43. [https://doi.org/10.1016/S0163-7258\(02\)00297-8](https://doi.org/10.1016/S0163-7258(02)00297-8)
- Schneider, B., & Prvulovic, D. (2013). Novel biomarkers in major depression. *Current Opinion in Psychiatry*, *26*(1), 47–53. <https://doi.org/10.1097/YCO.0b013e32835a5947>
- Shokolenko, I., Venediktova, N., Bochkareva, A., Wilson, G. I., & Alexeyev, M. F. (2009). Oxidative stress induces degradation of mitochondrial DNA. *Nucleic Acids Research*, *37*(8), 2539–2548. <https://doi.org/10.1093/nar/gkp100>
- Shoshan-Barmatz, V., Pittala, S., & Mizrachi, D. (2019). VDAC1 and the TSPO: Expression,

- Interactions, and Associated Functions in Health and Disease States. *International Journal of Molecular Sciences*, 20(13), 3348.
<https://doi.org/10.3390/ijms20133348>
- Siciliano, G., Tessa, A., Petrini, S., Mancuso, M., Bruno, C., Grieco, G. S., ... Murri, L. (2003). Autosomal dominant external ophthalmoplegia and bipolar affective disorder associated with a mutation in the ANT1 gene. *Neuromuscular Disorders*, 13(2), 162–165. [https://doi.org/10.1016/S0960-8966\(02\)00221-3](https://doi.org/10.1016/S0960-8966(02)00221-3)
- Siklós, L., Engelhardt, J., Harati, Y., Smith, R. G., Joó, F., & Appel, S. H. (1996). Ultrastructural evidence for altered calcium in motor nerve terminals in amyotrophic lateral sclerosis. *Annals of Neurology*, 39(2), 203–216.
<https://doi.org/10.1002/ana.410390210>
- Sluzewska, A. (1999). Indicators of immune activation in depressed patients. *Advances in Experimental Medicine and Biology*, 461(59–73).
- Sonnenberg, C. M., Deeg, D. J. H., Comijs, H. C., van Tilburg, W., & Beekman, A. T. F. (2008). Trends in antidepressant use in the older population: Results from the LASA-study over a period of 10 years. *Journal of Affective Disorders*, 111(2–3), 299–305.
<https://doi.org/10.1016/j.jad.2008.03.009>
- Spinelli, J. B., & Haigis, M. C. (2018). The multifaceted contributions of mitochondria to cellular metabolism. *Nature Cell Biology*, 20(7), 745–754.
<https://doi.org/10.1038/s41556-018-0124-1>
- Steckler, T., Holsboer, F., & Reul, J. M. H. M. (1999). Glucocorticoids and depression. *Bailliere's Best Practice and Research in Clinical Endocrinology and Metabolism*, 13(4), 597–614. <https://doi.org/10.1053/beem.1999.0046>
- Steinlechner-Maran, R., Eberl, T., Kunc, M., Schröcksnadel, H., Margreiter, R., & Gnaiger, E. (1997). Respiratory defect as an early event in preservation-reoxygenation injury of endothelial cells. *Transplantation*, 63(1).
- Stetler, C., & Miller, G. E. (2011). Depression and hypothalamic-pituitary-adrenal activation: A quantitative summary of four decades of research. *Psychosomatic Medicine*, 73(2), 114–126. <https://doi.org/10.1097/PSY.0b013e31820ad12b>
- Stork, C., & Renshaw, P. F. (2005). Mitochondrial dysfunction in bipolar disorder: Evidence from magnetic resonance spectroscopy research. *Molecular Psychiatry*, 10(10), 900–919. <https://doi.org/10.1038/sj.mp.4001711>
- Strüber, N., Strüber, D., & Roth, G. (2014a). Impact of early adversity on glucocorticoid regulation and later mental disorders. *Neuroscience and Biobehavioral Reviews*, 38(1), 17–37. <https://doi.org/10.1016/j.neubiorev.2013.10.015>
- Strüber, N., Strüber, D., & Roth, G. (2014b). Impact of early adversity on glucocorticoid regulation and later mental disorders. *Neuroscience and Biobehavioral Reviews*, 38(1), 17–37. <https://doi.org/10.1016/j.neubiorev.2013.10.015>
- Suwanjang, W., Wu, K. L. H., Prachayasittikul, S., Chetsawang, B., & Charngkaew, K. (2019). Mitochondrial Dynamics Impairment in Dexamethasone-Treated Neuronal Cells. *Neurochemical Research*, 0(0), 0. <https://doi.org/10.1007/s11064-019-02779-4>
- Swerdlow, R. H. (2009). The neurodegenerative mitochondriopathies. *Journal of Alzheimer's Disease*, 17(4), 737–751. <https://doi.org/10.3233/JAD-2009-1095>
- Takahashi, K., & Yamanaka, S. (2006). Induction of Pluripotent Stem Cells from Mouse Embryonic and Adult Fibroblast Cultures by Defined Factors. *Cell*, 126(4), 663–676.
<https://doi.org/10.1016/j.cell.2006.07.024>
- Tanaka, T., Hosoi, F., Yamaguchi-Iwai, Y., Nakamura, H., Masutani, H., Ueda, S., ... Yodoi, J. (2002). Thioredoxin-2 (TRX-2) is an essential gene regulating mitochondria-dependent apoptosis. *EMBO Journal*, 21(7), 1695–1703.
<https://doi.org/10.1093/emboj/21.7.1695>

- Velliquette, R. A., O'Connor, T., & Vassar, R. (2005). Energy inhibition elevates β -secretase levels and activity and is potentially amyloidogenic in APP transgenic mice: Possible early events in Alzheimer's disease pathogenesis. *Journal of Neuroscience*, *25*(47), 10874–10883. <https://doi.org/10.1523/JNEUROSCI.2350-05.2005>
- Vergara, R. C., Jaramillo-Riveri, S., Luarte, A., Moënne-loccoz, C., Fuentes, R., Couve, A., & Maldonado, P. E. (2019). The Energy Homeostasis Principle: Neuronal Energy Regulation Drives Local Network Dynamics Generating Behavior. *13*(July), 1–18. <https://doi.org/10.3389/fncom.2019.00049>
- Videbeck, P. (2000). PET measurements of brain glucose metabolism and blood flow in major depressive disorder: A critical review. *Acta Psychiatrica Scandinavica*, *101*(1), 11–20. <https://doi.org/10.1034/j.1600-0447.2000.101001011.x>
- Vojtíšková, A., Ješina, P., Kalous, M., Kaplanová, V., Houštěk, J., Tesařová, M., ... Godinot, C. (2004). Mitochondrial Membrane Potential and ATP Production in Primary Disorders of ATP Synthase. *Toxicology Mechanisms and Methods*, *14*(1–2), 7–11. <https://doi.org/10.1080/15376520490257347>
- Vreeburg, S. A., Hoogendijk, W. J. G., van Pelt, J., DeRijk, R. H., Verhagen, J. C. M., van Dyck, R., ... Penninx, B. W. J. H. (2009). Major Depressive Disorder and Hypothalamic-Pituitary-Adrenal Axis Activity. *Archives of General Psychiatry*, *66*(6), 617. <https://doi.org/10.1001/archgenpsychiatry.2009.50>
- Walker, U. A., & Collins, S. (1996). Respiratory chain encephalomyopathies: a diagnostic classification. *European Journal of Neurology*, *36*, 260–267.
- Wang, X., Sundquist, K., Rastkhani, H., Palmér, K., Memon, A. A., & Sundquist, J. (2017). Association of mitochondrial DNA in peripheral blood with depression, anxiety and stress- and adjustment disorders in primary health care patients. *European Neuropsychopharmacology*, *27*(8), 751–758. <https://doi.org/10.1016/j.euroneuro.2017.06.001>
- Weissman, M. M., Bland, R. C., Canino, G. J., Faravelli, C., Greenwald, S., Hwu, H.-G., ... Yeh, E.-K. (1996). Cross-National Epidemiology of Major Depression and Bipolar Disorder. *JAMA*, *276*(4), 293–299. <https://doi.org/10.1001/jama.1996.03540040037030>
- Wong, L.-J. C., Naviaux, R. K., Brunetti-Pierri, N., Zhang, Q., Schmitt, E. S., Truong, C., ... Copeland, W. C. (2008). Molecular and clinical genetics of mitochondrial diseases due to POLG mutations. *Human Mutation*, *29*(9), 150–172. <https://doi.org/10.1002/humu.20824>
- Wong, P. C., Pardo, C. A., Borchelt, D. R., Lee, M. K., Copeland, N. G., Jenkins, N. A., ... Price, D. L. (1995). An adverse property of a familial ALS-linked SOD1 mutation causes motor neuron disease characterized by vacuolar degeneration of mitochondria. *Neuron*, *14*(6), 1105–1116. [https://doi.org/10.1016/0896-6273\(95\)90259-7](https://doi.org/10.1016/0896-6273(95)90259-7)
- Wood, G. E., Young, L. T., Reagan, L. P., Chen, B., & McEwen, B. S. (2004). Stress-induced structural remodeling in hippocampus: Prevention by lithium treatment. *Proceedings of the National Academy of Sciences of the United States of America*, *101*(11), 3973–3978. <https://doi.org/10.1073/pnas.0400208101>
- Wu, Z., Huang, X., Feng, Y., Handschin, C., Feng, Y., Gullicksen, P. S., ... Stevenson, S. C. (2006). Transducer of regulated CREB-binding proteins (TORCs) induce PGC-1 α transcription and mitochondrial biogenesis in muscle cells. *Proceedings of the National Academy of Sciences of the United States of America*, *103*(39), 14379–14384. <https://doi.org/10.1073/pnas.0606714103>
- Yan, Y., Shin, S., Jha, B. S., Liu, Q., Sheng, J., Li, F., ... Vemuri, M. C. (2013). Efficient and Rapid Derivation of Primitive Neural Stem Cells and Generation of Brain Subtype Neurons From Human Pluripotent Stem Cells. *STEM CELLS Translational Medicine*, *2*(12),

- 1022–1022. <https://doi.org/10.5966/sctm.2013-0080erratum>
- Yonashiro, R., Sugiura, A., Miyachi, M., Fukuda, T., Matsushita, N., Inatome, R., ... Yanagi, S. (2009). Mutant SOD1 and Attenuates Mutant SOD1-induced Reactive Oxygen Species Generation. *Molecular Biology of the Cell*, 20, 4524–4530. <https://doi.org/10.1091/mbc.E09>
- Young, A. H., Sahakian, B. J., Robbins, T. W., & Cowen, P. J. (1999). The effects of chronic administration of hydrocortisone on cognitive function in normal male volunteers. *Psychopharmacology*, 145(3), 260–266. <https://doi.org/10.1007/s002130051057>
- Young, J. J., Silber, T., Bruno, D., Galatzer-Levy, I. R., Pomara, N., & Marmar, C. R. (2016). Is there progress? An overview of selecting biomarker candidates for major depressive disorder. *Frontiers in Psychiatry*, 7(72), 1–15. <https://doi.org/10.3389/fpsy.2016.00072>
- Yu, H., & Chen, Z. Y. (2011). The role of BDNF in depression on the basis of its location in the neural circuitry. *Acta Pharmacologica Sinica*, 32(1), 3–11. <https://doi.org/10.1038/aps.2010.184>
- Zheng, X., Boyer, L., Jin, M., Mertens, J., Kim, Y., Ma, L., ... Hunter, T. (2016). Metabolic reprogramming during neuronal differentiation from aerobic glycolysis to neuronal oxidative phosphorylation. *ELife*, 5(13374), 1–25. <https://doi.org/10.7554/eLife.13374>

List of figures

Figure 1 The organization of the mitochondrion.....	16
Figure 2 The ETC and the mechanism of OXPHOS in mitochondria.....	18
Figure 3 The ATP synthase.....	19
Figure 4 Mitochondria in the cellular metabolism.....	20
Figure 5 Fission and Fusion events.....	22
Figure 6 Symptoms of MDD and its increasing impact on daily performance.....	25
Figure 7 The Hypothalamic-Pituitary-Adrenal Axis.....	28
Figure 8 Mitochondrial functions in the stress response.....	32
Figure 9 ETC inhibitors.....	52
Figure 10 Mito Stress Test in the Seahorse XFp Flux Analyzer.....	53
Figure 11 Luciferase reaction for ATP quantification.....	54
Figure 12 Emission spectra of the cationic dye JC-1.....	55
Figure 13 Emission spectra and complex forming of the ratio metric dye Fura-2.....	56
Figure 14 Graphs and values for primer efficiency for mtDNA copy number determination.....	59
Figure 15 Seahorse XFp Flux Analyzer results of fibroblasts.....	65
Figure 16 Mito Stress Test in fibroblasts.....	66
Figure 17 Energy map of fibroblasts.....	67
Figure 18 Energy maps of fibroblasts for the three conditions.....	69
Figure 19 ATP content in fibroblasts.....	70
Figure 20 Fibroblasts loaded with the cationic dye JC-1.....	71
Figure 21 Mitochondrial membrane potential of fibroblasts.....	72
Figure 22 Cytosolic Ca ²⁺ homeostasis in fibroblasts.....	74
Figure 23 MtDNA copy number in 16 MDD and patient fibroblast cell lines.....	75
Figure 24 Fibroblasts in cell cultur.....	76
Figure 25 Reprogramming and iPSC clone separation.....	76
Figure 26 Immunostaining of NPC line MDD4.....	78
Figure 27 Seahorse XFp Flux Analyzer results of NPCs.....	80
Figure 28 Mito Stress Test in NPCs.....	82
Figure 29 Energy map of NPCs.....	82
Figure 30 Energy map for NPCs for the two conditions.....	84

Figure 31 ATP content in NPCs.....	85
Figure 32 Mitochondrial Membrane Potential measurements of NPCs..	86
Figure 33 Cytosolic Ca ²⁺ homeostasis in NPCs	87

List of tables

Table 1 Lab supplies used in the present study	41
Table 2 Chemicals required for the experiments of the study.....	41
Table 3 Kits	42
Table 4 Antibodies for Immunocytochemistry	43
Table 5 Primary Fibroblast Medium.....	43
Table 6 Primary fibroblast freezing medium	43
Table 7 E7 Medium	43
Table 8 mTeSR Medium	43
Table 9 Neural Induction Medium.....	43
Table 10 Neural Expansion Medium.....	44
Table 11 Blocking buffer.....	44
Table 12 Antibody buffer	44
Table 13 Seahorse Assay Medium pH=7.4.....	44
Table 14 Ringer's solution, pH=7.4.....	44
Table 15 Phosphate Buffered Saline pH=7.3	44
Table 16 Study participants and controls.....	45
Table 17 Volumes for fibroblast splitting procedure	46
Table 18 Coating conditions.....	49
Table 19 Target genes, sequences, concentrations and manufacturer of the primers used for mtDNA quantification.....	58
Table 20 Ragencies and volumes for RT-PCR.....	59
Table 21 Mean and SEM of clinical characteristics of n=16 MDD patients and n=16 controls.....	61
Table 22 Results of the PluriTest for pluripotency of iPSC lines.	77
Table 23 Percentage of PAX6/SOX2 positively stained NPCs.....	78
Table 24 Mean and SEM values for respiratory parameters of fibroblasts	118
Table 25 Single values (non-treated) for OCR and ECAR for 16 MDD and control fibroblast lines.....	118
Table 26 Single values (dexamethasone) for OCR and ECAR of 16 MDD patients and control fibroblast lines	119

Table 27 Single values (galactose) for OCR and ECAR of 16 MDD patients and control fibroblast lines	119
Table 28 Mean and SEM values for ATP measurements of fibroblast lines for 16 MDD patient and control pairs	120
Table 29 Single RLU values of 16 MDD patient and control pairs of fibroblast cell lines	120
Table 30 Mean and SEM values for JC-1 ratios of 16 MDD patients and controls fibroblast pairs	120
Table 31 Single red/green ratios for all 16 paired MDD and control cell lies	121
Table 32 Table 30 Mean and SEM values for Fura-2 ratios of 16 MDD patient and control pairs	121
Table 33 Single ratio values for Fura-2 measurements in fibroblasts.....	121
Table 34 Mean and SEM values of mtDNA copy numbers in fibroblasts.....	122
Table 35 mtDNA copy numbers for 16 MDD and control fibroblast cell lines.	122
Table 36 Mean and SEM values of respiratory parameters of 9 MDD and control NPC pairs.....	122
Table 37 OCR and ECAR values for 9 NPC MDD and control pairs.	123
Table 38 Mean and SEM values for JC-1 ratios of nine NPC MDD and control pairs.....	123
Table 39 Mean and SEM values for ATP measurements of 9 NPC MDD patients and control pairs	123
Table 40 Single RLU values of 9 MDD patient and control pairs of NPC lines	123
Table 41 Single JC-ratios for 9 MDD and control NPC lines.....	124
Table 42 Mean and SEM values for Fura-2 ratios of 9 NPC MDD and control pairs.....	124
Table 43 Single Fura-2 ratios for 9 MDD and control NPC cell lines.....	124

Appendix

Table 24 Mean and SEM values for respiratory parameters of fibroblasts

	Basal Respiration		Maximal Respiration		Spare Respiratory Capacity	
	mean OCR	SEM	mean OCR	SEM	mean OCR	SEM
MDD N	16.09	0.88	32.20	2.23	16.11	1.81
Control N	18.53	0.95	37.01	2.40	18.95	2.29
MDD DEX	22.96	1.14	48.76	3.88	25.28	3.15
Control DEX	23.25	1.12	45.03	2.32	27.76	3.92
MDD GAL	22.31	1.70	57.86	2.64	35.91	3.19
Control GAL	22.64	1.58	60.04	3.41	37.33	3.65
	non-mitochondrial Respiration		Proton Leak		ATP -related Respiration	
	mean OCR	SEM	mean OCR	SEM	mean OCR	SEM
MDD N	7.90	0.71	2.38	0.20	13.71	0.76
Control N	9.65	0.91	2.80	0.22	15.72	0.82
MDD DEX	11.08	0.95	2.94	0.31	19.91	0.90
Control DEX	11.84	0.79	2.72	0.29	20.52	0.97
MDD GAL	15.43	1.34	3.99	0.58	18.32	1.26
Control GAL	18.05	1.60	3.76	0.37	18.88	1.27

Table 25 Single values (non-treated) for OCR and ECAR for 16 MDD and control fibroblast lines

Pair	N			
	MDD		Control	
	OCR	ECAR	OCAR	ECAR
#1	22.49	18.03	23.45	10.99
#2	30.03	11.27	31.44	12.65
#3	29.63	13.82	28.19	12.15
#4	24.63	10.67	22.91	9.52
#5	18.01	12.25	19.59	12.54
#6	26.13	16.30	26.05	16.01
#7	22.07	10.39	46.04	12.23
#8	20.75	15.47	32.40	13.46
#9	25.23	16.86	29.46	8.36
#10	28.59	10.35	37.79	15.66
#11	26.74	24.38	30.16	16.53
#12	25.97	14.54	25.92	9.76

#13	22,69	9.84	30.25	9.37
#14	30.48	9.16	33.19	20.23
#15	17.96	11.41	20.76	12.98
#16	21.41	14.07	31.49	12.29

Table 26 Single values (dexamethasone) for OCR and ECAR of 16 MDD patients and control fibroblast lines

Pair	Dexamethasone			
	MDD		Control	
	OCR	ECAR	OCR	ECAR
#1	53.55	17.93	58.86	14.18
#2	37.21	5.89	64.30	20.29
#3	45.31	7.38	40.41	7.48
#4	34.90	19.33	33.07	10.53
#5	23.23	8.33	28.63	9.59
#6	46.83	15.69	43.97	11.81
#7	24.39	8.07	42.41	10.24
#8	28.61	7.51	48.86	10.24
#9	37.49	11.52	43.16	12.29
#10	36.73	13.79	42.97	9.53
#11	35.87	10.55	42.57	13.05
#12	44.58	15.01	49.54	16.93
#13	47.74	1.69	48.17	8.60
#14	18.94	3.29	20.30	5.57
#15	40.94	14.80	40.03	13.68
#16	79.48	11.08	50.68	5.46

Table 27 Single values (galactose) for OCR and ECAR of 16 MDD patients and control fibroblast lines

Pair	Galactose			
	MDD		Control	
	OCR	ECAR	OCR	ECAR
#1	29.74	15.76	30.53	15.39
#2	30.36	17.90	39.13	22.72
#3	46.32	18.51	41.86	16.67
#4	30.50	12.11	29.84	8.79
#5	41.26	15.28	28.96	17.27
#6	39.81	12.32	40.85	13.87
#7	32.15	12.02	40.54	16.82
#8	36.66	13.14	43.41	13.89
#9	59.61	18.47	63.51	19.12
#10	89.13	43.59	72.84	26.04
#11	52.29	15.59	59.37	16.09
#12	68.26	31.40	69.54	18.35
#13	56.03	17.51	62.29	13.05

#14	57.89	11.30	51.49	8.50
#15	82.35	37.22	73.74	21.74
#16	42.71	18.54	47.60	10.63

Table 28 Mean and SEM values for ATP measurements of fibroblast lines for 16 MDD patient and control pairs

	mean (RLU)	SEM
MDD N	59908	11595
Control N	73315	12402
MDD DEX	52419	10382
Control DEX	58836	11328
MDD GAL	89158	15043
Control GAL	99162	14537

Table 29 Single RLU values of 16 MDD patient and control pairs of fibroblast cell lines

Pair	MDD N	Control N	MDD DEX	Control DEX	MDD GAL	Control GAL
#1	28725	31958	6698	8282	74970	35427
#2	40717	65304	33293	33580	38739	47343
#3	44159	35897	17237	23195	44297	32185
#4	30804	42182	32253	54649	13624	116515
#5	21119	37008	26295	34799	57752	79691
#6	44089	110166	19703	29094	47092	118424
#7	22327	42185	13633	21345	110430	107092
#8	17573	87942	32355	9829	43236	26867
#9	51614	33690	31646	31861	53646	47419
#10	134620	149176	129238	143042	193662	193708
#11	41377	43084	38246	39944	66356	65851
#12	33585	32753	66047	75252	80235	97240
#13	100628	52306	91536	92541	150930	129138
#14	130534	144061	142213	149269	154589	163588
#15	49801	75492	65629	84681	75637	103046
#16	166859	189832	92688	110006	221335	223062

Table 30 Mean and SEM values for JC-1 ratios of 16 MDD patients and controls fibroblast pairs

	mean	SEM
MMD N	1.401	0.008
Control N	1.348	0.008

MDD DEX	1.449	0.006
Control DEX	1.421	0.006
MDD GAL	1.455	0.008
Control GAL	1.421	0.009

Table 31 Single red/green ratios for all 16 paired MDD and control cell lies

Pair	MDD N	Control N	MDD DEX	Control DEX	MDD GAL	Control GAL
#1	1.31	1.30	1.44	1.36	1.35	1.19
#2	1.43	1.39	1.42	1.54	1.49	1.58
#3	1.31	1.40	1.32	1.25	1.24	1.23
#4	1.26	1.18	1.44	1.30	1.32	1.35
#5	1.33	1.40	1.37	1.42	1.39	1.32
#6	1.18	1.00	1.31	1.30	1.33	1.39
#7	1.43	1.39	1.43	1.40	1.41	1.35
#8	1.50	1.43	1.38	1.30	1.62	1.47
#9	1.41	1.46	1.36	1.41	1.31	1.18
#10	1.57	1.41	1.54	1.56	1.49	1.60
#11	1.50	1.27	1.36	1.39	1.44	1.50
#12	1.41	1.55	1.61	1.40	1.55	1.66
#13	1.55	1.55	1.53	1.56	1.52	1.70
#14	1.50	1.50	1.53	1.48	1.56	1.42
#15	1.23	1.33	1.57	1.52	1.51	1.45
#16	1.54	1.41	1.55	1.51	1.43	1.63

Table 32 Table 30 Mean and SEM values for Fura-2 ratios of 16 MDD patient and control pairs

	mean	SEM
MDD N	0.6767	0.0128
Control N	0.6727	0.0088
MDD DEX	0.6262	0.0054
Control DEX	0.6204	0.0057
MDD GAL	0.6262	0.0054
Control DEX	0.6204	0.0057

Table 33 Single ratio values for Fura-2 measurements in fbroblasts.

Pair	MDD N	Control N	MDD DEX	Control DEX	MDD GAL	Control GAL
#1	0.66	0.64	0.58	0.61	0.62	0.64
#2	0.67	0.66	0.61	0.58	0.62	0.63
#3	0.65	0.65	0.62	0.61	0.64	0.63
#4	0.57	0.69	0.62	0.60	0.64	0.66
#5	0.73	0.73	0.63	0.61	0.65	0.63
#6	0.70	0.72	0.62	0.62	0.62	0.62
#7	0.64	0.66	0.61	0.61	0.63	0.61
#8	0.58	0.60	0.61	0.62	0.61	0.62

#9	0.63	0.69	0.64	0.64	0.66	0.64
#10	0.72	0.72	0.62	0.62	0.64	0.68
#11	0.68	0.66	0.67	0.65	0.64	0.61
#12	0.72	0.71	0.64	0.61	0.62	0.65
#13	0.72	0.65	0.61	0.62	0.65	0.64
#14	0.71	0.64	0.62	0.63	0.65	0.66
#15	0.72	0.67	0.63	0.66	0.69	0.68
#16	0.72	0.68	0.66	0.61	0.67	0.63

Table 34 Mean and SEM values of mtDNA copy numbers in fibroblasts.

	mean mtDNA copy number	SEM
MDD	654	28.04
Control	636	31.68

Table 35 mtDNA copy numbers for 16 MDD and control fibroblast cell lines.

Pair	mtDNA copy number	
	MDD	Control
#1	623	582
#2	634	618
#3	760	711
#4	577	584
#5	606	540
#6	728	501
#7	564	819
#8	486	738
#9	829	609
#10	767	375
#11	882	893
#12	578	668
#13	655	745
#14	512	545
#15	587	589
#16	681	652

Table 36 Mean and SEM values of respiratory parameters of 9 MDD and control NPC pairs.

	Basal Respiration		Maximal Respiration		Spare Respiratory Capacity	
	mean OCR	SEM	mean OCR	SEM	mean OCR	SEM
MDD N	88.49	3.42	114.94	5.55	27.40	1.44
Control N	103.72	4.52	131.15	11.54	34.81	7.46
MDD DEX	94.53	5.94	114.61	9.84	20.08	5.59

Control DEX	107.26	6.49	121.34	12.04	14.21	10.62
	non-mitochondrial Respiration		Proton Leak		ATP Production	
	mean OCR	SEM	mean OCR	SEM	mean OCR	SEM
MDD N	25.54	1.20	16.63	0.79	72.55	2.70
Control N	30.82	1.81	19.56	1.01	82.94	4.77
MDD DEX	25.62	1.52	16.22	0.70	75.87	3.83
Control DEX	28.00	1.40	21.02	2.96	85.27	4.64

Table 37 OCR and ECAR values for 9 NPC MDD and control pairs.

pair	N				DEX			
	MDD		CNTL		MDD		CNTL	
	OCAR	ECAR	OCR	ECAR	OCR	ECAR	OCR	ECAR
#1	121.86	71.63	152.73	64.38	137.21	50.61	144.61	42.83
#2	131.55	51.59	182.37	66.68	110.32	50.92	143.62	54.09
#3	139.35	60.91	158.93	61.84	176.87	46.20	173.42	46.58
#4	132.63	57.81	140.58	63.23	158.79	64.52	153.43	62.44
#5	117.89	53.65	157.87	57.19	116.99	47.83	177.98	56.41
#6	139.44	53.97	157.13	61.30	132.44	58.83	141.63	74.13
#7	133.88	50.13	126.95	49.57	86.91	37.86	119.85	39.15
#8	101.48	47.04	143.15	68.20	126.40	50.57	130.09	44.35
#9	127.26	55.84	152.46	61.55	130.74	50.92	148.08	52.50

Table 38 Mean and SEM values for JC-1 ratios of nine NPC MDD and control pairs.

	mean ratio	SEM
MDD N	1.696	0.065
Control N	1.839	0.092
MDD DEX	1.996	0.071
Control DEX	2.079	0.115

Table 39 Mean and SEM values for ATP measurements of 9 NPC MDD patients and control pairs

	mean	SEM
MDD N	341064	49780
Control N	324275	47085
MDD DEX	362357	65367
Control DEX	369576	57303

Table 40 Single RLU values of 9 MDD patient and control pairs of NPC lines

Pair	MDD N	Control N	MDD DEX	Control DEX
#1	210591	311489	127779	253116
#2	532401	187508	496569	406236

#3	475031	381469	703305	748366
#4	294678	335491	264349	257377
#5	331633	595669	320698	280280
#6	53072	224110	202532	168750
#7	487705	474044	549283	499086
#8	350901	169162	436798	352978
#9	333564	239534	159903	359999

Table 41 Single JC-ratios for 9 MDD and control NPC lines.

pair	MDD N	Control N	MDD DEX	Control DEX
#1	1.63	1.80	1.56	1.51
#2	1.36	1.68	2.18	2.60
#3	1.72	1.52	2.28	2.49
#4	1.75	2.08	1.94	1.84
#5	1.69	1.83	1.90	2.03
#6	1.89	2.21	2.00	1.95
#7	1.75	1.74	2.18	2.37
#8	2.00	2.22	1.91	2.01
#12	1.47	1.48	2.01	1.92

Table 42 Mean and SEM values for Fura-2 ratios of 9 NPC MDD and control pairs

	mean ratio	SEM
MDD N	0.62	0.01
Control N	0.60	0.01
MDD DEX	0.62	0.01
Control DEX	0.61	0.00

Table 43 Single Fura-2 ratios for 9 MDD and control NPC cell lines.

pair	MDD	Control	MDD DEX	Control DEX
#1	0.60	0.62	0.62	0.61
#2	0.64	0.60	0.62	0.59
#3	0.62	0.60	0.63	0.59
#4	0.59	0.60	0.58	0.60
#5	0.62	0.60	0.62	0.62
#6	0.63	0.62	0.60	0.63
#7	0.65	0.57	0.66	0.60
#8	0.62	0.56	0.62	0.62
#9	0.62	0.62	0.63	0.60